

# **Performance and Thermo-Mechanical Cost Evaluation of API 661 Air-Cooled Heat Exchangers**

by  
Mogamat Sadley Ackers

*Thesis presented in fulfilment of the requirements for the degree of  
Master of Engineering (Mechanical) in the Faculty of Engineering at  
Stellenbosch University*



Supervisor: Prof. Hanno Carl Rudolf Reuter

December 2012

## **Declaration**

By submitting this thesis electronically, I declare that the entirety of the work contained therein is my own, original work, that I am the sole author thereof (save to the extent explicitly otherwise stated), that reproduction and publication thereof by Stellenbosch University will not infringe any third party rights and that I have not previously in its entirety or in part submitted it for obtaining any qualification.

Signature: .....

Date: .....

## **Abstract**

The optimal design of a heat exchanger for a specified heat transfer, pressure drop and set of ambient conditions entails minimising space, weight, material usage and overall cost. However, the variables which influence the performance as well as the overall cost of a heat exchanger are not related in a simple way and it is not obvious which variables play the most important roles (Perry & Green, 1997:11-44).

Air cooled heat exchangers (ACHEs) are normally designed in three stages, by different experts in the field, and with the aid of specially designed software. This project combines these thermal, mechanical and cost estimation processes into a MS Excel model which makes it easier to see the influence that design parameters have on the overall cost of the heat exchanger.

A thermal model was created to design an API 661 (2006) ACHE. The results from this model compared well with those of HTRI Xchanger Suite 6.0 software, with HTRI being more conservative in its design mode.

A mechanical design model was then developed, which uses as inputs the outputs of the thermal design. The output from this mechanical design model is the minimum material thicknesses based on the stress criteria of Appendix 13 of ASME VIII div 1 (2007) Boiler and Pressure Vessel Code.

An experiment on a finned tube bundle was performed in a wind tunnel facility to determine performance characteristics and compare these to existing correlations in literature. The results showed that both the heat transfer coefficient ( $h$ ) and loss coefficient ( $E_u$ ) correlations proposed by Ganguli et al. (1985) closely predict the measured data, and were consequently used in the thermal design model. During this experiment it was also shown that the tube bundle reached 8 % - 9 % of its allowable internal fouling factor, due to rust build up inside the tubes, and in a testing period of only nine days.

The thermal and mechanical models were then combined with a cost estimation process to perform both a thermal and mechanical parametric study. The thermal study showed that to obtain an optimal solution, the design must attempt to maximise the length, increase the width rather than the number of bays, make use of two bundles per bay with fewer but larger fans and employ a large number of tube rows with the least number of tube passes. These guidelines were used to create an initial design; Excel Solver was then applied to locate the optimum combination of bundle length and width that result in the minimum heat exchanger cost.

Two mechanical considerations were investigated, both requiring additional welding and thus increased welding cost. Firstly the use of stay plates result in reduced required plate thicknesses according to the stress criteria since it provides additional stiffness in the header box design. Secondly the use of more (but smaller) nozzles as opposed to less (but larger) nozzles was also considered. The mechanical parametric study showed no specific trends, but both considerations should still be checked as it can be cost beneficial in a specific design.

## Opsomming

Optimale ontwerp van 'n warmteoordraer vir 'n gespesifiseerde warmteoordrag, drukval en stel van omgewingstoestand behels die minimalisering van ruimte, gewig, materiaalverbruik en algehele koste. Die veranderlikes wat egter die werkverrigting, sowel as die algehele koste, van 'n warmteoordraer beïnvloed, hou nie in 'n eenvoudige sin met mekaar verband nie, en dit is nie vanselfsprekend watter veranderlikes die belangrikste rolle speel nie (Perry & Green, 1997:11-44).

Lugverkoelde warmteoordraers (*air-cooled heat exchangers* of ACHEs) word normaalweg in drie fases ontwerp deur verskillende kundiges in die veld en met behulp van spesiaal ontwerpte programmatuur. Hierdie studie kombineer dié termiese, meganiese en kosteberamingsprosesse in 'n MS Excel-model, wat dit makliker maak om van te stel wat die invloed wat ontwerpparameters op die algehele koste van die hittedruiser is.

'n Termiese model is geskep om 'n "API 661 (2006) ACHE" te ontwerp. Die resultate van hierdie model het goed vergelyk met dié van die HTRI Xchanger Suite 6.0-program, met HTRI meer konserwatiew in die ontwerp af.

Na die termiese model geskep is, is 'n meganieseontwerp-model ontwikkel, wat as insette die uitsette van die termiese ontwerp gebruik het. Die uitset van hierdie meganieseontwerp-model is die minimum materiaaldikte gebaseer op die spanningskriteria van Bylae 13 van "ASME VIII div 1 (2007) Boiler and Pressure Vessel Code."

Daar is 'n eksperiment op 'n vinbuisbundel in 'n windtonnelfasiliteit uitgevoer om werkverrigtingskarakteristieke te bepaal en dit met bestaande korrelasies in die literatuur te vergelyk. Die resultate het getoon dat sowel die warmteoordragskoeffisiënt ( $h$ ) en die verlieskoeffisiënt ( $Eu$ ) korrelasies, voorgestel deur Ganguli et al. (1985), die data wat gemeet is akkuraat voorspel, en gevolglik is die korrelasies in die termieseontwerp-model gebruik. Gedurende die eksperiment is ook getoon dat die buisbundel 8 % - 9 % van sy toelaatbare interne-aanpakkingfaktor bereik het vanweë roesopbou binne-in die buise, en dit in 'n toetsingtydperk van slegs nege dae.

Die termiese en meganiese modelle was toe gekombineer met 'n kosteberamingsproses om 'n termiese sowel as 'n meganiese parametriese studie uit te voer. Die termiese studie het getoon dat, om 'n optimale oplossing te verkry, die ontwerp moet poog om die lengte te maksimeer; die wydte eerder as die aantal strate (*bays*) te vermeerder; van twee bundels per straat gebruik te maak met minder, maar groter waaiers; en 'n groot aantal buisrye met die kleinste hoeveelheid

buisdeurvloeiweë in te span. Hierdie riglyne is gebruik in 'n aanvanklike ontwerp, waarna die Excel Solver gebruik is om die optimale kombinasie van bundellengte en –wydte vas te stel met die oog op die laagste moontlike warmteoordraerkoste.

Twee meganiese oorwegings is ondersoek wat albei addisionele sweiswerk sou vereis en dus tot verhoogde sweiskoste sou lei. Eerstens lei die gebruik van ankerplate (*stay plates*) tot 'n vermindering in die vereiste plaatdiktes volgens die spanningskriteria, aangesien dit addisionele stewigheid in die spuitstukhouerontwerp bied. Tweedens is die gebruik van meer (maar kleiner) spuitstukke teenoor minder (maar groter) spuitstukke ook oorweeg. Die meganiese parametrisiese studie het geen spesifieke voorkeurings getoon nie, maar altwee oorgewings moet nog getoets word want dit kan koste voordelig word in 'n spesifieke ontwerp.

## **Acknowledgements**

I would like to express my sincerest gratitude to the following people/organisations for their contribution towards making this study possible:

- Prof H.C.R Reuter for his support, knowledge and guidance.
- My family and friends for their support, patience and encouragement.
- GEA Aircooled systems (Pty) Ltd for the funding and information applicable to this project.
- To Mr C Zietsmann and Julian Stanfliet for their assistance with the finned tube performance testing in the wind tunnel laboratory.

## Table of contents

Declaration.....	i
Abstract.....	ii
Opsomming.....	iv
Acknowledgements.....	vi
Table of contents.....	vii
List of figures.....	x
List of tables.....	xii
Nomenclature.....	xiv
1. Introduction.....	1
1.1. Background.....	1
1.2. Motivation.....	6
1.3. Objectives.....	6
1.4. Thesis outline.....	7
2. Thermal design according to API 661 (2006).....	7
2.1. Introduction.....	7
2.2. System description.....	8
2.3. Thermal model.....	9
2.3.1. Geometry.....	10
2.3.2. Draft equation.....	14
2.3.3. Fan characteristics.....	17
2.3.4. Water side pressure drop.....	18
2.4. Thermal model.....	20
2.4.1. Thermal model algorithm explained.....	20
2.4.2. Thermal rating mode.....	23
2.4.3. Thermal model design mode.....	24
3. Mechanical design of an air-cooled heat exchanger header box according to ASME VIII Div 1 (2007) Addenda 2009b.....	26



3.1.	Introduction .....	26
3.2.	Mechanical design procedure.....	26
3.2.1.	Design Inputs and outputs.....	27
3.2.2.	Vessel configuration .....	29
3.2.3.	Overall dimensions .....	30
3.2.4.	Corrosion allowance (Ca) .....	30
3.2.5.	Corroded condition .....	35
3.2.6.	Header design .....	36
3.2.7.	Nozzle design.....	42
3.2.8.	Tube-to-tubesheet welds .....	44
4.	Finned tube bundle performance characteristics .....	48
4.1.	Introduction .....	48
4.2.	Literature review .....	48
4.3.	Description of test facility.....	49
4.4.	Measurement devices and techniques .....	52
4.4.1.	Temperatures .....	52
4.4.2.	Pressures .....	53
4.4.3.	User interface .....	53
4.4.4.	Mass flow rates .....	54
4.5.	Test procedure .....	55
4.6.	Data Processing.....	56
4.7.	Results .....	57
4.7.1.	Isothermal test.....	57
4.7.2.	Energy balance.....	57
4.7.3.	Row effect.....	58
4.7.4.	Heat transfer coefficient.....	59
4.7.5.	Pressure drop.....	60
4.7.6.	Rust effect .....	61

4.8.	Summary of results and conclusion .....	64
5.	Parametric study .....	65
5.1.	Cost estimation.....	65
5.2.	Parametric study procedure.....	66
5.3.	Results of thermal parametric study.....	67
5.3.1.	Length versus width.....	67
5.3.2.	Length versus number of bays .....	67
5.3.3.	Width versus number of bays .....	68
5.3.4.	Fans per bay versus fan diameter.....	68
5.3.5.	Number of bundles per bay versus number of bays.....	68
5.3.6.	Passes versus width.....	69
5.4.	Cumulative thermal parametric study .....	69
5.4.1.	Case 1.....	69
5.4.2.	Case 2.....	70
5.5.	Excel solver.....	70
5.6.	Results of mechanical parametric study.....	72
5.6.1.	Nozzles.....	72
5.6.2.	Stay plates .....	73
5.7.	Cost breakdown.....	73
6.	Conclusions and recommendations .....	75
6.1.	Conclusions .....	75
6.2.	Recommendations .....	77
7.	References.....	78
	Appendix A – Properties of fluids .....	80
	Appendix B - Thermal design sample calculation.....	83
	Appendix C - Mechanical design sample calculation.....	98
	Appendix D – Measured data and results of wind tunnel experiment.....	108
	Appendix E - Wind tunnel experiment sample calculation .....	116

## List of figures

Figure 1.1: Components of an air-cooled heat exchanger (API 661, 2006) .....	2
Figure 1.2: Construction of a tube bundle with a plug-type header (API, 2006) .....	3
Figure 1.3: Exploded view of a tube bundle configuration (Basics of air cooled heat exchangers, [S.a]).....	5
Figure 1.4: Types of finned tubes (Basics of air cooled heat exchangers, [S.a]) .....	5
Figure 2.1: Schematic of an air-cooled heat exchanger .....	9
Figure 2.2: G-fin type finned tube .....	9
Figure 2.3: Fan dispersion angle (API 661, 2006).....	16
Figure 2.4: Heat exchanger bundle .....	20
Figure 2.5: Flow diagram of thermal model algorithm .....	22
Figure 2.6: Thermal model algorithm.....	23
Figure 3.1: Nozzle loads as in Figure 6 of API 661 (2006).....	28
Figure 3.2: Sketch 1 .....	31
Figure 3.3: Sketch 7 .....	31
Figure 3.4: Sketch 8 .....	31
Figure 3.5: Side plate length .....	32
Figure 3.6: Tubesheet length calculation .....	33
Figure 3.7: Stay plate .....	34
Figure 3.8: Multidiameter holes.....	34
Figure 3.9: Membrane stress.....	37
Figure 3.10: Bending stress .....	38
Figure 3.11: Attachment of nozzle to header.....	42
Figure 3.12: Tube-to-tubesheet welds as in Figure UW-20.1 of ASMEVIII div 1 (2007) .....	45
Figure 4.1: Test wind tunnel (Kröger, 2004).....	51
Figure 4.2: Heat exchanger bundle in the wind tunnel .....	51
Figure 4.3: Complete setup of the experiment.....	53

Figure 4.4: Scale and bucket used to check water mass flow rate.....	55
Figure 4.5: Tank used to check water mass flow rate.....	55
Figure 4.6: U-bend used to connect adjacent rows .....	56
Figure 4.7: Variable speed drive that control fan speed .....	56
Figure 4.8: Isothermal loss coefficient and Euler number .....	57
Figure 4.9: Energy balance .....	58
Figure 4.10: Effect of using $Q_a$ , $Q_m$ or $Q_w$ .....	58
Figure 4.11: Row effect .....	59
Figure 4.12: Sum of rows vs bundle.....	59
Figure 4.13: Heat transfer coefficient of bundle.....	60
Figure 4.14: Heat transfer coefficient comparison ratio .....	60
Figure 4.15: Pressure loss coefficient of bundle.....	62
Figure 4.16: Pressure loss coefficient comparison ratio .....	62
Figure 4.17: Heat transfer coefficient vs time .....	62
Figure 4.18: Rust factor .....	62
Figure 5.1: Flow chart of combined model.....	65

## List of tables

Table 1.1: Advantages and disadvantages of forced and induced draft configurations (Makhema, 2000).....	2
Table 2.1: Crossflow with four tube rows and four tube passes.....	12
Table 2.2: Thermal rating mode .....	24
Table 2.3: Thermal design mode .....	25
Table 3.3: Minimum nozzle neck nominal thickness as in Table 3 of API 661 (2006) .....	27
Table 3.4: Maximum allowable nozzle loads as in Table 4 of API 661 (2006).....	28
Table 3.5: Minimum thickness of header components as in Table 1 of API 661 (2006) .....	29
Table 3.6: Membrane stress, constants for equation (3.27).....	39
Table 3.7: Bending stress, constants for equation (3.28) and Figure 3.2.....	39
Table 3.8: Bending stress, constants for equation (3.28) and Figure 3.3.....	40
Table 3.9: Bending stress, constants for equation (3.28) and Figure 3.4.....	40
Table 3.10: Total stress .....	40
Table 3.11: Acceptance criteria .....	41
Table 4.1: Percentage difference between tests .....	63
Table 5.1: Costs taken into consideration for this project .....	66
Table 5.2: Results of thermal parametric study .....	67
Table 5.3: Results of cumulative thermal parametric study .....	69
Table 5.4: Excel solver results.....	71
Table 5.5: Results of parametric study of number of nozzles versus nozzle size.....	72
Table 5.6: Results of parametric study of the use of stay plates.....	73
Table 5.7: Percentage contribution of each section to total cost of the heat exchanger .....	73
Table D.1: Isothermal Test .....	108
Table D.2: Measured data of whole bundle (Test 1) .....	108

Table D.3: Results of whole bundle (Test 1) .....	108
Table D.4: Measured data of whole bundle (Test 2) .....	109
Table D.5: Results of whole bundle (Test 2) .....	109
Table D.6: Measured data of whole bundle (Test 3) .....	109
Table D.7: Results of whole bundle (Test 3) .....	110
Table D.8: Measured data of whole bundle (Test 4) .....	110
Table D.9: Results of whole bundle (Test 4) .....	110
Table D.10: Measured data of whole bundle (Test 5) .....	111
Table D.11: Results of whole bundle (Test 5) .....	111
Table D.12: Measured data of row 1 .....	111
Table D.13: Results of row 1 .....	112
Table D.14: Measured data of row 2 .....	112
Table D.15: Results of row 2 .....	112
Table D.16: Measured data of row 3 .....	113
Table D.17: Results of row 3 .....	113
Table D.18: Measured data of row 4 .....	113
Table D.19: Results of row 4 .....	114
Table D.20: Measured data of row 5 .....	114
Table D.21: Results of row 5 .....	114
Table D.22: Measured data of row 6 .....	115
Table D.23: Results of row 6 .....	115

## Nomenclature

A	Area, m <sup>2</sup>
a	Length of tube-to-tubesheet welds, mm
C	Coefficient; heat capacity rate $mc_p$ , W/K
$C_{af}$	Attachment factor
Ca	Corrosion allowance
$c_j$	Distance from neutral axis, mm
$c_p$	Specific heat at constant pressure, J/kgK
$c_v$	Specific heat at constant volume, J/kgK
D	End plate long side length, mm
DALR	Dry adiabatic lapse rate, K/m
d	Diameter, mm; end plate length, mm; short side length, mm
E	Ligament efficiency; joint efficiency
E	Effectiveness
F	Force, N; correction factor
f	Strength factor; friction factor
G	Mass velocity, kg/m <sup>2</sup> s
g	Gasket
H	Height, m ; side plate (short) length, mm
h	Distance to stay plate, mm; heat transfer coefficient, W/m <sup>2</sup> K
I	Moment of inertia, mm <sup>4</sup>
K	Loss coefficient; Vessel parameter
k	Thermal conductivity, W/mK
L	Length, m; tubesheet (long) length, mm
M	Mass, kg; Molecular weight, kg/mole; moment, N.m
m	Mass flow rate, kg/s
N	Revolutions per minute, rpm
NTU	Number of transfer units, $UA/C_{\min}$
$Ny$	Characteristic heat transfer parameter, m <sup>-1</sup>
n	Number
P	Pitch, mm; power, W

p	Pressure, Pa
Q	Heat transfer rate, W
R	Gas constant, J/kgK; thermal resistance, m <sup>2</sup> K/W
R <sub>y</sub>	Characteristic flow parameter, m <sup>-1</sup>
S	Stress, MPa; Allowable stress, MPa; spacing, mm
T	Temperature, K
t	Thickness, mm
V	Volume flow rate, m <sup>3</sup> /s, volume, m <sup>3</sup>
v	velocity, m/s
W	Width, m
w	Humidity ratio, kg water vapour/kg dry air
Z	Non-circular head factor or Section modulus

### Greek symbols

$\alpha$	Rectangular vessel parameter
$\Delta$	Differential
$\eta$	Efficiency
$\mu$	Dynamic viscosity, kg/ms
$\rho$	Density, kg/m <sup>3</sup>
$\sigma$	Area ratio
$\tau$	Shear stress, Pa

### Dimensionless Groups

Eu	Euler number, $\Delta p/(\rho v^2)$
Nu	Nusselt number, $hL/K$
Re	Reynolds number, $\rho v d/\mu$

### Subscripts

a	Allowable; air or based on air-side area
av	mixture of dry air and water vapor
b	Bending; bundle



c	Casing; compartment; combined; contraction
corr	Corroded
D	Darcy; drag
d	Design
do	Downstream
e	Expansion
F	Fan
f	Fillet; fin
fr	Frontal
g	Gas, groove
h	Height; hole
i	Inlet; inside; inch
j	Joint
l	Longitudinal
lm	Logarithmic mean
LMTD	Logarithmic mean temperature difference
m	Mean; membrane; model
max	Maximum
min	Minimum
N	Nozzle
o	Outlet; outside
p	passes; per
pl	Plenum chamber
pp	Partition plate
r	Resultant; reference; required; root; rows
rec	Recovery
s	Side
st	Stay plate
t	Transversal; tube; tensile
tot	Total
up	Upstream

v	Vapor; vessel
w	Water; weld; windwall
wb	Wetbulb
x	Co-ordinate
y	Co-ordinate
z	Co-ordinate

### **Superscripts**

c	Compartments
l	Tubesheet (long) plate
s	Side (short) plate
st	Stay plate

## 1. Introduction

The optimal design of a heat exchanger for a specified heat transfer, pressure drop and set of ambient conditions entails minimising space, weight, material usage and overall cost. However, the variables which influence the performance as well as the overall cost of a heat exchanger are not related in a simple way and it is not obvious which variables play the most important roles (Perry & Green, 1997:11-44).

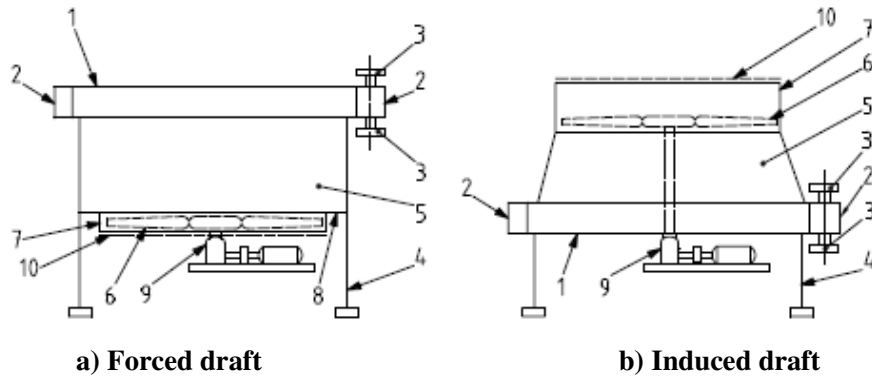
### 1.1. Background

Air-cooled heat exchangers (ACHEs) use air as the cooling medium to cool process fluids. They are typically used in the petrochemical, air-conditioning and power generating industries. These systems are often preferred over wet-cooled systems based on its environmental and economic advantages. Using an air-cooled system reduces the need for water and the treatment thereof. It also reduces the thermal and chemical pollution of water (Beiler, 1991:1.1). Although the initial installed cost of an air-cooled heat exchanger is usually greater than that of a water-cooled alternative, the savings in operation and maintenance costs frequently make the air-cooled heat exchanger the more economical selection (Mahajan, 1990:281).

An ACHE can be as small as a car radiator or large enough to cover acres of land, as in the case of large power plants. The ACHEs considered in this project comply with the American Petroleum Institute (API) 661 international standard, which gives requirements and recommendations with regard to the design, materials, fabrication, inspection and preparation for shipments of use in the petroleum and natural gas industries.

The basic components of an ACHE are shown in Figure 1.1. Cooling air, provided by one or more fans (6), is forced over a finned tube bundle (1) where heat is exchanged with the process fluid flowing inside the tubes. The space between the fan and the finned tube bundle is the plenum (5) which directs the air across the surface area. The fan is driven by a motor coupled with a speed reduction device (9) to supply the required amount of power. A fan guard (10) is also provided as protection for the tube bundle and a barrier to the rotating equipment. The process fluid enters and exits the system via nozzles (3) attached to the headers (2). The structure is supported by columns (4) to offer sufficient elevation for the ambient air to be extracted.

If the fan is located upstream of the heat exchanger, the ACHE is of the forced draft type as in Figure 1.1(a). In the induced draft type ACHE, the fan is located downstream of the ACHE as in Figure 1.1(b). Table 1.1 summarises the advantages and disadvantages of forced and induced draft heat exchangers, the main advantage of the forced draft configuration being that it requires a lower fan power consumption due to lower air inlet temperatures.



- |                     |                  |
|---------------------|------------------|
| 1 Tube bundle       | 6 Fan            |
| 2 Header box        | 7 Fan ring       |
| 3 Nozzle            | 8 Fan deck       |
| 4 Supporting column | 9 Drive assembly |
| 5 Plenum            | 10 Fan guard     |

**Figure 1.1: Components of an air-cooled heat exchanger (API 661, 2006)**

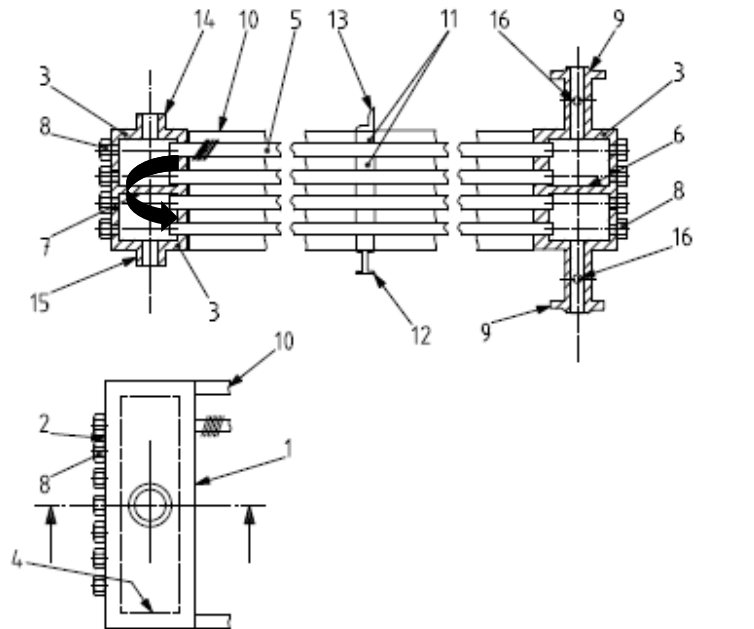
**Table 1.1: Advantages and disadvantages of forced and induced draft configurations (Makhema, 2000)**

Type	No.	Advantages	Disadvantages
<b>Forced draft</b>	1	Lower fan shaft power consumption due to lower inlet air temperatures	Poor air distribution across bundle
	2	Location of fan drives offers better accessibility for maintenance work	Low discharge velocity increases the risk of plume recirculation
	3	Fan drives not exposed to high temperatures making the choice of construction material less critical	Exposure of the finned surfaces to the atmosphere can affect performance due to wind, rain or hail
<b>Induced draft</b>	1	Better distribution of air across the bundle	High fan shaft power consumption since fan is in outlet air stream
	2	Relatively high escape velocity of the air reduces plume recirculation	Low accessibility of fan components for maintenance work
	3	Bundle is protected in part by plenum from weather conditions	Fan and drive system exposed to the warm air stream making the choice of construction material more critical

Figure 1.2 shows the typical construction of a four-row two pass tube bundle with a plug-type header, which provides a more detailed view of (1), (2) and (3) in Figure 1.1.

The pass partition plate (6) separates the header into two passes thus making it two rows per pass. The inlet/outlet header is situated on the right, where the nozzle (9) allows for the entry of the process fluid to the first two tube rows (5) via the header. The return header, on the left, sends the process fluid through the other two tube rows to the outlet header, where it exits through the outlet nozzle. The stiffener (7), in the return header, is known as a stay plate. It contains holes that allow the process fluid to pass through and thus does not separate tube passes. Pass partition plates and stiffeners (7) are welded into the headers. Tube spacers (11) are also provided at designated locations along the length of the tube bundle to keep the tubes in place.

The plug type header is a rectangular steel box fabricated from plate and consists of a tubesheet (1), plugsheet (2), top and bottom plates (3) and end plates (4). In the standard configuration, the tubes are expanded in the holes of the tubesheet (1) where



- |                  |                              |                          |
|------------------|------------------------------|--------------------------|
| 1 tubesheet      | 7 stiffener                  | 13 tube keeper           |
| 2 plugsheet      | 8 plug                       | 14 vent                  |
| 3 side plates    | 9 nozzle                     | 15 drain                 |
| 4 end plates     | 10 side frame                | 16 instrument connection |
| 5 tube           | 11 tube spacer               |                          |
| 6 pass partition | 12 tube support cross-member |                          |

**Figure 1.2: Construction of a tube bundle with a plug-type header (API, 2006)**

it is then welded to form the tube-to-header joints. Holes are drilled and tapped in the plugsheet (2) opposite each tube to allow for maintenance of the tubes. A plug (8) with a soft iron gasket is threaded into each hole to seal under pressure. These plugs make tube expansion and cleaning easy since the plugs can be removed when necessary. Piping does not have to be disassembled for inspection or cleaning, since the nozzles are mounted at the top or bottom of the header.

The tube bundle is manufactured as an assembly of tubes, headers, nozzles, tube supports and side frames as shown in Figure 1.3. The side frames, (10) in Figure 1.2, completes the assembly of the tube bundle and has lifting lugs attached to it to assist with handling and transportation. Tube supports and spacers are provided to prohibit intermeshing of the fins and bunching of the tubes, which allows channelling of the airflow pass the tubes.

The header box is considered to be a pressure vessel and is therefore designed to comply with American Society of Mechanical Engineers (ASME) Boiler and Pressure Vessel Code, Section VIII, Division 1 (2007). Although many header designs exist, only plug type headers were considered in this project as it is the most common. If the design pressure reaches or exceeds 3 MPa, the use of plug type headers becomes mandatory according to API 661 (2006).

A bare tube is the simplest and least expensive configuration, but its application is limited since it poses a higher resistance to heat transfer. Fins can expose from eight to twenty times more tube surface and thus result in dissipation of more heat from a given diameter of tube (Mahajan, 1990:283). Round tubes with smooth helical fins are encountered in many industrial air-cooled systems. They are readily mass-produced in great lengths at a minimum cost (Kröger, 2004:330). The tube material is selected based on the corrosion, pressure and temperature limitations of the required design. Aluminum material is used for the fins as it has a good thermal conductivity, it is economical to manufacture and because of its weight.

Figure 1.4 shows the three most common types of finned tubes. The L-fin type is produced by wrapping an aluminum strip, that is footed at the base, around the tube. The ends of the fins are stapled to prevent losing the contact between the fin foot and the tube. The L-fin type is used in applications where the tube wall temperature does not exceed 120 °C. The core tube is steel and the fin material is aluminum. The thermal contact resistance may increase rapidly at higher temperatures due to the difference between the thermal expansion coefficients of the two materials (Kröger, 2004:331).

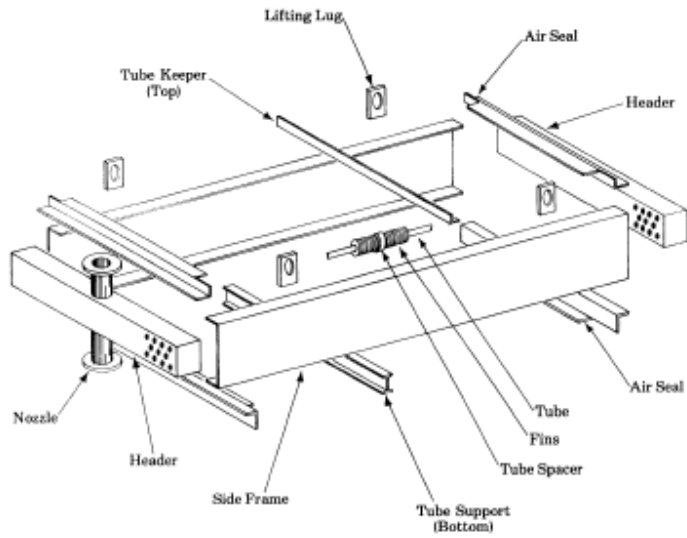
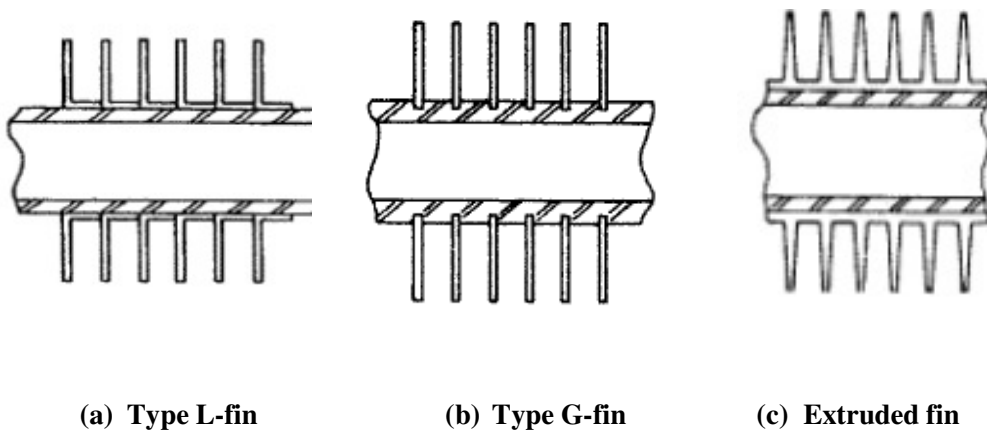


**Figure 1.3: Exploded view of a tube bundle configuration (Basics of air cooled heat exchangers, [S.a])**



**(a) Type L-fin**

**(b) Type G-fin**

**(c) Extruded fin**

**Figure 1.4: Types of finned tubes (Basics of air cooled heat exchangers, [S.a])**

The G-fin type tube is manufactured by cutting a groove into the core tube, the fin strip is inserted, and the tube material is then pushed back against the sides of the fin

material. This prevents differential expansion and thus G-fin tubes can be used for tube wall temperatures up to 400 °C. A thicker tube wall thickness must be used, since a groove is actually cut in it, to avoid over-pressuring the tube.

Where corrosion is a major consideration, the extruded fin is recommended for tube wall temperatures up to 200 °C. The finned surface is obtained by plastically deforming an outer aluminium muff onto the internal steel tube during a rolling process (Kröger, 2004:333).

Other less commonly used types of finned tubes such as double L-fin, I-fin and IW-fin are discussed in Kröger (2004:330-337).

## **1.2. Motivation**

There are always many possible designs to any given problem, but manufacturing limitations and client specifications or standards reduce this number of possible designs. The question that then arises is; which is the best possible design.

Generally company's main drive is to maximise value for their shareholders. Consequently one of the main considerations for the best possible design is the cost, while still producing a heat exchanger that meets all the design specifications.

Companies generally separate the design stages of an air-cooled heat exchanger into the thermal design, mechanical design and a cost estimation process. Each stage of the design process is performed by a different expert or department of the company using specialised software or databases. This mimics the classic "over-the-wall" design process as discussed by Ullman (1997:7). A characteristic of this design process is one-way communication, where information is "thrown over the wall" from one design stage to the next. This design process leads to information being interpreted incorrectly, which may result in poor quality products.

In contrast to the "over-the-wall" design process, this project will develop a design tool using MS Excel that combines all the stages of the design process thus including iteration between the design stages. This will make it easier to investigate the influence of changes to different parameters in the thermal and mechanical designs on the overall cost of the heat exchanger. The study is however limited to an air cooler design with water as the process fluid and it only considers plug type header boxes in the mechanical design.

## **1.3. Objectives**

The main objectives of this project are as follows:



- Evaluate the thermal performance of an API 661 type air-cooled heat exchanger.
- Perform a mechanical design of an API 661 type air-cooled heat exchanger which complies with the relevant sections of the ASME VIII Boiler and Pressure Vessel Code.
- Measure the performance characteristics of finned tube bundles and compare these characteristics to existing correlations.
- Complete a cost calculation for an API 661 air-cooled heat exchanger.
- Combine this with the thermal and mechanical model to perform a parametric study to investigate which design variables are the main cost drivers.

#### **1.4. Thesis outline**

Chapter 1 explains all the components of an API 661 air-cooled heat exchanger. It then gives the motivation and objectives of the project.

Chapter 2 provides an outline for the thermal design of an air-cooled heat exchanger which forms the basis of the thermal model. The results of the model is then checked by comparing the results to that of HTRI (Heat Transfer Research Institute) Xchanger suite 6.0, a commercial software package

Chapter 3 presents a summary of the relevant sections of the ASME VIII Boiler and Pressure Vessel Code for the mechanical design of an air-cooled heat exchanger.

Chapter 4 explains the setup of a wind tunnel test to evaluate the performance of a finned tube bundle. The results of the test are examined and compared to performance characteristics predicted by correlations found in the literature.

Chapter 5 discusses how the various design stages are combined to perform a parametric study to see which design variables are the main cost drivers. The results of the parametric study are presented for both thermal and mechanical design variables.

Chapter 6 summarises the results of this study. Conclusions are drawn and recommendations are made for future research.

## **2. Thermal design according to API 661 (2006)**

### **2.1. Introduction**

The first part of the section explains the forced-draft air-cooled heat exchanger configuration followed by various equations extracted from Kröger (2004) to

illustrate how the defined input parameters are used to calculate and obtain the thermal design. These equations include geometrical parameters, heat transfer and flow theory.

The theory is then used to design a heat exchanger as an example. The design calculations are carried out with the aid of MS Excel. The iterated solution is then used as input to a sample calculation created in Mathcad. Functions were created in visual basic for the fluid properties of air and water so that it can easily be used in MS Excel. These functions are according to Kröger (2004) and are shown in Appendix A.

The same heat exchanger is then designed or rated with HTRI software and certain key geometry as well as other parameters are compared.

## 2.2. System description

A schematic of a forced-draft air-cooled heat exchanger is shown in Figure 2.1. Ambient air (1) is accelerated by the fans (3), where upstream obstacles such as structural supports or a screen may be located. The air also flows across the heat exchanger supports (2). After leaving the fan (4), where further downstream obstacles may be located, the flow experiences losses in the plenum (5) before passing through the heat exchanger bundle, exiting at (6) (Kröger, 2004:137). Hot water flows inside the finned tubes and is cooled by blowing ambient air across the system by axial flow fans.

Two thermal models were developed; a design case and an off-design (rating) case. The design case is where the heat exchanger dimensions must be selected that will achieve a specified temperature change in a fluid stream of known mass flow rate, whereas the off-design case is where the heat exchanger dimensions are specified and the outlet temperatures of the hot and cold fluid streams must be predicted (Cengel, 2006:620). Therefore once a design case has been established the rating model can be used to evaluate the performance of that heat exchanger under different operating conditions.

A four-row four-pass water cooler with a grooved finned (G-fin) type of finned tube (shown in Figure 2.2) has been selected as an example case and a sample calculation is provided in Appendix B. This sample calculation provides all the details of the calculation since all the inputs, outputs, iteration parameters, equations and results are displayed.

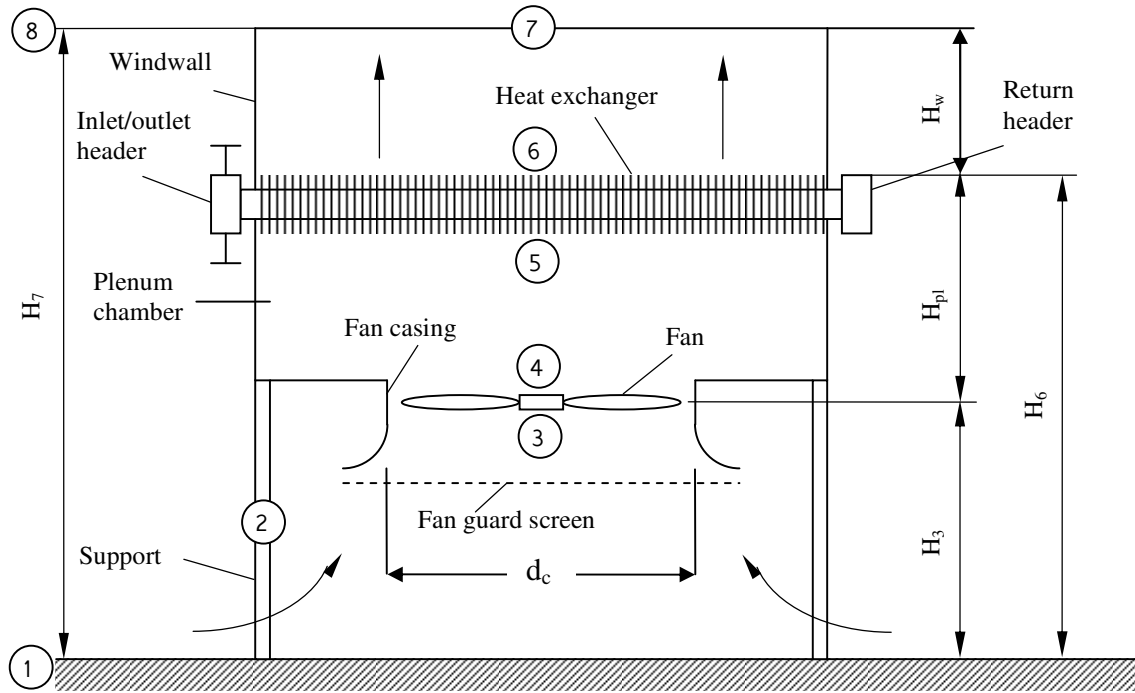


Figure 2.1: Schematic of an air-cooled heat exchanger

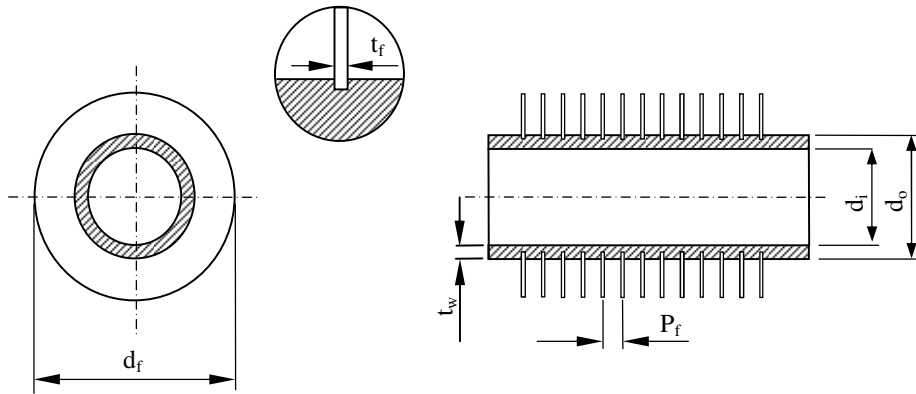


Figure 2.2: G-fin type finned tube

### 2.3. Thermal model

The thermal model was based on the work of Kröger (2004). There are two requirements that the model seeks to accomplish to have a successful heat exchanger

design. It must firstly be capable of rejecting the required amount of heat to the environment. Secondly the selected axial flow fan must generate the required amount of air mass flow rate. The energy equation allows for the calculation of the amount of heat transferred and the draft equation equates the pressure rise induced by the fan to the flow losses through the system (Bredell, 2006:18).

The sample calculation, shown in Appendix B, provides a detailed explanation of the thermal design while an overview of the calculation is also discussed below.

### 2.3.1. Geometry

The following equations regarding the geometry can be deduced when evaluating Figure 2.2.

Cross-sectional area per tube

$$A_t = \frac{\pi}{4} d_i^2 \quad (2.1)$$

Inside tube diameter

$$d_i = d_o - 2t_w \quad (2.2)$$

Inside width of bundle

$$W = d_{fo} + (n_{tr} - 0.5)P_{tr} \quad (2.3)$$

Water flow area required per pass

$$A_{req} = \frac{m_w}{\rho_w v_w} \quad (2.4)$$

Total exposed area per fin

$$A_{fin} = A_{r,fin} + A_{f,fin} \quad (2.5)$$

Exposed root area per fin

$$A_{r,fin} = \pi(P_f - t_f)d_r \quad (2.6)$$

Exposed area per fin

$$A_{f,fin} = \frac{2\pi}{4}(d_f^2 - d_r^2) + \pi d_f t_f \quad (2.7)$$

The thermal model uses the effectiveness-NTU (e-NTU) method as well as the logarithmic mean temperature difference (LMTD) method combined with fin efficiencies to evaluate the energy equation. These two methods are then compared and thereafter verified with HTRI Xchanger Suite 6.0.

A summary of the equations extracted from Kröger (2004) for use in the thermal design is shown below.

The heat transferred from the water inside the tubes to the air flowing over the tubes can be expressed as:

Water-side heat rate

$$Q_w = m_w c_{pw} (T_{wi} - T_{wo}) \quad (2.8)$$

Air-side heat rate

$$Q_a = m_a c_{pa} (T_{a6} - T_{a5}) \quad (2.9)$$

e-NTU method heat rate

$$Q_e = e C_{min} (T_{wi} - T_{a5}) \quad (2.10)$$

$$e = \frac{1 - \exp[-NTU(1 - C)]}{1 - C \exp[-NTU(1 - C)]} \quad (2.11)$$

where  $e$  is the effectiveness of the heat exchanger and other correlations exist depending on the heat exchanger configuration. Equation (2.11) is only valid for the counterflow arrangement.

LMTD method heat transferred

$$Q_{LMTD} = F_T U A \Delta T_{lm} \quad (2.12)$$

$$F_T = 1 - \sum_{i=1}^4 \sum_{k=1}^4 a_{i,k} (1 - \varphi_{cf})^k \sin \left[ 2i \arctan \frac{\varphi_h}{\varphi_c} \right] \quad (2.13)$$

$$\varphi_{cf} = \frac{(\varphi_h - \varphi_c)}{\ln \left[ \frac{(1-\varphi_c)}{(1-\varphi_h)} \right]} \quad (2.14)$$

$$\varphi_c = \frac{(T_{a6} - T_{a5})}{(T_{wi} - T_{a5})} \quad (2.15)$$

$$\Delta T_{lm} = \frac{(T_{wi} - T_{a5}) - (T_{wo} - T_{a6})}{\ln \left[ \frac{(T_{wi} - T_{a5})}{(T_{wo} - T_{a6})} \right]} \quad (2.16)$$

where the matrix  $a_{i,k}$  in equation (2.13) is dependent on the heat exchanger configuration and can be found in Kröger (2004:421-423). Table 2.1 shows an example of this matrix for a crossflow heat exchanger with four tube rows and four tube passes.

**Table 2.1: Crossflow with four tube rows and four tube passes**

$a_{i,k}$	<b>i = 1</b>	<b>2</b>	<b>3</b>	<b>4</b>
<b>k = 1</b>	-3.39E-01	2.77E-02	1.79E-01	-1.99E-02
<b>2</b>	2.38E+00	-9.99E-02	-1.21E+00	4.00E-02
<b>3</b>	-5.26E+00	9.04E-02	2.62E+00	4.94E-02
<b>4</b>	3.90E+00	-8.45E-04	-1.81E+00	-9.81E-02

Overall heat transfer coefficient

$$UA = \left[ \frac{1}{e_f h_a A_a} + \frac{\ln \left( \frac{d_o}{d_i} \right)}{2\pi k_t L_{tot}} + \frac{1}{h_w A_w} \right]^{-1} \quad (2.17)$$

Surface effectiveness  $e_f$

$$e_f = 1 - A_{f,fin} (1 - \eta_f) A_{fin} \quad (2.18)$$

Fin efficiency  $\eta_f$

$$\eta_f = \tanh \left[ \frac{bd_r \varphi / 2}{bd_r \varphi / 2} \right] \quad (2.19)$$

Fin efficiency parameter  $\varphi$

$$\varphi = (d_f/d_r - 1)[1 + 0.35 \ln(d_f/d_r)] \quad (2.20)$$

Fin efficiency parameter b

$$b^2 = \frac{2h_a}{t_f k_f} \quad (2.21)$$

Air-side heat transfer coefficient

$$h_a = \frac{k_a Nu_a}{d_r} \quad (2.22)$$

Air-side heat transfer coefficient (Ganguli et al., 1985)

$$Nu_a = 0.38 Re_a^{0.6} Pr_a^{0.333} (A/A_r)^{-0.15} \quad (2.23)$$

Air-side Reynolds number

$$Re_a = \frac{G_c d_r}{\mu_a} \quad (2.24)$$

Air mass velocity

$$G_c = \frac{m_a}{A_c} \quad (2.25)$$

Total air-side heat transfer area

$$A_a = L_t n_b n_{bay} n_{tr} n_r A_{fin} / P_f \quad (2.26)$$

Air-side heat transfer coefficient

$$h_w = \frac{k_w Nu_w}{d_i} \quad (2.27)$$

Water-side heat transfer coefficient (Gnielinski, 1975)

$$Nu_w = \frac{\left(\frac{f_D}{8}\right) (Re_w - 1000) Pr_w \left[1 + \left(\frac{d_i}{L_{tot}}\right)^{0.67}\right]}{1 + 12.7 \left(\frac{f_D}{8}\right)^{0.5} (Pr_w^{0.67} - 1)} \quad (2.28)$$

Friction factor (Filonenko, 1954)

$$f_D = (1.82 \log(Re_w) - 1.64)^{-2} \quad (2.29)$$

Water-side Reynolds number

$$Re_w = \frac{\rho_w v_w d_i}{\mu_w} \quad (2.30)$$

Total water-side heat transfer area

$$A_w = \pi n_b n_{bay} n_{tr} n_r d_i L_t \quad (2.31)$$

### 2.3.2. Draft equation

As the air moves through the heat exchanger and passes obstacles upstream or downstream of the heat exchanger, it experiences mechanical energy losses. These losses manifest themselves as a pressure drop that is defined by a dimensionless loss coefficient.

$$K = \Delta p / 0.5 \rho v^2 \quad (2.32)$$

where  $\Delta p$  is the pressure drop in question,  $\rho$  is the density and  $v$  is the velocity.

If the ambient air far from the heat exchanger is dry and the temperature distribution is according to the dry adiabatic lapse rate (DALR), the difference in pressure between (1) and (7) in Figure 2.1 follows from equation (2.33).

$$p_{a1} \left[ \left( 1 - DALR \frac{H_7 - H_6}{T_{a6}} \right)^{3.5} - \left( 1 - DALR \frac{H_7 - H_6}{T_{a1}} \right)^{3.5} \right] = p_{a1} - p_{a7} \quad (2.33)$$

Height 7 ( $H_7$ ) is shown in Figure 2.1

$$H_7 = H_w + H_6 \quad (2.34)$$

Height at outlet of heat exchanger ( $H_6$ )

$$H_6 = H_3 + H_{pl} \quad (2.35)$$

Fan height above ground level ( $H_3$ )



$$H_3 = \max \left( d_F, \frac{6.35 d_F X_1}{1 + \frac{45}{n_{Fbay}}} \right) \quad (2.36)$$

Where  $X_1$  is calculated from equation (8.3.2) and Figure 8.3.2 (Kröger, 2004) maintaining a ratio of actual air volume flow rate to ideal air volume flow rate ( $V/V_{id}$ ) of 0.96.

$$X_1 = -\ln(0.985 - 0.96) \quad (2.37)$$

Plenum height ( $H_{pl}$ )

$$H_{pl} = \begin{cases} 0.6 \text{ if } d_F < 1.828 \\ 1 \text{ otherwise} \end{cases} \quad (2.38)$$

Equation (2.38) must also take into account the requirement of paragraph 7.2.3.4 of API 661 (2006) which states that the air dispersion angle shall not exceed  $45^\circ$  as shown in Figure 2.3. Therefore the result of equation (2.38) is always checked to be greater or equal to the result of equation (2.39).

$$H_{pl} \leq \left[ \frac{\frac{L_t}{n_F} - d_F}{2} \right] \tan 45^\circ \quad (2.39)$$

Equation (2.40) represents the flow losses experienced by the air as it flows through the system. Equations (2.33) and (2.40), when set equal to each other, form the draft equation.

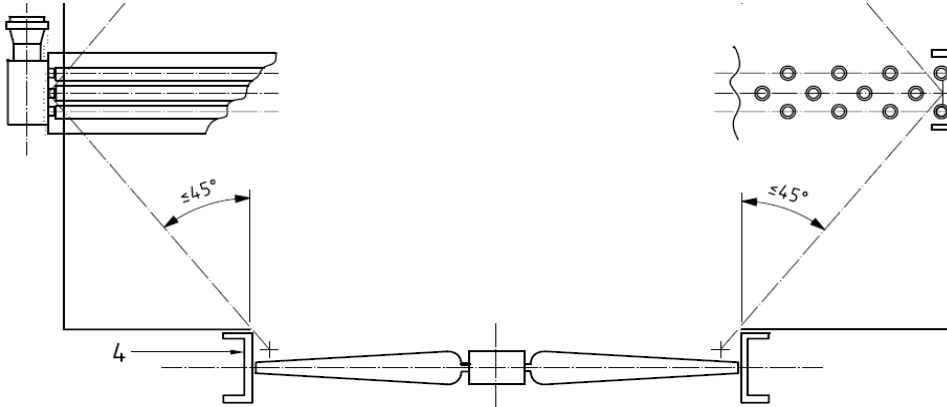


**Figure 2.3: Fan dispersion angle (API 661, 2006)**

$$\begin{aligned}
 p_{a1} - p_{a7} = & K_{ts} \frac{\left(\frac{m_a}{A_2}\right)^2}{2\rho_{a3}} + K_{Fsi} \frac{\left(\frac{m_a}{A_{fc}}\right)^2}{2\rho_{a3}} + K_{up} \frac{\left(\frac{m_a}{A_e}\right)^2}{2\rho_{a3}} + K_{do} \frac{\left(\frac{m_a}{A_e}\right)^2}{2\rho_{a3}} \\
 & - (K_{Fs} + K_{rec}) \frac{\left(\frac{m_a}{A_{fc}}\right)^2}{2\rho_{a3}} + K_{he} \frac{\left(\frac{m_a}{A_{frt}}\right)^2}{2\rho_{a56}} + \alpha_{e6} \frac{\left(\frac{m_a}{A_{frt}}\right)^2}{2\rho_{a6}}
 \end{aligned} \quad (2.40)$$

Support loss coefficient ( $K_{ts}$ )

$$K_{ts} = \frac{H_3 n_{ts} d_{ts} C_{Dts}}{A_2} \quad (2.41)$$

where the drag coefficient ( $C_{Dts}$ ) at the supports is obtained from Figure 2.5.1 (Kröger, 2004) once the air-side Reynolds number is known.

Fan static rise coefficient

$$K_{Fsi} = \frac{2\Delta p_{Fs} \rho_{a3}}{\left(\frac{m_a}{A_{fc}}\right)^2} \quad (2.42)$$

Heat exchanger loss coefficient

$$K_{he} = \frac{2EuG_c^2}{\left(\frac{m_a}{A_{frt}}\right)^2} \quad (2.43)$$

Euler number (Ganguli et al., 1985)

$$Eu = 2n_r \left[ 1 + 2 \exp \left\{ \frac{\left( \frac{-(P_t - d_f)}{4d_r} \right)}{1 + \frac{(P_t - d_f)}{d_r}} \right\} \right] \left[ 0.021 + 13.6 \frac{(d_f - d_r)}{Re(P_f - t_f)} + 0.25246 \left\{ \frac{(d_f - d_r)}{Re(P_f - t_f)} \right\}^{0.2} \right] \quad (2.44)$$

Heat exchanger effectiveness due to maldistribution of the air-side flow

$$e_{nu} = 1.05 - 0.05\alpha_{e6} \quad (2.45)$$

Corresponding heat exchanger outlet kinetic energy correction factor

$$\alpha_{e6} = 1.6 - 0.48 \frac{A_{fc}}{A_{ftr}} - 0.012K_{he} \quad (2.46)$$

Plenum recovery factor

$$K_{rec} = 0.3 \text{ since } 15 \leq K_{he} \leq 24 \quad (2.47)$$

The conical shroud inlet loss coefficient ( $K_{Fi}$ ) is obtained from Figure 6.4.7, the upstream loss coefficient ( $K_{up}$ ) from Figure 6.4.1 and the downstream loss coefficient ( $K_{do}$ ) from Figure 6.4.2 (Kröger, 2004).

### 2.3.3. Fan characteristics

Fan manufacturers specify the performance of their fans by means of performance curves. These curves usually give fan static pressure and fan power consumption as a function of volumetric flow rate through the fan. The curves are obtained from performance tests, either on the prototype fan or a scale model (Oosthuizen, 1995).

The thermal model uses a built-in fan curve to obtain the required air mass flow rate at the required pressure drop, which satisfies the draft equation. A 4.265 m diameter model fan was used, as in Kröger (2004:147), with all performance characteristics specified at a reference density of  $1.2 \text{ kg/m}^3$  and rotational speed of 216 rpm.

Reference fan static pressure curve

$$p_r = 140.2243 + 0.8776V_r - 0.014V_r^2 + 1.5075e^{-5}V_r^3 \quad (2.48)$$

Reference fan shaft power curve

$$P_{Fr} = 31.6268 - 0.9904V_r + 0.019V_r^2 - 1.427e^{-4}V_r^3 + 3.7075e^{-7}V_r^4 \quad (2.49)$$

Paragraph 7.2.3.3 of API 661 (2006) states that fans shall be sized such that the area occupied by the fan is at least 40 % of the total bundle face area served by that fan. Therefore as the bundle size changes in the design process, so does the diameter of the fan. The air mass flow rate is varied during the design calculations, which means that the rotational speed of the fan must also be varied. Since the model uses a specified fan curve; fan laws are employed to project the performance of fans that are smaller or larger than the reference fan. The following fan laws are used to convert the model fan data to data that is applicable for the prototype fan, operating at its own specified conditions.

Fan law for volume flow rate

$$V/V_m = N/N_m (d_F/d_{Fm})^3 \quad (2.50)$$

Fan law for fan static pressure

$$p/p_m = \rho/\rho_m (N/N_m)^2 (d_F/d_{Fm})^2 \quad (2.51)$$

Fan law for fan shaft power

$$P_F/P_{Fm} = \rho/\rho_m (N/N_m)^3 (d_F/d_{Fm})^5 \quad (2.52)$$

#### 2.3.4. Water side pressure drop

The header and finned tube configuration of a four-row four-pass heat exchanger bundle is shown in Figure 2.4. The water enters the bundle at the inlet nozzle (1) and exits at the outlet nozzle (6).

$$\Delta p_{12} = \Delta p_{vel} + \Delta p_{int} \quad (2.53)$$

The pressure drop of the flow exiting a system consists of a velocity loss term and an internal loss term as shown in equation (2.53) as explained by Fried & Idelchik (1989:343). If the internal loss term is ignored and it is assumed that the entire velocity term is lost when the fluid enters the inlet header (since it is negligibly small inside the header compared to inside the nozzle), the pressure drop can be expressed as in equation (2.54).

$$\Delta p_{12} = K_{12} \rho v_1^2 / 2 \quad (2.54)$$

The inlet nozzle loss coefficient  $K_{12}$  is equal to 1.06 for turbulent flow inside tubes with a velocity profile according to the one-seventh power law (Fried & Idelchik, 1989:77).

The pressure drop across the tube entrance is separated into two parts according to Kays and London (1984:109). Firstly the pressure drop which would occur due to flow-area change alone, without friction. The Second is the pressure loss due to the irreversible free expansion and momentum changes which follow the abrupt contraction contained in  $K_c$ .

$$\Delta p_{23} = \rho v_w^2 / 2 [(1 - \sigma_{23}^2) + K_c] \quad (2.55)$$

where  $v_w$  is the velocity in the tubes and  $\sigma_{23}$  is the core free-flow to frontal-area ratio. The loss coefficient  $K_c$  refers to the kinetic energy of the flow in the smaller cross sectional area and contains the irreversible component of the pressure drop (Kays & London, 1994:109).

$$K_c = 1 - 2/\sigma_c + 1/\sigma_c^2 \quad (2.56)$$

The area ratio  $\sigma_{23}$  is assumed to be zero and the jet contraction ratio is approximated by the following empirical relation for round tubes (Kröger, 2004:81).

$$\sigma_c = 0.61375 + 0.13318\sigma_{23} - 0.26095\sigma_{23}^2 + 0.51146\sigma_{23}^3 \quad (2.57)$$

The frictional pressure drop between any two sections of circular pipe is generally related to the pipe geometry and fluid properties (Kröger, 2004:61). Equation (2.58) represents the frictional pressure drop for all tube passes.

$$\Delta p_{f34} = f_D(n_p L_t / d_i) \rho v_w^2 / 2 \quad (2.58)$$

For uniform velocity distributions, the total outlet pressure drop due to reduction in the flow area resulting in an acceleration of the flow and a loss due to separation of the boundary layer can be expressed by equation (2.59) as mentioned by Kröger, (2004:79). This is identical to the two parts of the tube entrance pressure drop as explained by Kays & London (1984:109) except that in this case the second part is the irreversible free expansion and momentum changes, inherent in  $K_e$ , which follow an abrupt expansion and subtracts from the first part.  $K_e$  and  $\sigma_{56}$  are calculated in the same manner as equation (2.56) and equation (2.57) respectively.

$$\Delta p_{45} = \rho v_5^2 / 2 [(1 - \sigma_{45}^2) - K_e] \quad (2.59)$$

The same approach used for the inlet nozzle pressure drop into the inlet header is followed for the pressure drop across the tube exit into the header. The exit loss coefficient  $K_{56}$  is equal to 1.06 as with the inlet nozzle.

$$\Delta p_{56} = K_{56} \rho v_w^2 / 2 \quad (2.60)$$

The pressure drop across the bundle is simply the sum of the individual components.

$$\Delta p_{16} = \Delta p_{12} + n_p \Delta p_{23} + \Delta p_{f34} + n_p \Delta p_{45} + \Delta p_{56} \quad (2.61)$$

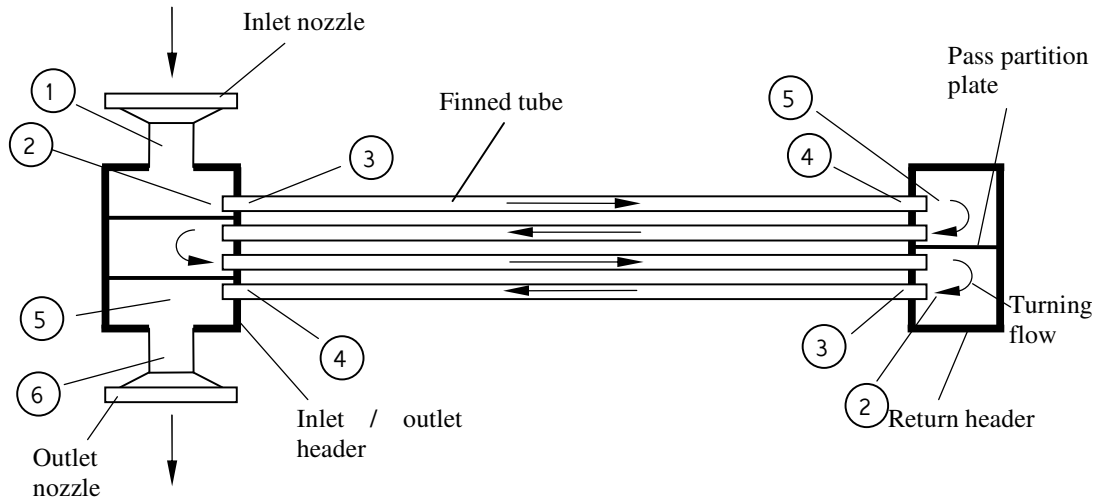


**Figure 2.4: Heat exchanger bundle**

## 2.4. Thermal model

### 2.4.1. Thermal model algorithm explained

The aim of the thermal model design case is to select the correct bundle dimensions such that an energy balance is obtained. This means that the heat transferred, equations (2.8), (2.9) and (2.10) or (2.12), must be equal. Appendix B shows the required input parameters for the thermal design model.

Figure 2.5 shows a flow chart of the thermal model algorithm. With the water mass flow rate given and an assumption made for the water velocity inside the tubes, the required tube area per pass can be calculated from equation 2.4. The total number of tubes per pass per bundle can then be calculated using equation 2.62. Process fluid velocities are kept between 1.2 m/s and 2.5 m/s as low fluid velocities permit fouling and high fluid velocities cause erosion.

$$n_{tp} = \frac{A_{req}}{n_b n_{bay} A_t} \quad (2.62)$$

With this known, the number of tubes per row can be determined and thus the bundle width can be calculated from equation 2.3. The bundle width must be limited to take into account some practical aspects such as transportation. Abnormal loads have a maximum object width of 3.6 m. When considering overseas deliveries, container size must also be taken into account. If the bundle width becomes too large in the calculation, another bundle is added in parallel which thus reduces the width of the individual bundles. The system can also have more than one bay in parallel, each containing one or more tube bundles. A bay is defined as one or more bundles, serviced by two or more fans, including the structure and plenum chamber.

An assumption must also be made for the air velocity through the bundle; the typical range is between 2.5 m/s and 4 m/s. This allows for the calculation of the air mass flow rate through the bundle. The air outlet temperature is then calculated such that the heat transferred is equal between the air-side and water side. Equation 2.17 through to equation 2.31 is then computed to obtain the overall heat transfer coefficient. The heat transferred by the heat exchanger ( $Q_{HX}$ ), by either method (e-NTU or LMTD), is calculated and compared to that of the water side heat transfer. If the bundle is not able to reject the required amount of heat, the bundle width must be increased.

Once the energy equation is satisfied, the model then calculates the LHS and RHS of the draft equation from equation (2.33) and equation (2.40) respectively. These results are then compared and if not satisfied, the air-side velocity and thus air mass flow rate must be recalculated to restart the iterative procedure.

Figure 2.6 shows the trend that the thermal model creates while performing a typical calculation. Since the tube side parameters are known, equation (2.18) can be used to compute the heat transferred on the water side ( $Q_w$ ). Each  $Q_{HX}$  curve is generated by varying the number of bundles (and thus bundle width) while keeping the fan speed (rpm) constant. Changing the speed of the fan shifts the curve vertically and thus results in a converged solution. Figure 2.6 illustrates that the quicker the fan rotational speed is increased the more rapidly a solution will be reached.

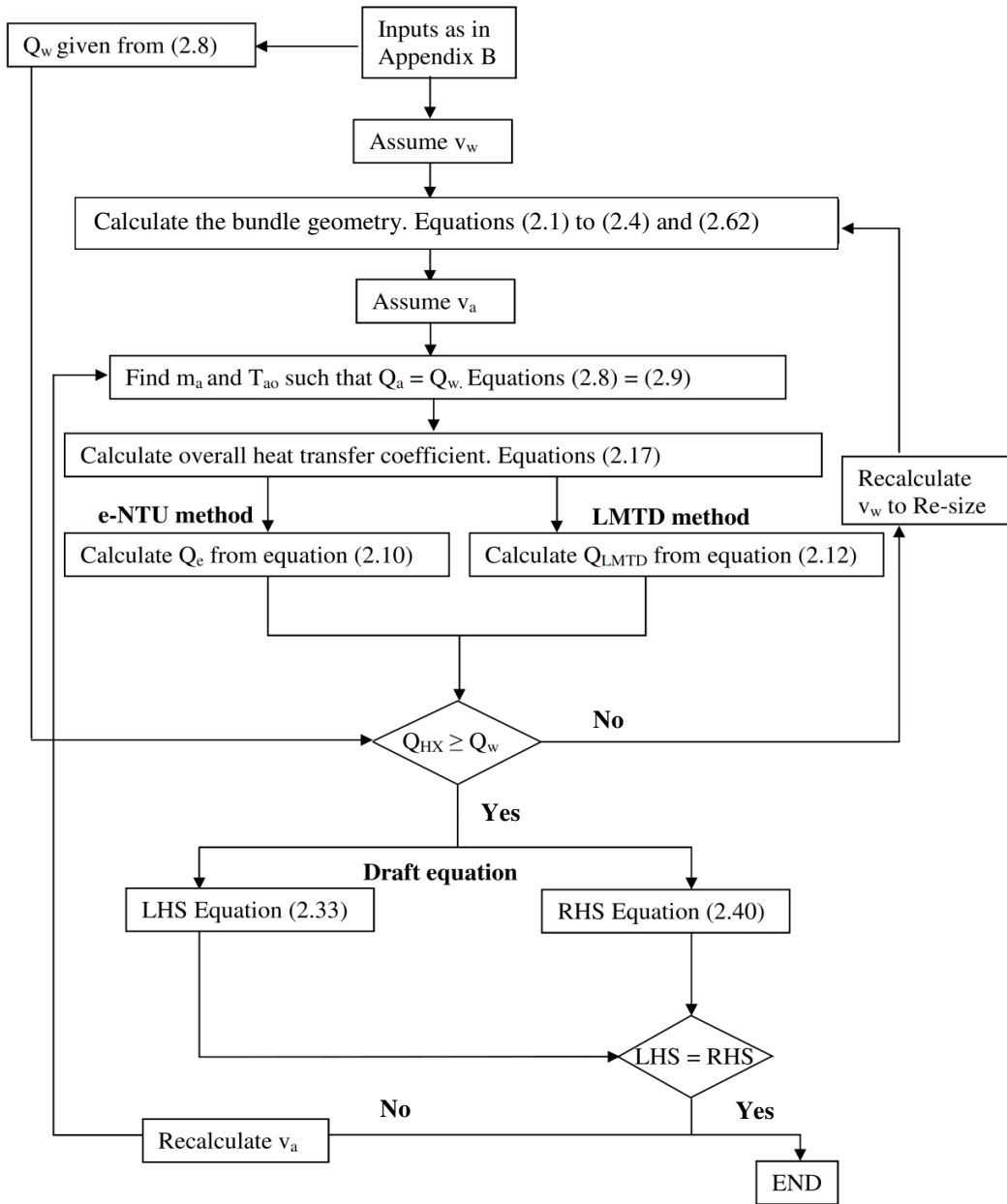
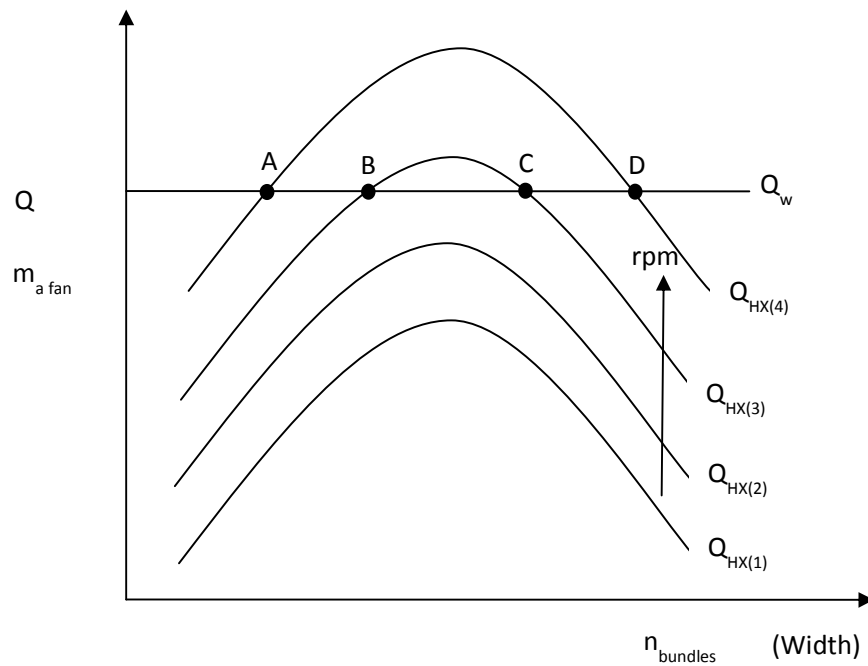


Figure 2.5: Flow diagram of thermal model algorithm



Points A, B, C and D in Figure 2.6 are all valid solutions to the thermal design of a heat exchanger, but C and D require a larger surface area which increases cost. Point A requires the same air mass flow rate as point B, but has a smaller surface area and thus a higher fan rotational speed. Therefore a limit must be placed on the fan rotational speed. Kröger (2004:14) recommends fan blade tip speeds of 60 m/s or less for relatively low noise levels. With this fan blade tip speed limitation in place, the thermal model converges to the one best solution by initially boosting the fan rotational speed to approximately its maximum and thereafter searching for the correct bundle width around that rotational speed.



**Figure 2.6: Thermal model algorithm**

The e-NTU and LMTD methods were programmed in adjacent columns in MS Excel, thus always comparing their results. The results of the thermal model were also compared to that of HTRI software to check the validity and accuracy of the model.

#### 2.4.2. Thermal rating mode

Before the design tools could be compared, the thermal model had to be verified that it was in fact producing valid results. For this validation, a heat exchanger was designed using the thermal model. The result, which is essentially the bundle

dimensions, was then entered into HTRI in its rating mode to check the performance of the bundle. Table 2.2 shows the results of this validation process. It illustrates that the e-NTU and LMTD methods are in good agreement. The last column (% diff) is the percentage difference between the results of the two methods and that of HTRI. Comparison with the HTRI results shows that most of the parameters are practically the same with the highest deviation being 12.96 % for the airside pressure drop. A suggestion for this difference is correlations used in the models to obtain the pressure drop. It is possible that HTRI uses a different correlation to that of the thermal model. The accuracy of these pressure drop correlations will be further explored in chapter 4. Table 2.2 therefore concludes that the thermal model performs an accurate calculation and thus is a suitable air cooled heat exchanger design tool.

**Table 2.2: Thermal rating mode**

	Units	e-NTU	LMTD	HTRI	% e-NTU diff	% LMTD diff
Duty	MW	14.47	14.47	14.465	0.01	0.01
Air mass flow rate	kg/s	491.10	491.11	496.839	1.15	1.15
Air outlet temperature	K	49.21	49.21	48.91	0.61	0.61
EMTD	K	27.82	27.49	27.6	0.79	0.41
Air-side pressure drop	Pa	93.72	93.70	107.67	12.96	12.97
Tube-side pressure drop	Pa	51.52	51.51	50.183	2.66	2.65
Bundle width	m	3.33	3.33	3.346	0.56	0.56
Bare tube area	m <sup>2</sup>	597.52	597.52	587.810	1.65	1.65
Face velocity	m/s	3.45	3.45	3.42	0.88	0.88
Driver power	kW	28.16	28.16	30.20	6.74	6.75

### 2.4.3. Thermal model design mode

Table 2.3 shows the comparison of the results of the thermal model and HTRI in design mode. Once more it can be seen that good correlation is achieved between the e-NTU and LMTD methods. The main aim of the design mode is to calculate the dimensions of the bundle given the performance; therefore the key parameter in this case is the width of the bundle.

HTRI provides a bundle that is 16.02 % wider than that of the thermal model. The other differences are mainly as a result of this area difference. The reason for this difference could be that the philosophies of the respective algorithms are different. A possible graphical explanation of these two designs could be that the thermal model provides design A and HTRI provides design B, as illustrated in Figure 2.6. The thermal model provides a smaller surface area which then translates to being a more cost effective design.

**Table 2.3: Thermal design mode**

	Units	e-NTU	LMTD	HTRI	% e-NTU diff	% LMTD diff
Duty	MW	14.47	14.47	14.465	0.01	0.01
Air mass flow rate	kg/s	498.15	498.22	478.816	4.04	4.05
Air outlet temperature	K	48.83	48.79	50.04	2.41	2.50
EMTD	K	27.97	27.68	27.1	3.21	2.16
Airside pressure drop	Pa	95.93	95.93	76.78	24.95	24.95
Tube-side pressure drop	Pa	51.24	51.23	37.830	35.45	35.43
Bundle width	m	3.33	3.33	3.962	16.02	16.02
Bare tube area	m <sup>2</sup>	597.52	597.52	695.199	14.05	14.05
Face velocity	m/s	3.67	3.67	2.79	31.62	31.62
Driver power	kW	24.78	24.78	20.21	22.64	22.64
Overdesign based on Q	%	2.29	3.99	---	---	---
Overdesign based on U	%	---	---	5.26	---	---

The basis for expressing overdesign margins is not always clear and could differ across software packages. Table 2.3 shows that HTRI basis the percentage overdesign margin on the percentage difference between the required and actual overall heat transfer coefficient (U), whereas the thermal model has based it on the percentage difference between the required and actual duty (Q).

Overdesign margins are added to heat exchangers to account for variable process and ambient conditions, fouling and uncertainties in fluid properties (Bennett et al. 2007). Referring to Figure 2.6, an oversized heat exchanger lies in the region above the  $Q_w$  line. This means that the heat exchanger is able to reject more heat than is actually required. There are several drawbacks of the excessive use of this design margin. The economic downside being that the increased heat transfer area translates directly to unnecessary capital and transportation cost. Table 2.3 shows that the larger bundle of the HTRI design has a larger overdesign value than the thermal model.

### **3. Mechanical design of an air-cooled heat exchanger header box according to ASME VIII Div 1 (2007) Addenda 2009b**

#### **3.1. Introduction**

The purpose of this section is to illustrate how to design a rectangular cross section pressure vessel by applying the formulas from ASME VIII div 1 (2007) for the design of a plug type header box. It also outlines the limitations on the design imposed by the API 661 (2006) standard.

It summarises the design procedure by showing the steps to be completed in the design process and thereafter each step is described separately in more detail. The air-cooled heat exchanger configurations are firstly discussed followed by the presentation of the various equations extracted from ASME VIII div 1 (2007) within the relevant sections.

This code summary will be used to program the mechanical design procedure in Microsoft Excel and a sample calculation will be produced using Mathcad as shown in Appendix C.

#### **3.2. Mechanical design procedure**

1. Design Inputs and Outputs
2. Determine the relevant configuration of the noncircular vessel from the thermal design by choosing one of the sketches from Figure 13-2(a) in ASME VIII div 1 (2007); depending on the requirement for and position of partition plates or stay plates.
3. Determine initial general dimensions for the geometry of the header (i.e. width, length, height) and thicknesses of the pressure containing plates.
4. Use (3) above to determine the dimensions in the corroded condition.
5. Complete the stress calculation for the selected header type and check that it meets the acceptance criteria. If not, return to (3) above and repeat until an acceptable design is achieved.
6. Perform a stress analysis on the design of the nozzles.
7. Determine if the tube-to-tubesheet weld sizes are satisfactory.

All calculations must be completed for both the inlet and return or outlet header.

### 3.2.1. Design Inputs and outputs

#### Pressure and Temperature

It should be checked that the design pressure and temperature complies with the specific purchaser/client requirements and that there is at least a margin between operating and design pressure and temperature. That is, the design pressure and temperature must be higher than the operating pressure and temperature.

#### Tube Geometry

The tube geometry results from the thermal design of the heat exchangers, which includes tube diameter, length, wall thickness and pitch; as well as the number of tubes, rows and passes.

The wall thickness for tubes with an outside diameter of 25.4 mm to 38.1 mm shall not be less than 2.11 mm for Carbon steel as stated in paragraph 7.1.11.3 of API 661 (2006).

#### Nozzles

The size of the required nozzles is also suggested by the thermal design. Table 3.3 shows the minimum nozzle neck nominal thicknesses based on the pipe size as in Table 3 of API 661 (2006). The nozzles are manufactured with a 12.5 % tolerance; therefore only 87.5 % of the wall thickness is used in the calculations to ensure that even a nozzle wall thickness that is at the lower tolerance limit will still be adequate.

**Table 3.1: Minimum nozzle neck nominal thickness as in Table 3 of API 661 (2006)**

Nominal Size [Inch]	OD [mm]	Nozzle neck thickness
1.50	48.30	5.58
2.00	60.30	6.35
3.00	88.90	7.14
4.00	114.30	8.74
6.00	168.30	11.13
8.00	219.10	13.49
10.00	273.00	10.97
12.00	323.80	12.70
14.00	355.60	15.09
16.00	406.40	17.48

Generally in the first round of calculations the piping has not been finalised and therefore the piping nozzle loads are not available. Table 3.4 shows recommended nozzle loads to be used in design calculations as extracted from API 661 (2006). The directions of the nozzle moments and forces, as indicated in Table 3.4, are illustrated in Figure 3.1.

**Table 3.2: Maximum allowable nozzle loads as in Table 4 of API 661 (2006)**

Nominal Size [Inch]	Moments [Nm]			Forces [N]		
	$M_x$	$M_y$	$M_z$	$F_x$	$F_y$	$F_z$
1.50	110	150	110	670	1020	670
2.00	150	240	150	1020	1330	1020
3.00	410	610	410	2000	1690	2000
4.00	810	1220	810	3340	2670	3340
6.00	2140	3050	1630	4000	5030	5030
8.00	3050	6100	2240	5690	13340	8010
10.00	4070	6100	2550	6670	13340	10010
12.00	5080	6100	3050	8360	13340	13340
14.00	6100	7120	3570	10010	16680	16680

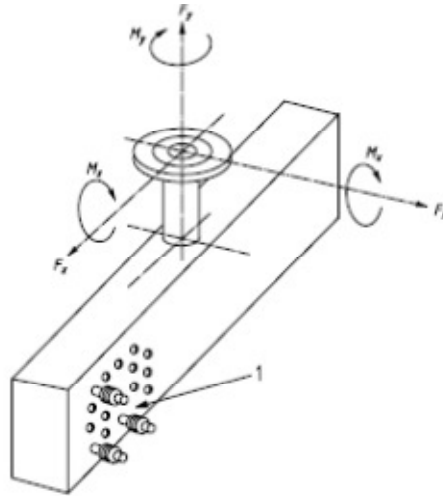


**Figure 3.1: Nozzle loads as in Figure 6 of API 661 (2006)**

### Materials

To limit the complexity of the project, Carbon steel was the only material considered for the heat exchanger design. The type of material is chosen in the mechanical

design for the different parts of the vessel and its respective properties must be extracted from ASME II Part D 2007 Customary. This code presents the material properties in metric units. The data must therefore be converted, interpolated if necessary, and thereafter reconverted to SI units to be used in the mechanical design process.

### Vessel thicknesses

The side plate, tubesheet, plugsheet, end plate and partition or stay plate thicknesses must be selected by the designer and used in the stress equations. If the results are satisfactory under the acceptance criteria, the design is acceptable. If not, the thicknesses must be re-chosen until it is satisfactory under the stress criteria of ASME VIII div 1 (2007), specified in Table 3.11. The thicknesses are therefore considered to be outputs of the mechanical design. Table 3.5 shows the minimum thicknesses of header components as given in API 661 (2006).

### Tube-to-tubesheet welds

As with the vessel thicknesses the tube-to-tubesheet weld lengths must initially be chosen and then used in the calculation to check if it is satisfactory. If it is not satisfactory, it must be re-chosen until it obeys the acceptance criteria of Section 3.2.8.

**Table 3.3: Minimum thickness of header components as in Table 1 of API 661 (2006)**

<b>Minimum nominal thickness (including a corrosion allowance of 3 mm) of header components</b>	
Tubesheet	19 mm
Side and end plates	12 mm
Partition or stay plates	12 mm

### **3.2.2. Vessel configuration**

The configurations are all rectangular cross sections with the opposite sides of the vessel having the same thickness. These sketches can be found in Figure 13-2(a) of ASME VIII div 1 (2007). Sketch 1 – A simple rectangular cross section with no partition or stay plates, shown in Figure 3.2. Sketch 7 – Shows a box with a single partition or stay plate, shown in Figure 3.3. Sketch 8 – Similar to Sketch 1 but having two opposite sides stayed by multiple stay or partition plates, shown in Figure 3.4. The inlet/outlet header in Figure 2.1 is an example of a Figure 3.3 header and the return header in Figure 2.1 is an example of a Figure 3.2 type header.

When a header box has two unequal compartments, analysis is based on Figure 3.3 with both compartments based on the larger size. Cases of three or more compartments is analysed with the techniques of Figure 3.4 with the design based on the largest compartment (Mahajan, 1990:291). This design consideration is also explained in 13-9 (f) of ASME VIII div 1 (2007). It states that the vessel must be analysed as if all the compartments had the same dimension, which is equal to the maximum compartment dimension. This rule is implemented in the mechanical design by calculating an effective tubesheet length for Figure 3.3 and Figure 3.4 as shown in equation (3.22). For a vessel with more than two compartments, use the geometry shown in Figure 3.4 with three compartments having the maximum dimensions of the actual vessel. This means that a five or six compartment vessel will be analysed as if it had only three compartments.

Evaluating the header box as explained above by 13-9 (f) of ASME VIII div 1 (2007) shows that the method is conservative. The same paragraph gives an option to use the provisions of U-2(g) using techniques of structural analysis for rigid frames, such as moment distribution and slope-deflection, but the stresses throughout shall not exceed the allowable values as established in Appendix 13 of ASME VIII div 1 (2007). U-2(g) states that the code does not cover all details of design and construction and where details are not given the manufacturer shall provide details which are as safe as those given by the ASME VIII div 1 (2007) code. Equations (3.22) and (3.23) reiterates the conservative nature of the calculation method, where it always makes use of the more conservative value between a partition and stay plate when both are included in the header design.

### **3.2.3. Overall dimensions**

The overall dimensions of the tube bundle that results from the thermal design of the heat exchanger, gives an indication of the width and depth of the header box. The thicknesses of the various plates must however still be chosen and verified in the stress analysis.

### **3.2.4. Corrosion allowance (Ca)**

Section UG-16(e) of ASME VIII div 1 (2007) states that all design equations in the code represent the dimensions in the corroded condition. Therefore all dimensions must be calculated in the corroded condition. According to paragraph 7.1.5 of API 661 (2006), the purchaser shall specify the corrosion allowance for all surfaces exposed to the process fluid, where the minimum is 3 mm for carbon steel.



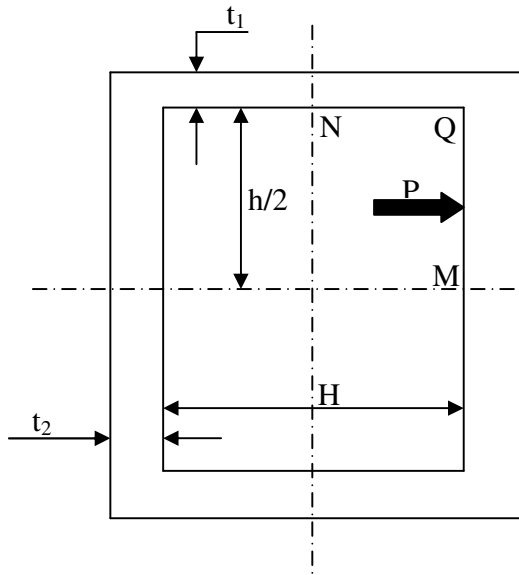


Figure 3.2: Sketch 1

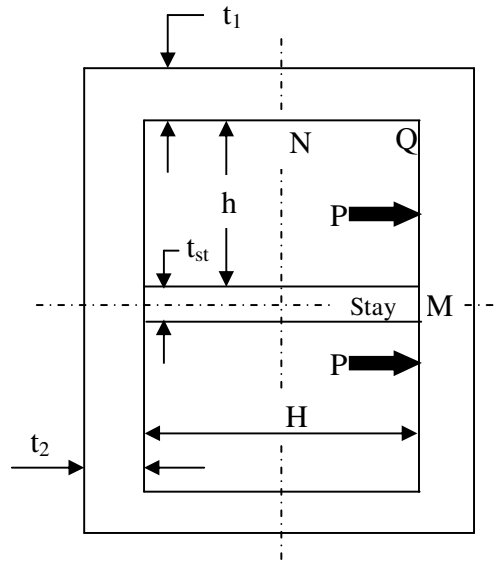


Figure 3.3: Sketch 7

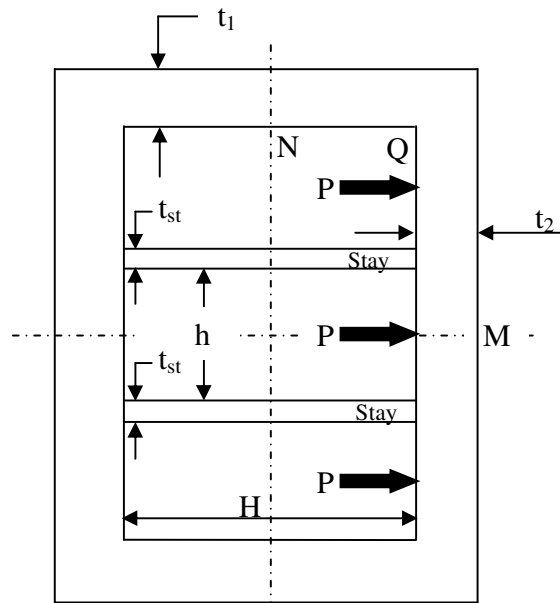
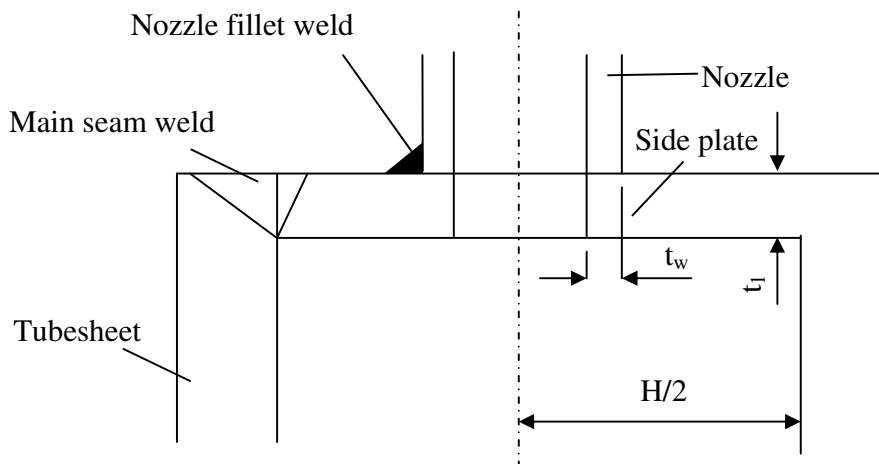


Figure 3.4: Sketch 8

### Side plate length (H)

In order to reduce material and welding costs, the overall dimensions of the vessel must be reduced where possible. The length of the plates used to construct the header box is therefore kept to a minimum. The width of the bundle and thus number of tubes per row determines the width of the header box. The tubesheet length (L) is determined by the number of tube rows used in the thermal design. The side plate length (H) is governed by the size of the nozzle attached to it with provision for welding such that welding does not overlap with the main seam weld as shown in Figure 3.5.



**Figure 3.5: Side plate length**

### Tubesheet length (L)

The tubesheet length is calculated based on the vertical pitch ( $p_l$ ) of the tubes, number of partition or stay plates ( $n_p$ ) and the spacing between the tubes and header plates, which is chosen to be 29 mm for one inch (1") tubes to provide sufficient space for welding.

$$L = n_T p_l + n_{pp}(2 \times 29 + t_{pp}) + n_{st}(2 \times 29 + t_{st}) + 2 \times 29 \quad (3.1)$$

where  $n_T$  is the sum of the number of tube rows in each compartment minus one ( $n_t - 1$ ). For example: For a Figure 3.2 type vessel, if there are 2 tube rows in the compartment,  $n_T$  would be equal to 1.

Equation (3.1) will always produce the correct length for Figure 3.2 type vessels but not Figure 3.3 and Figure 3.4. The front and rear headers must be considered simultaneously in the design process of these two types. It may be that two adjacent tube rows in the front header are opposite two tube rows separated by a partition/stay plate in the rear header. Thus if the tube rows in the front header is spaced by only using the vertical pitch, a resulting slope relative to the rear header will occur since the thickness of the partition plate has not been taken into account. This is illustrated with an example in Figure 3.6 where the vertical pitch is 67 mm and partition plate thickness is 12 mm, but the spacing between tube row 2 and tube row 3 should be 70 mm.

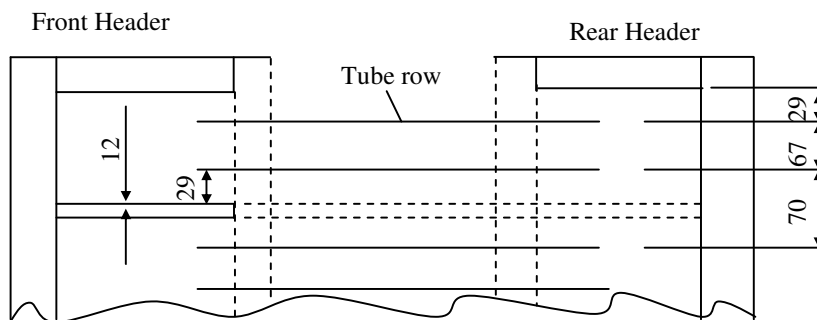


**Figure 3.6: Tubesheet length calculation**

### Stay plate design

Differentiation must be made between a partition plate and a stay plate in the design of header boxes. A partition plate is the plate that separates tube passes whereas a stay plate is used for reinforcement of the header box and does not separate tube passes.

A stay plate is designed in such a way that it is used as reinforcement for the header box which thus results in the use of slimmer side and tubesheet plates. The stay plate contains holes which allow the flow to pass through it and therefore does not separate tube passes. The use of stay plates may result in a more economical design since less material would be used, however the addition of stay plates results in more welding and thus additional welding cost.

Stay plates must be designed such that the minimum flow area through the stay plate holes is 100 % of the flow area through the tubes of that particular pass.

$$A_{holes} = A_{one\ pass} \quad (3.2)$$

$$A_{one\ pass} = \frac{\pi}{4} d_i^2 n_{tubes\ (one\ pass)} \quad (3.3)$$

The strength of a plate is weakened by the holes that it possesses. Therefore by applying a ligament efficiency to it, its new weakened strength in terms of its thickness is obtained. Figure 3.7 illustrates how to calculate the ligament efficiency of a stay plate.

$$\eta_1 = \frac{P - D_{hole}}{P} \quad (3.4)$$

$$\eta_2 = \frac{H - D_{hole}}{H} \quad (3.5)$$

$$\eta = \min(\eta_1, \eta_2) \quad (3.6)$$

$$t_{st\ (corr)} = \eta t_{st} - 2Ca \quad (3.7)$$

The new thickness found in equation (3.7) is then to be used in the stress analyses as described above.

#### Ligament efficiency of multidiameter holes in plates

For the case of a plate with uniform diameter holes, the ligament efficiency factors  $e_m$  and  $e_b$  for membrane and bending stresses, respectively, are considered to be the same. For multidiameter holes, the neutral axis of the ligament may no longer be at midthickness of the plate; thus for bending loads, the stress is higher at one of the plate surfaces than at the other surface (13-6 of ASME VIII div 1, 2007).

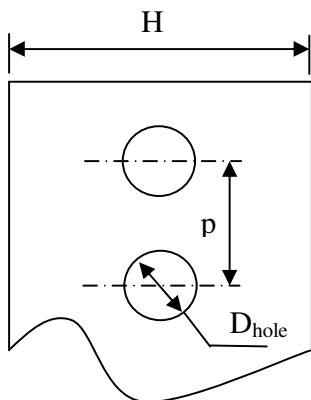


**Figure 3.7: Stay plate**

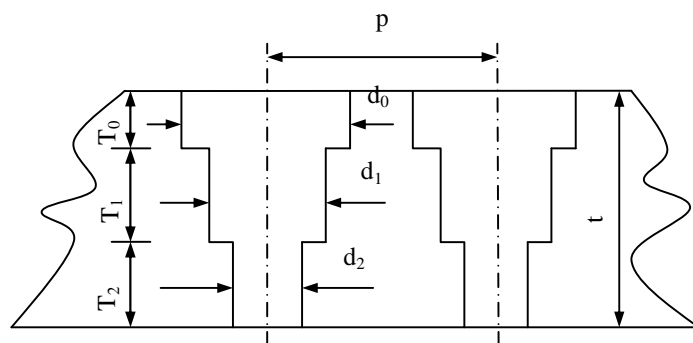


**Figure 3.8: Multidiameter holes**

Membrane stress

$$e_m = (p - D_E)/p \quad (3.8)$$

$$D_E = \frac{1}{t}(d_0T_0 + d_1T_1 + \dots + d_nT_n) \quad (3.9)$$

Bending stress

$$e_b = (p - D_E)/p \quad (3.10)$$

$$D_E = p - 6I/t^2c \quad (3.11)$$

$$I = \frac{1}{12} \sum_{k=0}^n b_k T_k^3 + \sum_{k=0}^{n-1} b_k T_k \left( \frac{T_k}{2} + \sum_{m=k+1}^n T_m - \bar{X} \right)^2 + b_n T_n \left( \bar{X} - \frac{T_n}{2} \right)^2 \quad (3.12)$$

$$b_k = p - d_k \quad (3.13)$$

$$\bar{X} = \left[ \sum_{k=0}^n b_k T_k \left( \frac{T_k}{2} + \sum_{m=k+1}^n T_m \right) \right] \left( \sum_{k=0}^n b_k T_k \right)^{-1} \quad (3.14)$$

$$c = \max(\bar{X}, (t - \bar{X})) \quad (3.15)$$

### 3.2.5. Corroded condition

As previously mentioned, the design equations of ASME VIII div 1 (2007) require that all parameters be used in their corroded condition, therefore the following initial calculations are necessary.

Side plate thickness (short plate):

$$t_{1corr} = t_1 - Ca \quad (3.16)$$

Tubesheet thickness (long plate):

$$t_{2corr} = t_2 - Ca \quad (3.17)$$

Partition plate thickness:

$$t_{pp/st(corr)} = t_{pp/st} - 2Ca \quad (3.18)$$

Side plate length:

$$H_{corr} = H + 2Ca \quad (3.19)$$

Tubesheet length:

$$L_{corr} = L + 2Ca \quad (3.20)$$

Effective tubesheet length:

$$L_{corr} = [n_c \max(h_c) + 2Ca] + (n_{pp} + n_{st})[\max(t_{st(corr)}, t_{pp(corr)})] \quad (3.21)$$

where  $h_c$  is the height of each compartment.

Distance to stay plate:

$$h = \frac{[L_{corr} - (n_{pp} + n_{st})\min(t_{pp(corr)}, t_{st(corr)})]}{n_c} \quad (3.22)$$

The first expression in equation (3.23) is the calculation of the ligament efficiency for a plate with uniform holes as is the case for tubesheets. The other two terms, from equations (3.8) and (3.10) respectively, are for multidiameter holes as is the case for plugsheets since it has a recess for the gasket and plug seating. Because of the difference in ligament efficiencies, the tubesheet and plugsheet could be designed to have different plate thicknesses. However, ASME VIII div 1 (2007) does not have a stayed figure, and thus corresponding stress equations, for different tubesheet and plugsheet plate thicknesses. The header box design is thus once more conservative in that it assumes the tubesheet plate thickness to be as thick as the plugsheet.

Ligament efficiency (13-4 and UG-53 of ASME VIII div 1 2007):

$$E_2 = \min \left[ \frac{(p_t - d_h)}{p_t}, e_m, e_b \right] \quad (3.23)$$

where  $d_h$  is the larger of the tube or plug hole diameter obtained from Table 11 of API 661 (2006).

### 3.2.6. Header design

The stress design equations are shown for all three types of configurations. Only use the equation for the applicable type when doing the actual calculation. All design

stress equations for Figure 3.2 are listed in section 13-7, and Figure 3.3 and Figure 3.4 are in section 13-9 of ASME VIII div 1 (2007).

The mechanical design is according to Appendix 13 of ASME VIII div 1 (2007), which is based on both membrane and bending stresses. Both are considered to be primary local stresses, produced by pressure.

The membrane stress is defined as the component of normal stress that is uniformly distributed and equal to the average value of stress across the thickness of the section under consideration as defined in 3-2 of ASME VIII div1 (2007). This average stress is shown in Figure 3.9.

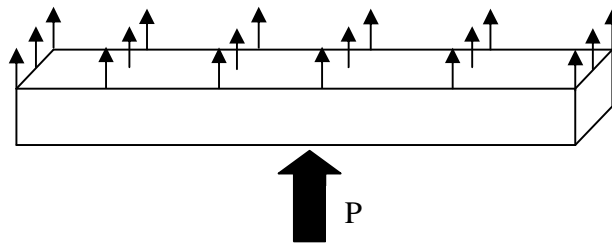


**Figure 3.9: Membrane stress**

There are two values of bending stress to be determined at each cross section. There is one stress value at the outermost surface of the plate and one stress value at the innermost surface of the plate. For this particular rectangular vessel under consideration the neutral axis is situated at the centre of the respective plate. The two stress values are therefore equal in magnitude. The bending stress can thus be defined as the stress originating in the central portion of a flat plate due to pressure, which varies from compression on the one side to tension on the opposite side. The bending stress is shown in Figure 3.10.

Moment of inertia with  $b = 1$  (unit width) as in 13-4(k) of ASME VIII div 1 (2007):

$$I_i = \frac{bt_i^3}{12} \quad (3.24)$$

where  $i = 1$  or  $2$ ; represents the side (short) or tubesheet (long) plate respectively.

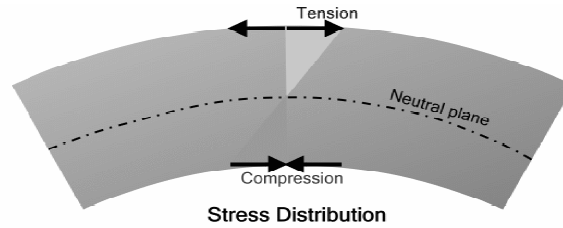


**Figure 3.10: Bending stress**

Section 13-5 of ASME VIII div 1 (2007) defines  $h$  as the inside length of the long side of Figure 3.2 (unstayed vessels), or the dimension perpendicular to  $H$  in Figure 3.3 and Figure 3.4 (stayed vessels) in which case  $h$  may be greater than, equal to, or less than  $H$ . Therefore if the side (short) plate length ( $H$ ) is longer than the tubesheet (long) plate length ( $L$ ) the header box should be rotated in the stress analysis so that the tubesheet (long) plate will be the actual long plate on the header box. The definition of  $h$ , previously mentioned, implies that this is only required for Figure 3.2 type vessels.

For example, if the side plate length ( $H$ ) is larger than the tubesheet plate length ( $L$ ),  $H > L$ , the new tubesheet plate length ( $L_{\text{new}}$ ) would become the side plate length ( $H$ ) and the new side plate length ( $H_{\text{new}}$ ) would become the tubesheet plate length ( $L$ ). Thus the header box has been rotated resulting in the tubesheet plate length being the actual long plate of the vessel.

Rectangular vessel parameter:

$$\alpha = \frac{H}{h} \quad (3.25)$$

Vessel parameter:

$$K = \frac{I_2}{I_1} \alpha \quad (3.26)$$

### Membrane stress

The general equation used to describe the membrane stress is:

$$S_m^j = \frac{Ph}{2at_i E_i} \left[ b - c \left( \frac{2d + K(e - \alpha^2)}{d + fK} \right) \right] \quad (3.27)$$



where  $j = s, l$  or  $st$ ; represents the side (short), tubesheet (long) or stay plate and the constants for different header designs are presented in Table 3.6.

**Table 3.4: Membrane stress, constants for equation (3.27)**

Plate	Symbol	i	h	Figure 3.2			Figure 3.3						Figure 3.4					
				a	b	c	a	b	c	d	e	f	a	b	c	d	E	f
Side plate	$S_m^s$	1	h	1	1	0	2	4	1	1	5	2	1	3	1	3	11	5
Tubesheet	$S_m^l$	2	H	1	1	0	1	1	0	0	0	0	1	1	0	0	0	0
Stay plate	$S_m^{st}$	3	h	N.A			1	0	-1	1	5	2	1	0	-1	3	11	5

### Bending stress

The general equation used to describe the bending stress is:

$$S_b^{jk} = \frac{Pac_j}{12I_iE_i} \left[ -bH^2 + c^2 \left( \frac{d + eK(f - \alpha^2)}{d + gK} \right) \right] \quad (3.28)$$

$$c_j = \frac{t_i}{2} \quad \text{represents distance from neutral axis} \quad (3.29)$$

where  $k = M, N$  and  $Q$  represent the location of the stress shown in Figures 3.2 to 3.4 and the constants for different header designs are presented in Tables 3.7 to 3.9. At location  $Q$ , the joint efficiency (E) is equal to 1.

**Table 3.5: Bending stress, constants for equation (3.28) and Figure 3.2**

Plate	Symbol	i	a	b	c	d	e	f	g
Side (short) plate at location Q:	$S_b^{sQ}$	1	1	0	h	1	-1	0	1
Side (short) plate at location N:	$S_b^{sN}$	1	1	1.5	h	1	-1	0	1
Tubesheet (long) plate at location M:	$S_b^{lM}$	2	$h^2$	$\frac{1.5}{H^2}$	1	1	-1	0	1
Tubesheet (long) plate at location Q:	$S_b^{lQ}$	2	1	0	h	1	-1	0	1

**Table 3.6: Bending stress, constants for equation (3.28) and Figure 3.3**

Plate	Symbol	i	a	b	c	d	e	f	g
Side (short) plate at location Q:	$S_b^{sQ}$	1	1	0	h	1	-2	0	2
Side (short) plate at location N:	$S_b^{sN}$	1	$\frac{1}{2}$	3	$\sqrt{2}h$	1	-2	0	2
Tubesheet (long) plate at location M:	$S_b^{lM}$	2	1	0	h	1	1	3	2
Tubesheet (long) plate at location Q:	$S_b^{lQ}$	2	1	0	h	1	-2	0	2

**Table 3.7: Bending stress, constants for equation (3.28) and Figure 3.4**

Plate	Symbol	i	a	b	c	d	e	f	g
Side (short) plate at location Q:	$S_b^{sQ}$	1	1	0	h	3	-5	0	5
Side (short) plate at location N:	$S_b^{sN}$	1	$\frac{1}{2}$	-3	$\sqrt{2}h$	3	-5	0	5
Tubesheet (long) plate at location M:	$S_b^{lM}$	2	1	0	h	3	1	6	5
Tubesheet (long) plate at location Q:	$S_b^{lQ}$	2	1	0	h	3	-5	0	5

#### Total Stress

The total stress in various members and locations in the header are calculated using the equations given in Table 3.10

**Table 3.8: Total stress**

Plate	Location	Formula	Equation number
Side (short) plate:	Q	$S_{TQ}^s = S_b^{sQ} + S_m^s$	(3.30)
	N	$S_{TN}^s = S_b^{sN} + S_m^s$	(3.31)
Tubesheet (long) plate:	M	$S_{TM}^l = S_b^{lM} + S_m^l$	(3.32)

	Q	$S_{TQ}^l = S_b^{lQ} + S_m^l$	(3.33)
Stay plate:		$S_T^{st} = S_m^{st}$	(3.34)

### Allowable Stress:

The allowable stress, defined for any combination of membrane plus bending stresses, is shown in equation (3.35) as in 13-4(b) (1) of ASME VIII div 1 (2007).

$$S_a = 1.5S_d \quad (3.35)$$

### Acceptance criteria:

The total stress in the various members and locations (defined in Table 3.10) must not exceed the allowable stress defined in equation (3.35). In addition, the membrane stress in all members (defined in Table 3.6) must not exceed the design stress ( $S_d$ ). The acceptance criteria is summarised in Table 3.11.

**Table 3.9: Acceptance criteria**

Side (short) plate:	$S_{TQ}^s \leq S_a$	(3.36)
	$S_{TN}^s \leq S_a$	(3.37)
Tubesheet (long) plate:	$S_{TM}^l \leq S_a$	(3.38)
	$S_{TQ}^l \leq S_a$	(3.39)
Membrane stresses	$S_m^j \leq S_d$	(3.40)

### End Plate Design

Minimum required thickness according to UG-34(c) with  $C = 0.2$  as in 13-4 (f) of ASME VIII div 1 (2007).

$$t = d \sqrt{\frac{ZCP}{S_{ap}E}} + Ca \quad (3.41)$$

where the non-circular head factor ( $Z$ ) is:

$$Z = 3.4 - \frac{2.4d}{D} \quad \text{Or not greater than 2.5} \quad (3.42)$$

where  $d$  is the short span of the end plate and  $D$  is the long span. End plates are added to the header box for each compartment. The short span ( $d$ ) can therefore be either

parallel or perpendicular to the side plate length (H) depending on the height of the compartment.

### 3.2.7. Nozzle design

The nozzles are attached to the header in one of two manners according to Figure UG-41.1 of ASME VIII Div 1 (2007), shown in Figure 3.11. However, only the set-on construction is used due to the sequence of fabrication. The minimum nominal thickness of the nozzle neck, of carbon steel flanged connections shall not be less than specified in Table 3.3. Table 3.4 shows the maximum allowable nozzle loads according to API 661 (2006). Each nozzle in its corroded condition must be able to withstand the simultaneous application of all the moments and forces as stated in paragraph 7.1.10 of API 661 (2006). It is therefore necessary to calculate an equivalent stress and compare it to the allowable stress of the nozzle material.

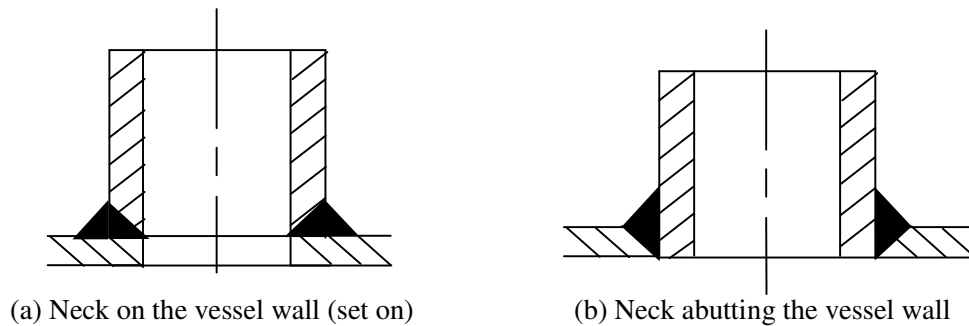


**Figure 3.11: Attachment of nozzle to header**

Thickness of nozzle:

$$t_n = t - Ca \quad (3.43)$$

Inside diameter of nozzle:

$$d_i = d_o - 2t_n \quad (3.44)$$

Minimum required wall thickness under internal pressure (UG-27 of ASME VIII div 1 2007):

$$t_{rn} = \frac{Pd_i}{2(SE_j - 0.6P)} \quad (3.45)$$

Circumferential stress due to pressure:

$$S_h = \frac{Pd_i}{2t_n} \quad (3.46)$$

Nozzle cross-sectional area:

$$A_{cross} = \frac{\pi}{4}(d_o^2 - d_i^2) \quad (3.47)$$

Tensile stress due to  $F_y$ :

$$S_t = \frac{F_y}{A_{cross}} \quad (3.48)$$

Section modulus  $Z$

$$Z = \frac{2I}{d_o} \quad (3.49)$$

Nozzle second moment of inertia:

$$I = \frac{\pi}{64}(d_o^4 - d_i^4) \quad (3.50)$$

Resultant bending moment:

$$M_r = \sqrt{M_x^2 + M_z^2} \quad (3.51)$$

Bending stress due to  $M_x$  and  $M_z$ :

$$S_b = \frac{M_r}{Z} \quad (3.52)$$

Resultant stress:

$$S_r = S_h + S_t + S_b \quad (3.53)$$

Shear stress:

$$\tau_x = \frac{2F_x}{\pi d_o t_n} \quad (3.54)$$

$$\tau_z = \frac{2F_z}{\pi d_o t_n} \quad (3.55)$$

$$\tau_y = \frac{2M_y}{\pi d_o^2 t_n} \quad (3.56)$$

Resultant shear stress:

$$\tau_r = \tau_x + \tau_y + \tau_z \quad (3.57)$$

Equivalent stress:

$$S_e = \sqrt{S_r^2 + 4\tau_r^2} \quad (3.58)$$

Acceptance criteria:

$$S_e \leq S_d \quad (3.59)$$

### 3.2.8. Tube-to-tubesheet welds

The rules provided in this section determine the weld sizes and allowable joint loads for full strength tube-to-tubesheet welds. A full strength tube-to-tubesheet weld is one in which the design strength is equal to or greater than the axial tube strength ( $F_t$ ) as explained in UW-20.2(a) of ASME VIII div 1 (2007).

When the weld meets the requirements of UW-20.4 of ASME VIII div 1 (2007), it is a full strength weld and the joint does not require qualification by shear load testing. This weld also provides tube joint leak tightness. The maximum allowable axial load ( $L_{max}$ ) in either direction on a tube-to-tubesheet joint is determined by the rules of UW-20.4(b) and the weld sizes are determined by UW-20.6 of ASME VIII div 1 (2007). There are four types of acceptable tube-to-tubesheet welds which are shown in Figure 3.12. The variables required for this section are defined in Figure 3.12.

Axial tube strength:

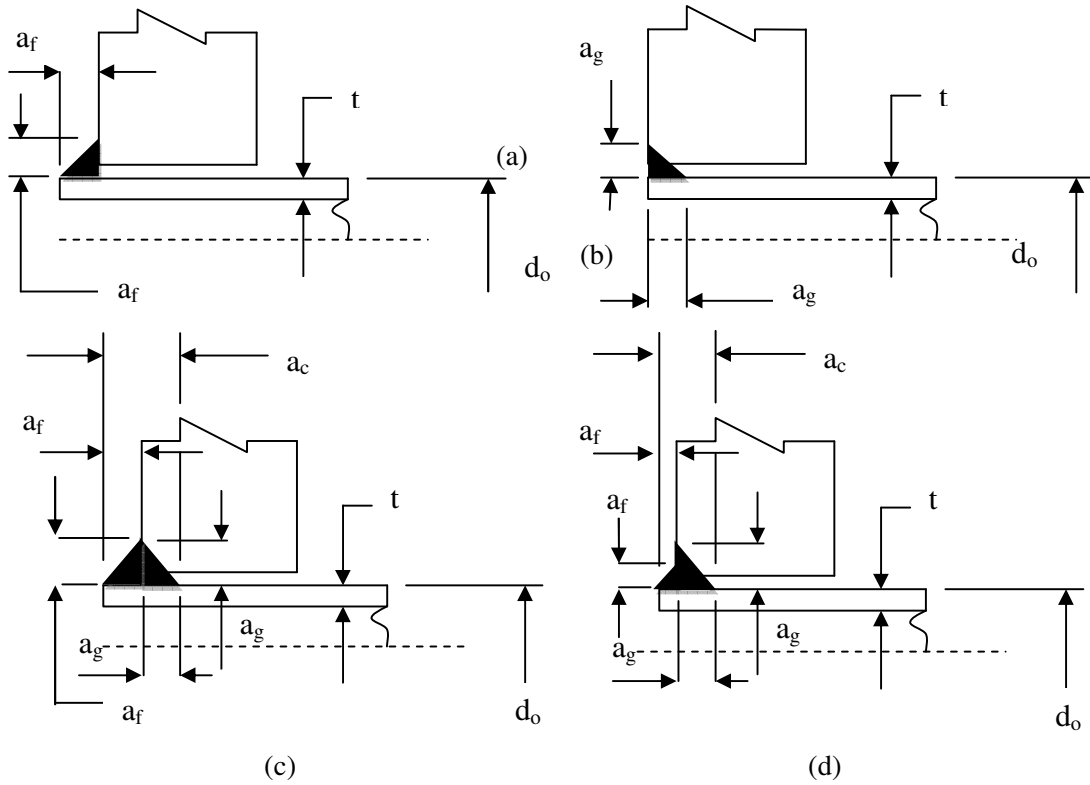
$$F_t = \pi t(d_o - t)S_a \quad (3.60)$$

Fillet weld strength, but not greater than  $F_t$ :

$$F_f = 0.55\pi a_f (d_o + 0.67a_f) S_w \quad (3.61)$$

Ratio of fillet weld's strength to the design strength:

$$f_f = 1 - \frac{F_g}{f_d F_t} \quad (3.62)$$



Groove weld strength, but not greater than  $F_t$ :

**Figure 3.12: Tube-to-tubesheet welds as in Figure UW-20.1 of ASMEVIII div 1 (2007)**

$$F_g = 0.85\pi a_g (d_o + 0.67a_g) S_w \quad (3.63)$$

Weld strength factor:

$$f_w = \frac{S_a}{S} \quad (3.64)$$

Maximum allowable axial load in either direction on the tube-to-tubesheet joint according to UW-20.4(b)(2)(a):

$$L_{max} = F_t \quad (3.65)$$

Ratio of design strength to the tube strength:

$$f_d = 1 \quad (3.66)$$

Minimum required length of weld, corresponding to Figure 3.12:

$$(a) \quad a_r = \sqrt{(0.75d_o)^2 + 2.73t(d_o - t)f_w f_d} - 0.75d_o \quad (3.67)$$

$$\text{and } a_{f(req)} \geq \max(a_r, t)$$

$$(b) \quad a_r = \sqrt{(0.75d_o)^2 + 1.76t(d_o - t)f_w f_d} - 0.75d_o \quad (3.67)$$

$$\text{and } a_{g(req)} \geq \max(a_r, t)$$

$$(c) \quad a_r = 2 \left[ \sqrt{(0.75d_o)^2 + 1.07t(d_o - t)f_w f_d} - 0.75d_o \right] \quad (3.67)$$

$$\text{and } a_{c(req)} \geq \max(a_r, t)$$

$$a_{f(req)} = 0.5a_{c(req)} \quad \text{and} \quad a_{g(req)} = 0.5a_{c(req)}$$

$$(d) \quad a_r = \sqrt{(0.75d_o)^2 + 2.73t(d_o - t)f_w f_d f_f} - 0.75d_o \quad (3.67)$$

$$\text{Choose } a_{g(req)}$$

$$\text{and } a_{c(req)} \geq \max(a_r + a_{g(req)}, t)$$

$$a_{f(req)} = a_{c(req)} - a_{g(req)}$$

The designer chooses the length of welds ( $a_f$  and/or  $a_g$ ) to perform the calculation and thereafter compares the required length of welds found in equation (3.67) to the initially chosen values.

#### Acceptance criteria

$$a_{f(required)} \leq a_f \quad (3.68)$$

$$a_{g(required)} \leq a_g \quad (3.69)$$



$$a_{c(\text{required})} \leq a_c \tag{3.70}$$

## **4. Finned tube bundle performance characteristics**

### **4.1. Introduction**

A critical part of designing a heat exchanger is the prediction of the air-side heat transfer coefficient ( $h$ ) and pressure loss coefficient ( $E_u$ ) across the finned tube bundle. It is therefore useful to know which existing correlations best describe the performance of the finned tube bundle. The aim of this experiment is to calculate these performance characteristics by measuring the necessary parameters in a wind tunnel test, and thereafter comparing it to existing correlations.

### **4.2. Literature review**

Ward & Young (1959) investigated the effects of tube geometry on the heat transfer and pressure drop characteristics of equilateral triangle pitch tube banks. Seven finned-tube banks ranging from four to eight rows were tested. Conclusions were that additional tube bank arrangements were required to improve heat transfer and pressure drop correlations.

Briggs & Young (1963) extended the study of Ward & Young (1959) by testing an additional nine banks of tubes. This led to an improved heat transfer correlation and a pressure drop correlation that included the effect of tube pitch but additional work was required to obtain a generalized pressure drop correlation.

Robinson & Briggs (1966) used a multiple regression analysis technique to analyze isothermal pressure drop data for seventeen finned-tube banks. The ratio of the root diameter to the transverse pitch was found to be the most important geometric factor. A generalized pressure drop correlation was obtained which had a reported standard error of 8.3 %.

Gianolio & Cuti (1981) performed tests on seventeen finned-tube banks with different numbers of rows under induced and forced draft conditions. Briggs and Young (1963) was reported as the most reliable correlation for heat exchangers having a number of rows greater than or equal to six and running under induced draft. This correlation over predicted results for banks having less than six rows; the difference increased with decrease in the number of rows.

Ganguli et al. (1985) investigated the effects of various finned tube design parameters on the thermal-hydraulic performance of a tube bundle. Generalized heat transfer and pressure drop correlations were presented. A bundle thermal conversion factor was introduced to characterize the thermal performance of heat exchangers. It is defined as a measure of how much heat flux may be expected per unit of pressure drop.

Beiler (1991) performed experiments to investigate the effect of flow maldistribution on the performance of air-cooled heat exchangers. It was observed that the thermal performance of downstream tube rows is influenced more by air flow maldistribution than the performance of upstream rows.

### 4.3. Description of test facility

The performance characteristics of extended surfaces are normally determined under idealized conditions in wind tunnels designed specifically for this purpose. An example of an atmospheric open-loop induced draft tunnel is shown schematically in Figure 4.1.

A radial fan (8) draws air uniformly through the rounded inlet section, across the heat exchanger bundle (1) which is heated by water flowing inside the tubes. The static pressure difference is measured across the bundle at points located in the duct wall (3). After the heat exchanger bundle, the air passes through a connecting section (2) and two sets of air mixers (4), followed by a venturi in which a sampling tube is located.

The air discharged from the heat exchanger may have a non-uniform temperature distribution together with a non-uniform velocity distribution. The most accurate means of measuring the mean temperature of the air stream under these conditions is to introduce air-mixers and then sample the stream at a number of points. Air-mixers may consist of a series of vanes arranged to divide the air flow into many small streams which are diverted across each other. The venturi arrangement after the mixers tends to minimize the non-uniformity of the air stream velocity. The sampling tube (5) permits the withdrawal of air from numerous points across the venturi throat and conveys it to a convenient location where the mean dry-bulb temperature may be measured. The air flow is determined by measuring the pressure drop across a 0.2509 m elliptical nozzle mounted in a plate (7) located between two perforated plates (6).

The wind tunnel is responsible for the air-side flow over the heat exchanger bundle, whereas water is the working fluid used inside the tubes. Water is heated to approximately 60 °C by electric heating elements placed inside a reservoir tank. The heater also has its own control unit, which switches the individual elements on or off as required to obtain the necessary water temperature. The water is pumped through the system, where it is cooled in the heat exchanger section, by the air, before it returns to the reservoir to be reheated. Since the water temperature difference is very small only two of the six elements were in use during the operation of the experiment.

Tests were conducted on a G-fin type tube bundle with a fin pitch of 2.8 mm as shown in Figure 4.4. The bundle has 6 rows, 13 tubes per row and it is arranged in a

staggered order. The general characteristics of the bundle are shown in Appendix E (Sample calculation).

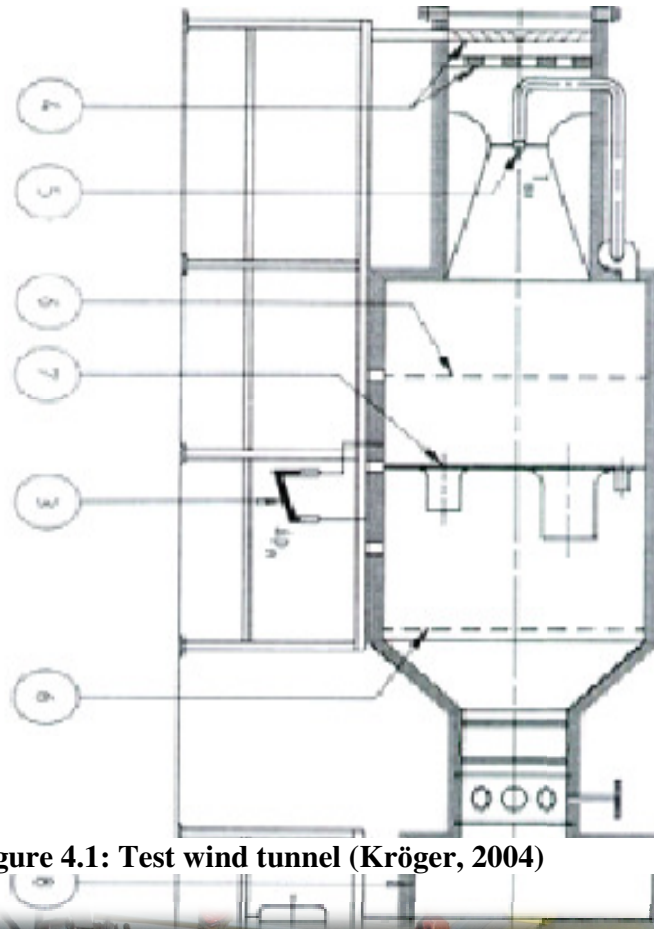


**Figure 4.1: Test wind tunnel (Kröger, 2004)**

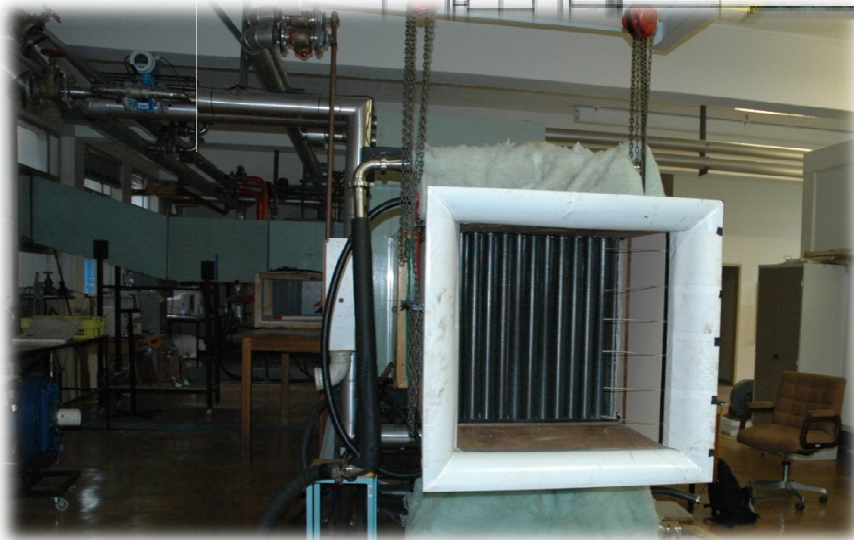


**Figure 4.2: Heat exchanger bundle in the wind tunnel**

#### **4.4. Measurement devices and techniques**

Temperatures, pressures, pressure drops and mass flow rates were measured during this experiment. These measuring devices and techniques will be explained using Figure 4.3 which shows the complete setup of the experiment.

##### **4.4.1. Temperatures**

The wet-bulb temperature, measured at the inlet of the wind tunnel, is measured using a wet-bulb thermometer. This is an ordinary thermometer with a wick at the bottom which is dipped in water. Since the air flows over the wick, the thermometer measures the wet-bulb temperature. This is accompanied by a thermometer that measures the atmospheric dry-bulb temperature.

Thermocouples (1) are placed inside the manifolds at the inlet and outlet of the tube bundle to measure the water temperature. It is also used at (5) in Figure 4.1 to measure the temperature of the outlet air.

The inlet air temperature is also measured using thermocouples, but this area is larger than the other areas where it is used. Since the temperature is measured over a large area, and the distribution is not uniform, an average temperature is measured at the inlet. Six equally spaced thermocouples (2) are positioned in this section to obtain an average temperature as shown in Figure 4.3.

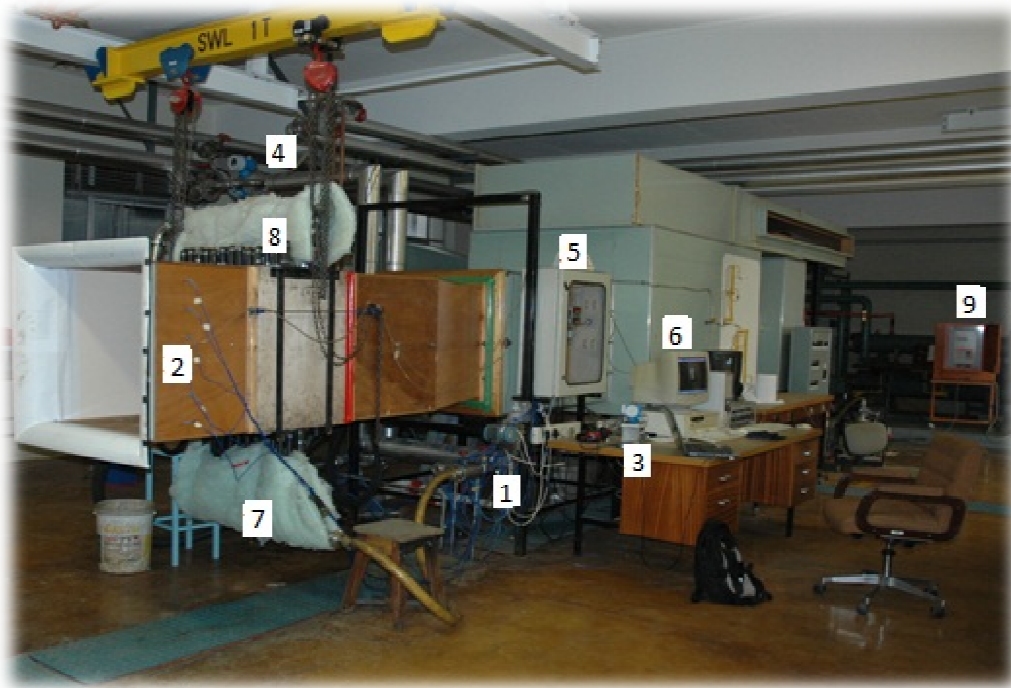


**Figure 4.3: Complete setup of the experiment**

#### **4.4.2. Pressures**

A mercury barometer is used to measure the atmospheric pressure in the test area. The Endress and Hauser Deltabar pressure transducer (3) was used for the experiment. The three pressure transducers were first calibrated using a Betz 2000 Micromanometer.

Pressure transducers, (3) in Figure 4.3, are placed at three locations in the experimental setup; two of the three measures a pressure drop across the tube bundle and elliptical nozzle respectively. This is marked (3) in Figure 4.1. The other transducer measures the absolute pressure before the elliptical nozzle to obtain the density of the air at that point as required in equation (4.2) for the air mass flow rate.

#### **4.4.3. User interface**

The system incorporates a computer which displays all the measured data. The measuring devices send an analogue signal to the Schlumberger data logger (5). The data logger converts the analogue to a digital signal which can be read by the

computer (6). This output signal is now measured in volts. This interface can only be used once the calibration of each measuring device has been completed.

Calibration is done by obtaining an expression that shows the relationship between the voltage reading and the SI unit of the respective measuring device. It also takes into account the zero readings of each device. These expressions are then entered into the computer program which results in the measured data being displayed and saved in its respective SI unit. Pressures are displayed in Pascal (Pa), temperatures in degrees Celsius (°C) and mass flow rate in kilograms per second (kg/s).

#### 4.4.4. Mass flow rates

There is a positive displacement mass flow rate measuring device (4) in the water pipeline, but a more conventional method was used to check this parameter. A section in the system contains a manually operated valve and a tank with known mass, which is used to measure and check the mass flow rate of the water. The bucket and scale, shown in Figure 4.4, was used to measure the mass of the water between points (1) and (2) in Figure 4.5. When the valve is closed, the time ( $t$ ) taken to fill the tank between these two points is measured. These measured values are then used to calculate the mass flow rate of the water in the following manner:

$$m = \frac{M}{t} \quad (4.1)$$

The mass flow rate of the air is determined by measuring the pressure drop across the nozzle as well as the pressure at the inlet of the nozzle. These pressures are then used to calculate the mass flow rate using the following equation (Kröger 2004):

$$m_a = C_n \dot{\Phi}_g Y A_n (2\rho_n \Delta P_n)^{0.5} \quad (4.2)$$

where:

- $C_n$  is the nozzle coefficient
- $\dot{\Phi}_g$  is the gas expansion factor
- $Y$  is the approach velocity factor
- $A_n$  is the cross sectional area of the elliptical nozzle
- $\rho_n$  is the air density after the bundle and before the nozzle
- $\Delta P_n$  is the pressure drop across the elliptical nozzle





**Figure 4.4: Scale and bucket used to check water mass flow**

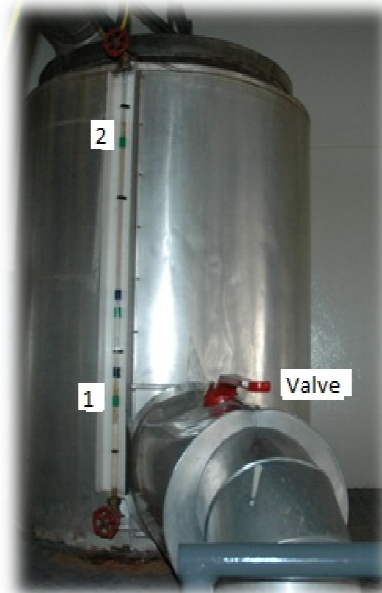


**Figure 4.5: Tank used to check water mass flow rate**

#### **4.5. Test procedure**

Firstly an isothermal test is done, where no water is involved in the experiment. This test is done to obtain the pressure drop number, the Euler number and the isothermal loss coefficient of the tube bundle.

Each row was tested individually, row 1 being the row closest to the air inlet, as well as the entire bundle (in counter flow). U-bends, shown in Figure 4.6, are connected to the ends of each tube, which is then connected to the adjacent tube row. In this way the tube bundle becomes a 6 pass heat exchanger. It is also shown as (8) in Figure 4.3. In order to reduce and prevent heat losses during the operation of the experiment; all manifolds, u-bends and all other pipe connections were insulated, shown as (7) in Figure 4.3.

Each test was run at six different fan speeds by changing the frequency on the variable speed drive (VSD) shown in Figure 4.7. This is done to obtain results over a range of data. It is also shown as (9) in Figure 4.3.

Five bundle tests were performed to check for repeatability and to suggest a reason for deterioration in the results, if any. Test 3 was used to display results of individual tests.



**Figure 4.6: U-bend used to connect adjacent rows**



**Figure 4.7: Variable speed drive that control fan speed**

#### 4.6. Data Processing

The measured data is collected and entered into an Excel program which obtains all the necessary performance characteristics of the tube bundle. A brief outline of this calculation is demonstrated below:

1. First calculate the heat transferred by each fluid (air and water side) and then compare them to obtain an energy balance, since the increase in air-stream energy must be equal to the heat transferred from the water.

$$Q = Q_a = m_a c_{pa} (T_{ao} - T_{ai}) \quad (4.3)$$

$$Q = Q_w = m_w c_{pw} (T_{wi} - T_{wo}) \quad (4.3)$$

2. Calculate the corresponding heat transfer coefficients ( $h_w$  and  $h_a$ ) and the dimensionless loss coefficient (Eu).
3. Use existing empirical correlations, which predict these parameters, and compare them to the results of the experiment.

All measured data and results are shown in Appendix D. A sample calculation, created in Mathcad, is also included in Appendix E to show all intermediate formulas and answers.

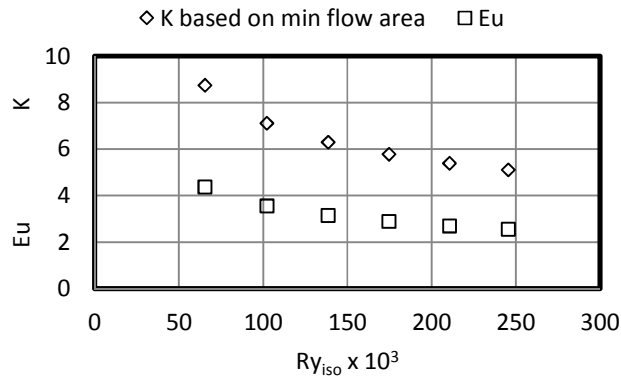
## 4.7. Results

This section presents the results of the isothermal test, a comparison of heat transfer coefficient from row to row as well as the complete bundle. It is followed by a comparison of the results for the complete bundle to the predictions of existing correlations found in the literature.

### 4.7.1. Isothermal test

The result of the isothermal test is shown in Figure 4.8. It shows that the loss coefficient (K) and the Euler number (Eu) differ by a factor of two.

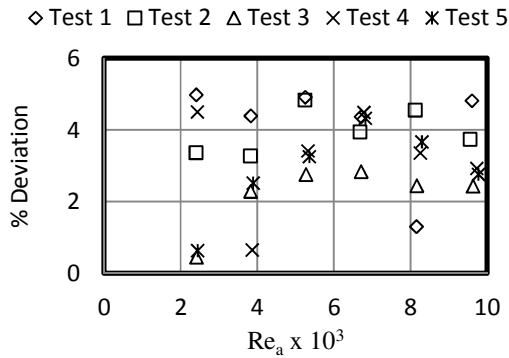
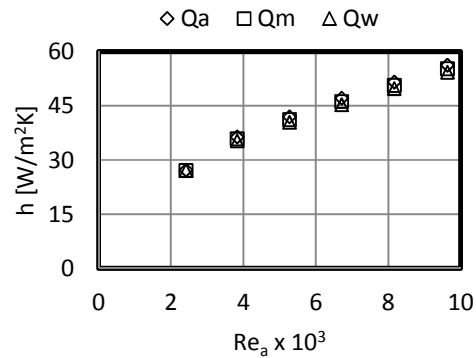
$$K \approx 2Eu \quad (4.4)$$



**Figure 4.8: Isothermal loss coefficient and Euler number**

### 4.7.2. Energy balance

Figure 4.9 shows the energy balance as a percentage deviation between the air side and the water side heat duty for all five tests. Since the respective air and water mass flow rates and the inlet and outlet temperatures are measured, the quality of the data can to a large extent be determined by the energy balance as given by equation (4.3).


**Figure 4.9: Energy balance**

**Figure 4.10: Effect of using Q<sub>a</sub>, Q<sub>m</sub> or Q<sub>w</sub>**

The effect of using  $Q_a$ ,  $Q_m$ , or  $Q_w$  in calculating the heat transfer coefficient is shown in Figure 4.9. The air side heat duty is always higher than the water side heat duty (also illustrated in Figure 4.9); it therefore also yields a higher heat transfer coefficient. The highest percentage difference between  $Q_a$  and  $Q_w$  is seen to be 3.8 % at a Reynolds number of 6700. It is therefore recommended by Gianolio & Cuti (1981) that the heat duty, used in the calculation of the overall heat transfer coefficient as shown in equation (4.5) and thus the air side heat transfer coefficient as shown in equation (4.6), should be calculated using the arithmetic mean of the values obtained from the air and water heat balance. The correction factor ( $F_T$ ) is assumed to be unity since the test is performed under counter flow conditions and due to the high temperature difference between the water and air.

$$U = \frac{Q_m}{A_a F_T \Delta T} \quad (4.5)$$

$$h_a = \left[ e_f A_a \left( U - 1/h_w A_w - \sum R_n/A_n \right) \right]^{-1} \quad (4.6)$$

### 4.7.3. Row effect

Figure 4.11 shows the heat transfer coefficient of the individual rows as well as for the bundle. The air flow entering the tube bank is not very turbulent and has almost exclusively axial velocity (perpendicular to the tube rows). The air after the first tube row is turbulent, with the turbulence level increasing with the number of tube rows; due to the wake effect of the preceding rows (Gianolio & Cuti, 1981). This is a possible explanation for the increase in air side heat transfer coefficient with increasing row number. The peak value is achieved at Row 6 where the turbulence is expected to be maximum. This reiterates the conclusions made by Beiler (1991) that

the performance of downstream tube rows is influenced more by air flow maldistribution than upstream tube rows.

Both the Nusselt number and Reynolds numbers contain an equivalent or hydraulic diameter and because of the arbitrary nature of its definition, different definitions are found in the literature. As explained by Kröger (2004:357-358), in the absence of the equivalent diameter, the characteristic flow parameter ( $Ry$ ) and characteristic heat transfer parameter ( $Ny$ ) may be preferred.

A function  $Ny = f(Ry)$  was computed for each row; these functions were then summed and compared to the values obtained for the bundle test at its respective  $Ry$  numbers. Figure 4.12 shows this comparison, where the results are identical for the tested range of  $Ry$  values.

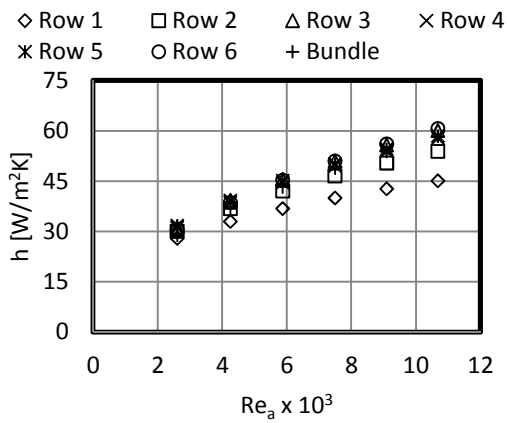


Figure 4.11: Row effect

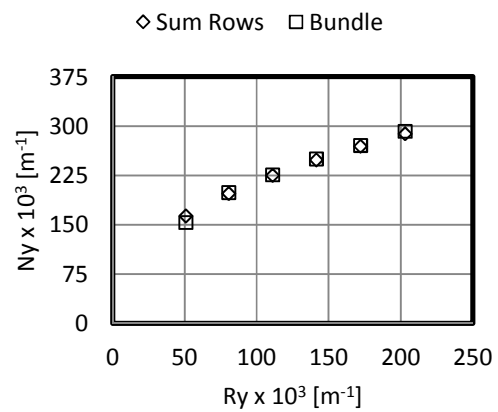


Figure 4.12: Sum of rows vs bundle

#### 4.7.4. Heat transfer coefficient

Two correlations, equations (4.7) and (4.8), found in the literature were used to predict the heat transfer coefficient of the bundle. These equations are only applicable within certain limits which are listed in Kröger (2004:377-379). Figure 4.13 shows the comparison between the measured data and that predicted by the correlations. The Reynolds number range of the tube bundle tests were  $2000 < Re < 10000$ , and therefore both correlations shown in equations (4.7) and (4.8) are valid. A power correlation fit (for Test 3) is also shown in Figure 4.13 as a line through the data.

Briggs & Young (1963) valid for  $1000 < Re < 18000$

$$\frac{hd_r}{k} = 0.134Pr^{0.33}Re^{0.681} \left[ \frac{2(P_f - t_f)}{d_f - d_r} \right]^{0.2} \left[ \frac{P_f - t_f}{t_f} \right]^{0.1134} \quad (4.7)$$

Ganguli et al. (1985) valid for  $1800 < Re < 100000$

$$\frac{hd_r}{k} = 0.138Pr^{0.33}Re^{0.6}(A/A_r)^{-0.15} \quad (4.8)$$

The measured data falls closer to the relation of Ganguli et al. (1985) as the Reynolds number increases. Figure 4.14 shows the comparison as a ratio of the experimental to the predicted value. It shows that the Ganguli et al. (1985) correlation is closer for predicting the heat transfer coefficient.

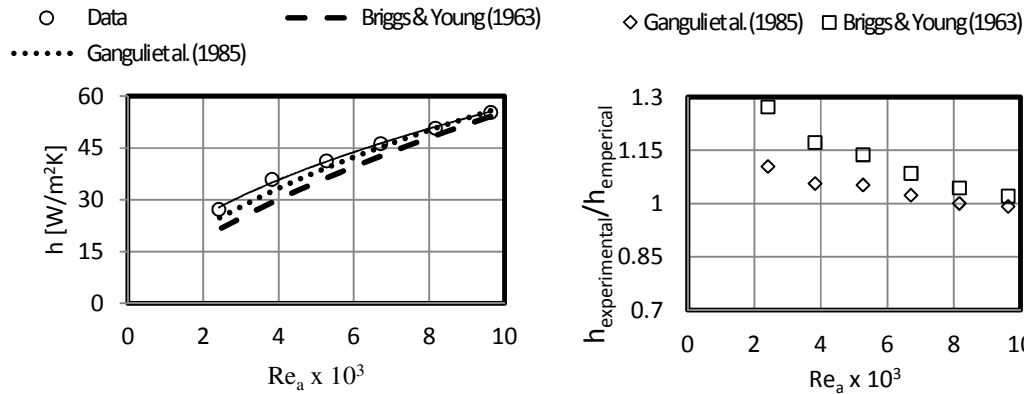


**Figure 4.13: Heat transfer coefficient of bundle**

**Figure 4.14: Heat transfer coefficient comparison ratio**

#### 4.7.5. Pressure drop

The pressure drop is expressed in dimensionless form using the Euler number (pressure loss coefficient). Two correlations, found in the literature, were used to predict the pressure drop of the bundle. The limits of applicability of these correlations are listed in Kröger (2004:382-383). Equations (4.9) and (4.10) are correlations for isothermal data, the tests were however non-isothermal since it had heated water inside the tubes. During non-isothermal operation there is a further term owing to the acceleration of the flow over the bundle. This acceleration is due to the density change across the bundle as a result of the increase in air temperature. The measured data must therefore be converted to isothermal data by subtracting the acceleration term so that it can be compared to the existing correlations, as shown in equation (4.11).

Robinson & Briggs (1966) valid for  $2000 < Re < 50000$

$$Eu = \frac{\rho \Delta p}{G_c^2} = 18.93 n_r Re^{-0.316} \left( \frac{P_t}{d_r} \right)^{-0.927} \left( \frac{P_t}{P_d} \right)^{0.515} \quad (4.9)$$

Ganguli et al. (1985)

$$Eu = \frac{\rho \Delta p}{G_c^2} = 2n_r \left[ 1 + 2e^{\frac{-(P_t - d_f)}{(4d_r)}} / \{1 + \frac{(P_t - d_f)}{(4d_r)}\} \right] \quad (4.10)$$

$$\left[ 0.021 + 13.6 (d_f - d_r) / Re(P_f - t_f) + 0.25246 \{ (d_f - d_r) / Re(P_f - t_f) \}^{0.2} \right]$$

Non-isothermal to isothermal Euler number

$$Eu = \frac{\rho_{am}}{G_c^2} \left[ \Delta p_{non-iso} - \frac{G_c^2}{2} (1 + \sigma^2) \left( \frac{1}{\rho_{ao}} - \frac{1}{\rho_{ai}} \right) \right] \quad (4.11)$$

Figure 4.15 shows a plot of the isothermal Euler number of the bundle as well as that predicted by the two correlations. The two correlations have the same trend but the Ganguli et al. (1985) correlation shows superior agreement with the measured data. The Robinson & Briggs (1966) correlation under predicts the pressure loss coefficient by about 18-24 % over the range of Reynolds numbers. Figure 4.16 shows the ratio of the measured Euler number to that predicted by the respective correlations, which reiterates the superiority of the Ganguli et al. (1985) correlation.

#### 4.7.6. Rust effect

Five tests were performed to check the repeatability of the results. Figure 4.17 shows a plot of the heat transfer coefficient for each of the five tests, at all six air speeds (Reynolds number), versus the time elapsed to complete all the tests. It illustrates that there is a general deterioration in the performance of the bundle with increasing time. Initially the tubes had an oil film protective layer to prevent corrosion during transportation and handling. Test 1 therefore washed away this oil film layer making the tubes susceptible to corrosion.

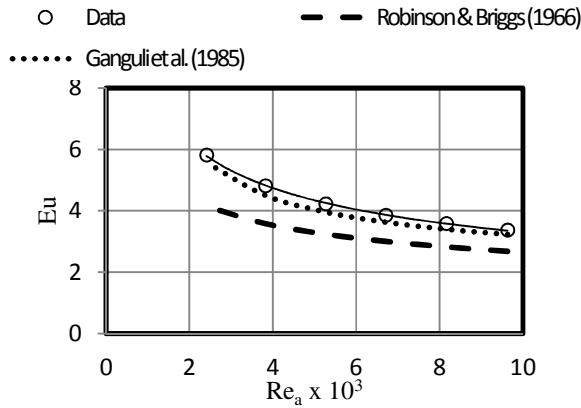


**Figure 4.15: Pressure loss coefficient of bundle**

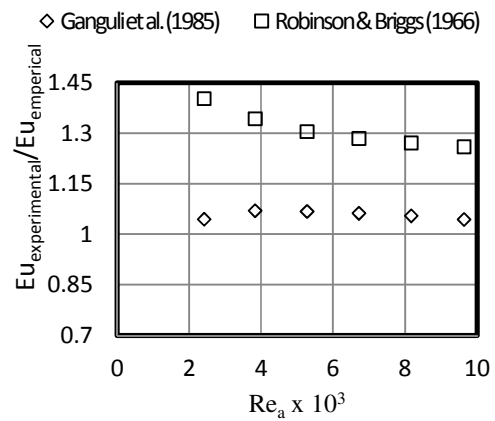


**Figure 4.16: Pressure loss coefficient comparison ratio**

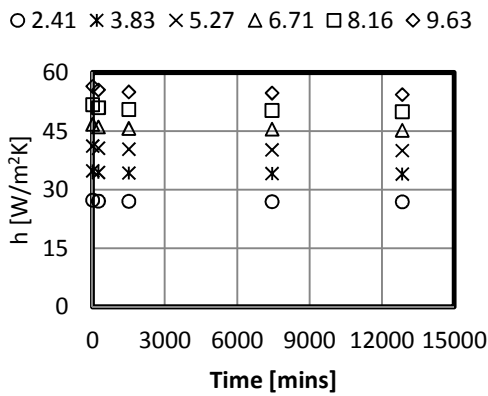


**Figure 4.17: Heat transfer coefficient vs time**

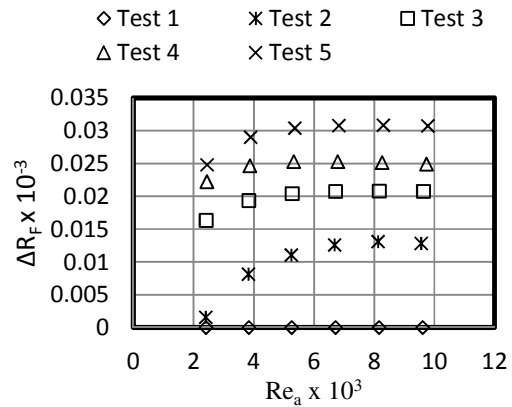


**Figure 4.18: Rust factor**

A suggestion for the reason in the deterioration in the performance of the bundle is due to corrosion. In the absence of fouling, the summation term in equation (4.6) includes resistances due to the tube wall and the fin root as well as the thermal contact resistance at the steel-aluminum interface (Kröger, 2004:370). The thermal contact resistance was not modeled in this project.

The oxygen in the water reacts with the steel tube and this causes a buildup of rust in the tube. The rust build up can be seen as fouling inside the tubes. It was thus modeled as an extra thermal resistance ( $\Delta R_f$ ) to the air flow in the calculation of the



air side heat transfer coefficient. Equation (4.12) was derived based on the air side heat transfer coefficient staying constant.

$$\Delta R_f = \frac{(\pi d_i) n_r n_{tr} L_t}{e_f A_a} [\{h_a(Re)^{-1}\}_i - \{h_a(Re)^{-1}\}_{Test1}] \quad (4.12)$$

A positive rust factor indicates a decrease in the heat transfer coefficient relative to Test 1. A correlation is required for the heat transfer coefficient as a function of Reynolds number, since they differ from test to test. Slight errors might occur when calculating the rust factor in this way since it is dependent on how well both correlations fits its respective data. The rust factor is shown in Figure 4.18 where all tests are compared to the base case (Test 1). It is a function of time since the time intervals between consecutive tests were not constant.

The results show that after performing five tests in a space of nine days, the internal fouling factor due to rust reaches a value of 0.0000308 m<sup>2</sup>K/W. Suggested fouling factors to be used in the design process of heat exchangers are 0.0004 m<sup>2</sup>K/W for city water above 50 °C (Sukhatme, 2005), 0.000352 m<sup>2</sup>K/W for treated make-up water (TEMA, 2007) and 0.000352 m<sup>2</sup>K/W for city or well water (H&C Heat transfer Solutions, [S.a]). The fouling factor specified in the design process can be seen as its allowable fouling during its operation. The bundle can thus be seen as to have fouled 8-9 % of its allowed fouling in a short period of about nine days.

Table 4.1 shows the percentage change in the heat transfer coefficient of each Reynolds number as depicted in Figure 4.17. The decrease in performance becomes more amplified with increasing Reynolds number. The intervals between tests were not constant but a time log was kept of the tests for comparison. There was an immediate decrease from Test 1 to Test 2, which means the corrosion occurred rapidly inside the tubes. More time was then allowed between tests to monitor the corrosion inside the tubes. A further decrease was shown in the performance with time, but this decrease became less between subsequent tests. This suggests that eventually the effect of rust will settle down thus giving constant performance.

**Table 4.1: Percentage difference between tests**

Test relative to Test 1	Time [mins]	Reynolds Number x 10 <sup>3</sup>					
		2.41	3.82	5.27	6.71	8.16	9.63
Test 2	240	0.90	1.13	1.29	1.41	1.51	1.59
Test 3	1500	1.06	1.56	1.90	2.17	2.38	2.55
Test 4	7440	1.43	1.98	2.35	2.63	2.86	3.06
Test 5	12840	1.59	2.31	2.81	3.19	3.49	3.74

#### **4.8. Summary of results and conclusion**

The performance characteristics of a finned tube bundle were determined by experiments in a wind tunnel. The results show that there is a row effect present that is directly proportional to the turbulence level of the air flow approaching the respective row. This confirms the work previously done by Gianolio & Cuti (1981) and Beiler (1991). Both heat transfer coefficient and pressure drop correlations, proposed by Ganguli et al. (1985), closely predicts the measured data and was thus used in the thermal design process. Corrosion inside the tubes caused deterioration in the heat transfer coefficient with time. This corrosion was modeled as an internal resistance, known as a rust factor.

## 5. Parametric study

It was mentioned in chapter 1 that companies split the design process of heat exchangers into three stages, each performed by a different expert in the field with specially designed software. This means that designers in the thermal and mechanical stages of the process make decisions regarding the design with limited knowledge about the effect it might have on the cost. Figure 5.1 shows how the three stages were linked to create a combined model.

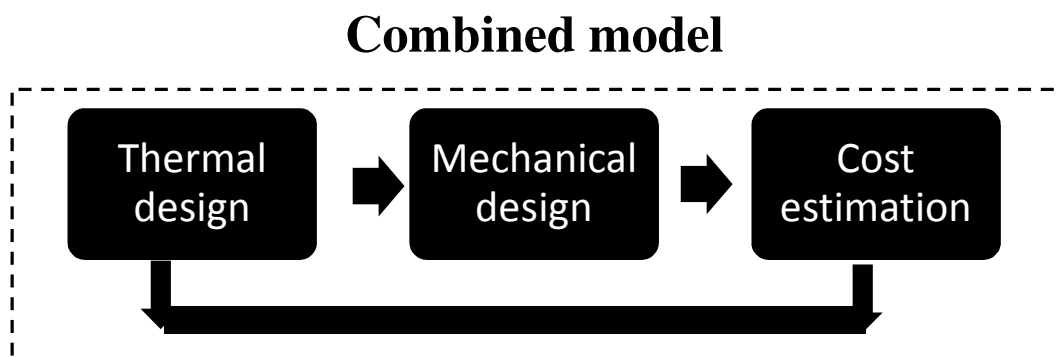


**Figure 5.1: Flow chart of combined model**

A thermal design is created using the thermal model described in chapter 2. The outputs of the thermal design are then transferred to the mechanical design model to obtain the minimum header thicknesses under the stress criteria of ASME VIII Div 1 (2007) as explained in chapter 3. The cost estimation is then done based on the outputs of both the thermal and mechanical designs of the heat exchanger. In this way if a change is made to the thermal design, the mechanical design is updated and the effect that the change has on the cost can immediately be seen. This assists designers in making an informed decision on which is the best possible design based on the minimum cost while satisfying the design specifications.

### 5.1. Cost estimation

The cost estimation was done according to equations and confidential specific costs obtained from GEA Aircooled Systems (Pty) Ltd. The equations are for example functions of the tube bundle dimensions from the thermal design and lengths and thicknesses of the header box from the mechanical design. Table 5.1 shows a detailed

breakdown of all the costs considered in this project. It includes the cost of the header box, tube bundle, labour, support structure, fans and motors.

**Table 5.1: Costs taken into consideration for this project**

<b><u>Header box material</u></b>	<b><u>Tube bundle</u></b>
Plate	Finned tubes
Plugs	Side frames + tube support
Nozzles	Tube spacers
Gaskets	
Corrosion protection	<b><u>Labor</u></b>
NDE, stress relieving, data books	Welding header plates
	Pass partition plates
<b><u>Other</u></b>	Tube to tubesheet welds
Assembly of bundles	Filler material
Support structure	Boilermaking (Cut, Tack, Set)
Fans	Weld Preps (Machining)
Bearing box + drives	Set up per header box
Motor	Drilling tubesheet holes
	Drilling and tapping plugsheet holes

## 5.2. Parametric study procedure

The goal of the parametric study is to vary only one design parameter in a specific design and examine the effect that it has on the cost. Table 5.1 shows that only the material and manufacturing cost of the heat exchanger was taken into account and not the cost of operating the heat exchanger. Therefore when comparing two designs the fan power consumption was kept constant to compensate for this cost of operation. The only way that this is possible is to allow a secondary parameter to vary thus striving to keep the fan power consumption constant.

Two different designs were considered in the parametric study. The one was very large with the original design consisting of 18 bundles and a smaller design that consisted on only 8 bundles. This was done to check the trend of the results across designs of different scales. It also incorporates different tube pass arrangements which results in the inclusion of all the header box sketches shown in Figure 3.2, Figure 3.3 and Figure 3.4.

Two separate studies were done, firstly the thermal design parameters followed by the mechanical design parameters.

### 5.3. Results of thermal parametric study

Table 5.2 shows a summary of the results obtained in the thermal parametric study which will be discussed individually.

**Table 5.2: Results of thermal parametric study**

No.	Case	Primary Parameter	Changed from .. to ..	Secondary parameter	Units	Changed from .. to ..	% $\Delta$ Cost
1	A	Length	5.15 $\rightarrow$ 6	Width	m	3.5 $\rightarrow$ 3	-5.19
	B		6 $\rightarrow$ 8.2			3 $\rightarrow$ 2.2	-7.00
2	A	Length	6 $\rightarrow$ 9	no. of bays		18 $\rightarrow$ 14	-5.00
	B		6 $\rightarrow$ 9			7 $\rightarrow$ 5	-13.07
3	A	Width	2.5 $\rightarrow$ 3.5	no. of bays		16 $\rightarrow$ 12	-2.47
	B		2.45 $\rightarrow$ 3.2			5 $\rightarrow$ 4	-2.87
4	A.i	Fans per bay	1 $\rightarrow$ 2	Fan shaft power	kW	26.2 $\rightarrow$ 13.1	1.88
	A.ii		2 $\rightarrow$ 4			13.1 $\rightarrow$ 7.9	7.66
	B.i		1 $\rightarrow$ 2			37.4 $\rightarrow$ 18.7	3.07
	B.ii		2 $\rightarrow$ 4			18.7 $\rightarrow$ 9.5	6.32
5	A	bundles per bay	1 $\rightarrow$ 2	no. of bays		4 $\rightarrow$ 2	-5.11
	B		1 $\rightarrow$ 2			14 $\rightarrow$ 7	-7.11
6	A	passes	6 $\rightarrow$ 3	Water velocity	m/s	2.5 $\rightarrow$ 1.23	-0.64
	B		4 $\rightarrow$ 2			2.5 $\rightarrow$ 1.23	-0.32

#### 5.3.1. Length versus width

The length is the primary parameter and the width is the secondary parameter. These parameters are changed accordingly to keep the frontal area of the bundle constant. Case A shows an increase in the length from 5.15 m to 6 m, the width changes from 3.5 m to 3 m; which results in a 5.19 % decrease in cost. Case B further increases the length which results in a 7 % decrease in cost. This concludes that increasing the length of the bundle, while decreasing the width results in a more economical design for the same heat transfer area. This result proves that making use of longer tubes is cheaper than adding to the required plate material of the header box and additional welding costs.

#### 5.3.2. Length versus number of bays

Instead of having a large number of bays, the length of individual bundles can be increased to reduce the number of bays. The length was increased from 6 m to 9 m; this reduced the number of bays from 18 to 13, which resulted in an 11.63 % decrease in the cost of the heat exchanger for Case A. Case B examines the same change in the

design for the smaller scale design; the length is increased from 6 m to 9 m, which resulted in a 13.07 % decrease in cost. This means that increasing the length while decreasing the number of bays results in a more cost-effective design.

### **5.3.3. Width versus number of bays**

This case is similar to that of section 5.3.2, but having the width as the primary parameter. In Case A the width was increased from 2.5 m to 3.5 m; this allowed a reduction in the number of bays from 16 to 12, which results in a 2.47 % decrease in the cost. The same trend is seen with Case B, where the width is increased from 2.45 m to 3.2 m, allowing the number of bays to decrease from 5 to 4 with a 2.87 % decrease in cost. Therefore simply increasing the width of each bundle and reducing the total number of bays obtains a more economical design.

### **5.3.4. Fans per bay versus fan diameter**

In this example there are two bundles per bay which means that the option is available to have many small fans per bay or fewer large fans for each bay. The diameter of the fan is governed by the requirement that it must at least occupy 40 % of the bay area as mentioned in section 2.3.4. The results show that increasing the number of fans per bay from 1 to 2, increases the cost of the heat exchanger by 1.88 % for Case A.i. A further cost increase of 7.66 % is observed when increasing the number of fans from 2 to 4 for Case A.ii. The same trend is observed when applying the test to Case B.i and Case B.ii, where the cost increases by 3.07 % and 6.32 % respectively. It is therefore more costly to have more, but smaller, fans per bay than having less, but larger, fans per bay. In this example, the fan shaft power cannot be kept constant. It is inversely proportional to the number of fans in the system, as the number of fans is halved; the fan shaft power doubles for each fan. It must be noted, as mentioned in section 5.2, that the cost of operation was not taken into account in this study.

### **5.3.5. Number of bundles per bay versus number of bays**

This investigation is done to see whether it is more cost-effective to have one bundle per bay or two bundles per bay and thus fewer bays. Case A shows that using two bundles per bay reduces the number of bays from 4 to 2, which decreases the cost by 5.11 %. Case B, with the larger design case, shows that using two bundles per bay reduces the required number of bays from 14 to 7 resulting in a 7.11 % decrease in the cost of the heat exchanger. It is thus more cost-effective to use two bundles per bay rather than one bundle per bay.

### 5.3.6. Passes versus width

The effect of changing the number of tube passes was also investigated. Changing the number of tube passes in this manner has a direct effect on the velocity of the water inside the tubes. Care must be taken to ensure that the velocity inside the tubes stays within the limits of 1 m/s to 2.5 m/s as discussed in section 2.4. The number of passes in Case A was changed from 6 to 3; which resulted in a decrease in the water velocity from 2.5 m/s to 1.23 m/s and thus a 0.64 % decrease in the cost. In the same way Case B varies the number of passes from 4 to 2; which resulted in a decrease in cost by 0.32 %. Reducing the number of tube passes reduces the required amount of partition plates and welding thereof in each header box.

## 5.4. Cumulative thermal parametric study

The next step in the study is to evaluate the effect of changing more than one primary design parameter. The aim is to obtain the cumulative improvement in the cost of the heat exchanger by combining the individual changes of Table 5.2 and noting the cumulative effect. Table 5.3 shows the results of this cumulative parametric study.

### 5.4.1. Case 1

It was previously mentioned that two different designs were investigated to check the results and trends across different design scales. The first case is that of the smaller design. It combines the changes of Case 2B and Case 5A of Table 5.2, where the length is changed from 6 m to 9 m and making use of two bundles per bay rather than one. These combined changes bring about a decrease in the number of bays from 8 to 3, with a decrease of 17.5 % in the cost of the heat exchanger. This decrease in cost is roughly the sum of the individual decreases of the respective cases of Table 5.2, 13.07 % for Case 2B and 5.11 % for Case 5A, which is the sum 18.18 %.

**Table 5.3: Results of cumulative thermal parametric study**

No.	Primary Parameter	Changed from ... to ...	Secondary parameter	Units	Changed from ... to ...	% $\Delta$ Cost
1	Length	6 $\rightarrow$ 9	number of bays		8 $\rightarrow$ 3	-17.5
	bundles per bay	1 $\rightarrow$ 2				
2	Length	6 $\rightarrow$ 9	Width	m	3 $\rightarrow$ 3.5	-11.7
	bundles per bay	1 $\rightarrow$ 2	number of bays		18 $\rightarrow$ 6	
	passes	4 $\rightarrow$ 2	Fan shaft power	kW	9.8 $\rightarrow$ 15.7	

### 5.4.2. Case 2

Case 2 varies the length from 6 m to 9 m, uses two bundles per bay and reduces the amount of tube passes from 4 to 2. This allows for a reduction in the bundle width and overall number of bays with a resulting 11.7 % decrease in the cost of the heat exchanger. Although operational costs were not included in this study, it should be noted that the fan power consumption also increased in this example as a consequence of the design changes. Case 2 consists of the combination of Case 2A (5.00 %), Case 5B (7.11 %) and Case 6B (0.34 %) from Table 5.2, which has a sum of 12.45 % decrease in cost. Case 1 and Case 2 shows that the cumulative decrease in cost is approximately the sum of the individual cases as listed in Table 5.2.

### 5.5. Excel solver

The results of Table 5.2 show which individual design variables should be changed in order to obtain a cost effective design. The cumulative study verifies the consistency of the results by applying many design changes collectively. A further improvement in the results can be obtained by applying MS Excel's built-in optimiser, Solver, to the given problem.

Since most of the cost of the heat exchanger is owing to the material used in the design, the hypothesis is that the optimum design of a heat exchanger requires that the minimum design area be used to satisfy the design specifications using the minimum fan shaft power. The optimisation problem is therefore stated as follows; minimise the cost by varying the length, the width of the bundle which is dependent on the water velocity inside the tubes determined from equations (2.3), (2.4) and (2.53) and the air-side velocity through the bundle. This is stated mathematically below:

$$\text{Minimise:} \quad F = R \quad (5.1)$$

$$\text{By changing variables:} \quad L, v_w, v_a, \quad (5.2)$$

$$\text{Such that:} \quad 1.2 \text{ m/s} \leq v_w \leq 2.5 \text{ m/s} \quad (5.3)$$

$$2.5 \text{ m/s} \leq v_a \leq 4 \text{ m/s} \quad (5.4)$$

$$W \leq 3.5 \text{ m} \quad (5.5)$$

$$\text{Overdesign} \geq 0 \quad (5.6)$$



Table 5.4 shows the results obtained by applying Excel Solver to the two cases in Table 5.3 from different initial design points (A and B). The  $\Delta$ Cost column, in Table 5.4, refers to the percentage change in cost relative to the respective case in Table 5.3.

**Table 5.4: Excel solver results**

No.	Width [m]	Length [m]	Water velocity [m/s]	Overdesign [%]	Fan power [kW]	Frontal Area [m <sup>2</sup> ]	$\Delta$ Cost [%]
1.A	2.3→2.37	9→8.04	1.3→1.28	6.4→3.6	17.1→20.8	128→114	-7.1
1.B	2.5→2.5	8→7.49	1.2→1.2	1.6→2.1e-7	16→18	120→112	-8.9
2.A	3→3.2	10→8	1.3→1.2	7.5→0.38	23.2→27.1	420→361	-1.17
2.B	3.2→2.78	9→9.64	1.23→1.4	3.7→4.5	22.3→28	403→376	-2.54
3	2.3→2.18	12→11.8	1.7→1.8	1.7→9.5e-7	21.4→24.2	386→360	-10.06

In Case 1.A the Solver increased the width from 2.3 m to 2.37 m while decreasing the length of the bundle from 9 m to 8.04 m, which brought about a higher fan power consumption but a lower frontal area resulting in a 7.1 % decrease in the cost of the heat exchanger. Case 1.B, starting from different initial design parameters, results in an 8.9 % decrease in cost. The same trend is seen for Case 2, where Case 2.A decreases by 1.17 % and Case 2.B decreases by 2.54 %. Vanderplaats (2007:19) states that the best practical approach is to start an optimisation process from several different design points, and if the optimisation results are essentially the same final design, it can be assured to be the true optimum. Therefore the reason for using two different initial design points is to demonstrate that the problem at hand has many local optima, since the each final design differs.

Case 3 is another design variation of Case 2, but the initial design was produced using the knowledge gained from the results of the parametric study in Table 5.2 in an attempt to find the most economical design. Firstly make use of the maximum length of 12 m, two bundles per bay, with fewer (larger) fans, utilize minimum amount of bays and choose the width of the bundle such that the percentage overdesign tends to zero. Once this feasible design is obtained, apply Excel Solver to locate the correct combination of length and width to minimise the cost.

The result of Case 3 showed a further 10.06 % decrease in the cost of the heat exchanger relative to Case 2 in Table 5.3. This 10.06 % is large compared to the 1.17 % and 2.54 % obtained from Case 2.A and Case 2.B respectively, which shows

the effectiveness of the technique applied in Case 3. Therefore the method of applying the knowledge obtained from the trends of the parametric study to the initial design and thereafter applying Excel Solver to the problem is considered a good way of acquiring the optimum design of a heat exchanger.

## 5.6. Results of mechanical parametric study

As explained in chapter 3, the output of the mechanical design is the minimum header thicknesses under the stress criteria of Appendix 13 of ASME VIII div 1 (2007). This means the design obtained from the mechanical design model is always an optimum in terms of the minimum required material thicknesses. However, as with the fans per bay in the thermal study, the option is available to use many small nozzles or fewer but larger nozzles. Also if the header box plate material becomes too thick, a stay plate that acts as a stiffener can be added resulting in reduced header box thicknesses. These two design changes were therefore investigated in the study.

### 5.6.1. Nozzles

The results are shown in Table 5.5 for the parametric study of the number of nozzles versus the nozzle size. Case 1 reduces the nozzle size from 6" to 4" which results in a 0.67 % decrease in cost, but Case 2 performs the same resulting in a 0.79 % increase in cost. Case 3 shows that the nozzle diameter was firstly decreased from 8" to 6" and thereafter further decreased to 4" with both instances resulting in a decrease in the cost of the heat exchanger. Although the same design change is made in Case 1 and Case 2, there is an increase in cost for Case 2 and a decrease in cost for Case 1. The results therefore show that there is no particular trend when changing the number of nozzles versus the size of the nozzle across different design cases. It is recommended to be checked in each design case to see which design is more economical.

Table 5.5 also shows that the side plate length (H) decreases as the nozzle size decreases. This was previously shown in equation (3.1), where the side plate length (H) is directly proportional to the diameter of the nozzle. Another trend resulting from the study is that using smaller nozzle sizes allows the header plate thicknesses ( $t_1$  and  $t_2$ ) to be decreased while satisfying the stress criteria of ASME VIII div 1 (2007).

**Table 5.5: Results of parametric study of number of nozzles versus nozzle size**

No.	Nozzle size	Number of nozzles	H	$t_1$	$t_2$	% $\Delta$ Cost
1	6 → 4	1 → 2	180 → 124	25 → 16		-0.67
2	6 → 4	1 → 3	180 → 124	25 → 16		0.79
3	8 → 6	1 → 2	180 → 238	35 → 25	25 → 20	-0.27
	6 → 4	2 → 4	180 → 124	25 → 16		-3.01

### 5.6.2. Stay plates

Table 5.6 shows the results of the parametric study of the use of stay plates. A stay plate is especially useful for Figure 3.2 type vessels, which become Figure 3.3 type vessels when adding one stay plate. Stay plates contain holes which allows the fluid to flow through, as shown in Figure 3.6, thus it does not separate passes but only acts as a stiffener plate which then results in reduced header plate thicknesses under the stress criteria of Appendix 13 of ASME VIII div 1 (2007). This phenomenon can be seen for all the cases in Table 5.6, where upon the addition of a stay plate the tubesheet thickness ( $t_2$ ) is reduced. As with the case of the study of the number of nozzles versus the nozzle size, there is no particular trend in the results across different designs. Case 1 and Case 2 both result in an increase in the cost, whereas Case 3 results in a decrease in the cost of the heat exchanger. Case 1 and Case 3 are the same in that a stay plate was only added to the return header, but they yield the opposite result in terms of cost. Once more it should be noted that each case number was for a different design case.

**Table 5.6: Results of parametric study of the use of stay plates**

No.	Stays	Figure	$t_2$	$t_{\text{stay}}$	% $\Delta$ Cost
1	Return header	3.2 → 3.3	40 → 25	0 → 16	0.69
2	Both headers	3.3 → 3.4	40 → 20	0 → 16	0.86
	Outlet Header	3.3 → 3.4	40 → 20	0 → 16	0.27
3	Return header	3.2 → 3.3	40 → 20	0 → 16	-0.02

### 5.7. Cost breakdown

Table 5.1 showed a breakdown of the cost considered in this project. Two different designs were used to check the percentage contribution of each section, as in Table 5.1, to the total cost of the heat exchanger.

**Table 5.7: Percentage contribution of each section to total cost of the heat exchanger**

Section as in Table 5.1	Percentage contribution	
	Case 1	Case 2
Header Box material	9.72	11.96
Tube bundle	32.97	32.71
Labor	11.48	9.87
Other	45.83	45.47

The results of this percentage contribution are shown in Table 5.7. It shows that across different designs, the percentage contribution of each section is approximately constant. Most of the cost ( $\pm 45\%$ ) is due to fans, motors, bearing box and drives and the support structure. The header box material constitutes  $\pm 10\%$ , labour another  $\pm 10\%$  and the tube bundle  $\pm 35\%$  of the total heat exchanger cost. The header box components are basically the sum of the header box material and the labour cost as listed in Table 5.1. Therefore it can also be seen that  $\pm 20\%$  of the total cost is due to the header box.

## 6. Conclusions and recommendations

Companies separate the design process into thermal design, mechanical design and cost estimation, each performed by a different expert in the field with specially designed software. Often a few possible designs exist to satisfy a given problem, thus a combined model assists in choosing the best design in terms of cost of the heat exchanger. The purpose of this project was to create a model in MS Excel that combines the three stages of the design of a heat exchanger in order to perform a parametric study to investigate which trends provide the best possible design based on the cost of the heat exchanger.

### 6.1. Conclusions

A simplified schematic of an air-cooled heat exchanger is shown in Figure 2.1, which was used to create a model to perform the thermal design according to equations extracted from Kröger (2004). Both the e-NTU and LMTD methods were considered in the model. Two models were developed; the design case which calculates the dimensions of the bundle given the performance and the off-design (rating) case which calculates the performance given the dimensions of the bundle. The model uses a built-in fan curve together with fan laws to satisfy the draft equation. A flow diagram of the thermal model algorithm is shown in Figure 2.5. The model was verified with HTRI software for both the design case and off-design case.

The results produced by the thermal model compared very well with HTRI results apart from for the air-side pressure drop that differed slightly. A possible explanation for this difference was that the two programs use different correlations to predict the pressure drop. A G-finned tube bundle was therefore tested in a wind tunnel facility to compare the measured performance characteristics to that predicted by existing correlations. Chapter 4 provides all the details of the wind tunnel tests. The results showed that both the heat transfer coefficient ( $h$ ) and pressure loss coefficient ( $E_u$ ) correlations proposed by Ganguli et al (1985) predict the measured data well and were thus used in the thermal design model. It also showed that there is a general deterioration in the performance of the tubes with time in Figure 4.19. This deterioration is as a result of rust build-up inside the tubes and thus equation (4.12) was derived which expresses the rust factor relative to the first test. Table 4.1 shows the percentage deterioration in heat transfer coefficient relative to Test 1. It concludes that eventually the effect of rust will stabilise thus resulting in constant performance of the tubes.

Chapter 3 underlines the mechanical design procedure of a plug-type header box according to ASME VIII div 1 (2007). This procedure was programmed in MS Excel to create the mechanical design model, which includes nozzle design and tube-to-

tubesheet welds. The model uses the geometry of the thermal design as inputs and produces the minimum header thicknesses as outputs; based on the stress criteria of Appendix 13 of ASME VIII div 1 (2007) Boiler and Pressure Vessel Code.

A cost estimation model was also created using equations and confidential specific costs obtained from GEA Aircooled Systems (Pty) Ltd. The three models were then combined thus allowing a parametric study to be performed to see what effect changing a design variable has on the cost of the heat exchanger. This parametric study was split into the thermal and mechanical design sections. The results presented in Table 5.2 show that to obtain an optimal solution, the design must attempt to maximise the length, increase the width rather than the number of bays, make use of two bundles per bay with fewer but larger fans and employ a large number of tube rows with the least number of passes. The design must strive to implement these guidelines while adhering to all the design specifications and requirements.

Table 5.3 shows the results of applying many design changes collectively. It shows that altering many design parameters together is the sum of the individual changes as in Table 5.2.

Excel Solver was used to optimise the designs, but different starting points resulted in different final designs. This is explained in Section 5.5 with Table 5.4 displaying the results. Different final designs imply that many local optima exist in the design space. An informed strategy was then created to obtain the optimum design of a heat exchanger. The knowledge obtained from the individual parametric study (Table 5.2) is used to create an initial design; Excel Solver is then applied to it to find the correct combination of length and width to minimise the cost of the heat exchanger.

Table 5.5 shows no specific trend for using bigger and less nozzles or smaller and more nozzles. The same conclusion was drawn from Table 5.6 for the use of stay plates in the header box. Both studies showed that the percentage change in cost is small compared to that of the thermal parametric study. The usage of these mechanical considerations should therefore be based on more practical aspects, such as pressure drop across nozzles or the need to strengthen the header box utilising stay plates.

Chapter 5 shows the capability of the combined model. It can create a thermal design given the performance required by any system. The thermal design exports the bundle dimensions to the mechanical design to calculate the minimum header thicknesses required under the stress criteria. The cost estimation model then uses the necessary parameters from the thermal and mechanical design to calculate all costs as shown in Table 5.1 to produce the overall cost of the heat exchanger. Any changes made to the

design, at either the thermal or mechanical design stage of the design process is immediately reflected in the cost of the heat exchanger.

## **6.2.Recommendations**

The thermal design model uses a built-in fan curve to satisfy the draft equation, whereas it might be simpler to calculate the pressure drop across the fan and thereafter choose a fan accordingly. Only water was considered as the working fluid in the design, but this can easily be extended to take into account other fluids by adding a library of other fluid's properties.

Only a plug-type header was considered in the mechanical design and although it is the most commonly used type, others types can be included. Other plate materials can also be included since only carbon steel was considered in the design of the header boxes.

Section 3.2.2 states that according to 13-9 (f) of ASME VIII div 1 (2007) even though compartments of a header box are of unequal size, it is analysed as if they are equal with the maximum compartment dimension. An alternative method could be to analyse the header box with rigid frame theory or moment distribution and slope deflection calculations.

Current design practice evaluates the tubesheet and plugsheet of stayed vessels to have the same plate thicknesses since ASME VIII div 1 (2007) is limited to unstayed vessels with different tubesheet and plugsheet plate thicknesses. This is especially disadvantageous since plugsheets are evaluated with multidiameter hole ligament efficiencies because it has a recess for the seating of gaskets and plugs. ASME VIII div 1 (2007) code can be expanded to include stayed vessels with different tubesheet and plugsheet thicknesses with corresponding stress equations.

In these ways ASME VIII div 1 (2007) is conservative in its design; it might therefore be useful to compare it to a different design code or by designing the header box with the proposed alternative methods.

Only a G-finned type tube was tested in the wind tunnel facility, more types of tubes, such as L-fin and Extruded fin as in Figure 1.4, can be tested for comparison.

The results presented in Chapter 5 are based on a limited number of design cases; similar problems should therefore be independently verified.

The costing information can be refined to include more detail as well as the cost of operation for more accurate cost representations.

## 7. References

API Standard 661, Air-Cooled Heat Exchangers for General Refinery Service, 2006, Sixth Edition, American Petroleum Institute.

*Basics of Air-Cooled Heat Exchangers.* [S.a]. [Online]. Available: <http://www.onsitepowerinc.com/documents/supplierDocs/amercool/Basics%20of%20Air%20cooled%20Heat%20Exchangers%20rev1.pdf>. [2011, November 15].

ASME Boiler and Pressure Vessel Code, Section VIII, Division 1, 2007 Edition, American Society of Mechanical Engineers.

ASME Boiler and Pressure Vessel Code, Section II, Part D, Properties (Customary), Materials, 2007 Edition, American Society of Mechanical Engineers.

ASME B16.5, Pipe Flanges and Flanged Fittings, NPS ½ through NPS 24 Metric/Inch Standard, 2003, American Society of Mechanical Engineers.

Beiler, M.G. 1991. *Effect of flow maldistribution on performance on induced and forced draft air-cooled heat exchangers.* Stellenbosch, South Africa: University of Stellenbosch (MSc thesis).

Bennett, C.A., Kistler, R.S., Lestina, T.G. & King, D.C., 2007. Improving Heat Exchanger Designs. *Chemical Engineering Progress Symposium Series*, pp. 40-45.

Bredell, J.R. & Kröger, D.G. 2006. Numerical Investigation of Fan Performance in a Forced Draft Air-Cooled Steam Condenser. California Energy Commission, PIER Energy-Related Environmental Research.

Briggs, D.E & Young, E.H. 1963. Convection heat transfer and pressure drop of air flowing across triangular pitch banks of finned tubes. *Chemical Engineering Progress Symposium Series*, 59(41):1-10.

Cengel, Yunus A. 2006. Heat and mass transfer: a practical approach. 3<sup>rd</sup> ed. New York: McGraw-Hill.

Fried, E. & Idelchik, I. E., 1989. *Flow Resistance: A Design Guide For Engineers.* Philadelphia: Taylor & Francis.

Ganguli, A., Tung, S.S. & Taborek, J. 1985. Parametric study of air-cooled heat exchanger finned tube geometry. *American Institute of Chemical Engineers Symposium Series*, 81(245):122-128.



Gianolio, E. & Cuti, F. 1981. Heat transfer coefficients and pressure drops for air coolers with different numbers of rows under induced and forced draft. *Heat Transfer Engineering*, 3(1):38-47.

H&C Heat Transfer Solutions. [S.a]. {Online}. Available: [www.hcheattransfer.com/fouling\\_factors2.html](http://www.hcheattransfer.com/fouling_factors2.html). [2012, November 20].

Kays, W. M. & London, A. L. 1984. *Compact Heat Exchangers*. 3rd ed. Malabar, Florida: Krieger Publishing Company.

Kröger, D.G. 2004. *Air-Cooled Heat Exchangers and Cooling Towers*. Tulsa, Oklahoma: PennWell Corp.

Mahajan, K. K., 1990. *Design of Process Equipment*. Tulsa, Oklahoma: Pressure Vessel Handbook Publishing, Inc.

Makhema, T. 2000. *Performance evaluation of air-cooled heat exchangers*. Stellenbosch, South Africa: University of Stellenbosch (MSc thesis).

Oosthuizen, P.C. 1995. *Performance characteristics of hybrid cooling towers*. Stellenbosch, South Africa: University of Stellenbosch (MSc Thesis).

Perry, R. H., & Green, D. W. 1997. *Perry's Chemical Engineers' Handbook*. 7<sup>th</sup> ed. United States of America: McGraw-Hill.

Robinson, K.K & Briggs, D.E. 1966. Pressure drop of air flowing across triangular pitch banks of finned tubes. *Chemical Engineering Progress Symposium Series*, 62(64):177-184.

Sukhatme, S.P. 2005. *A textbook of heat transfer*. 4<sup>th</sup> ed. India: Universities Press (India) Private Limited Ullman, D.G. 1997. *The Mechanical Design Process*. 2<sup>nd</sup> ed. Singapore: McGraw-Hill.

TEMA *Standards of the Tubular Exchanger Manufacturers Association*. (2007). 9<sup>th</sup> ed. TEMA New York.

Vanderplaats, G.N. 2007. *Multidiscipline Design Optimization*. California Office: Vanderplaats Research & Development, Inc.

Ward, D.J & Young, E.H. 1959. Heat transfer and pressure drop of air in forced convection across triangular pitch banks of finned tubes. *Chemical Engineering Progress Symposium Series*, 55(29):37-44.

## Appendix A – Properties of fluids

### A.1 Functions for the thermophysical properties of dry air:

Density

$$\rho_a(p_a, T_a) := \frac{p_a}{287.08 T_a}$$

Specific heat

$$c_{pa}(T_a) := \left( 1.04535610^3 - 3.16178310^{-1} \cdot T_a + 7.08381410^{-4} \cdot T_a^2 - 2.70520910^{-7} \cdot T_a^3 \right)$$

Dynamic viscosity

$$\mu_a(T_a) := \left( 2.28797310^{-6} + 6.25979310^{-8} \cdot T_a - 3.13195610^{-11} \cdot T_a^2 + 8.1503810^{-15} \cdot T_a^3 \right)$$

Thermal conductivity

$$k_a(T_a) := -4.93778710^{-4} + 1.01808710^{-4} \cdot T_a - 4.62793710^{-8} \cdot T_a^2 + 1.25060310^{-11} \cdot T_a^3$$

### A.2 Functions for the thermophysical properties of saturated vapour:

Vapour pressure

$$z_1(T_a) := 10.79586 \left( 1 - \frac{273.16}{T_a} \right) \quad a_2(p_a, p_{vwb}) := \frac{0.62509 p_{vwb}}{p_a - 1.005 p_{vwb}}$$

$$z_2(T_a) := 5.02808 \log \left( \frac{273.16}{T_a} \right)$$

$$z_3(T_a) := 1.5047410^{-4} \cdot \left[ 1 - 10^{-8.29692 \cdot \left[ \left( \frac{T_a}{273.16} \right) - 1 \right]} \right]$$

$$z_4(T_a) := 4.287310^{-4} \cdot \left[ 10^{4.76955 \cdot \left( 1 - \frac{273.16}{T_a} \right)} - 1 \right]$$

$$z_5 := 2.78611831$$

$$z(T_a) := z_1(T_a) + z_2(T_a) + z_3(T_a) + z_4(T_a) + z_5$$

$$p_v(T_a) := 10^{z(T_a)}$$

Humidity ratio

$$a_1(T_{db}, T_{wb}) := \frac{2501.6 - 2.3263(T_{wb} - 273.15)}{2501.6 + 1.8577(T_{db} - 273.15) - 4.184(T_{wb} - 273.15)}$$

$$a_2(p_a, p_{vwb}) := \frac{0.62509 p_{vwb}}{p_a - 1.005 p_{vwb}}$$

$$a_3(T_{db}, T_{wb}) := \frac{1.00416(T_{db} - T_{wb})}{2501.6 + 1.8577(T_{db} - 273.15) - 4.184(T_{wb} - 273.15)}$$

$$w(T_{db}, T_{wb}, p_a, p_{vwb}) := a_1(T_{db}, T_{wb}) \cdot a_2(p_a, p_{vwb}) - a_3(T_{db}, T_{wb})$$

Specific heat

$$c_{pv}(T_a) := \left( 1.3605 \cdot 10^3 + 2.31334 T_a - 2.46784 \cdot 10^{-10} \cdot T_a^5 + 5.91332 \cdot 10^{-13} \cdot T_a^6 \right)$$

Dynamic viscosity

$$\mu_v(T_a) := \left( 2.562435 \cdot 10^{-6} + 1.816683 \cdot 10^{-8} \cdot T_a + 2.579066 \cdot 10^{-11} \cdot T_a^2 - 1.067299 \cdot 10^{-14} \cdot T_a^3 \right)$$

Thermal conductivity

$$k_v(T_a) := 1.3046 \cdot 10^{-2} - 3.75619 \cdot 10^{-5} \cdot T_a + 2.217964 \cdot 10^{-7} \cdot T_a^2 - 1.111562 \cdot 10^{-10} \cdot T_a^3$$

### A.3 Functions for the thermophysical properties of mixtures of air and water vapour:

Density

$$\rho_{av}(w, p_a, T_a) := (1 + w) \cdot \left( 1 - \frac{w}{w + .62198} \right) \cdot \frac{p_a}{287.08 T_a}$$

Specific heat

$$c_{pav}(T_a, w) := \frac{c_{pa}(T_a) + w c_{pv}(T_a)}{1 + w}$$

Dynamic viscosity

$$M_a := 28.97 \quad M_v := 18.016 \quad X_a(w) := \frac{1}{1 + 1.608 w} \quad X_v(w) := \frac{w}{w + .622}$$

$$\mu_{av}(T_a, w) := \frac{X_a(w) \cdot \mu_a(T_a) \cdot M_a^{.5} + X_v(w) \cdot \mu_v(T_a) \cdot M_v^{.5}}{X_a(w) \cdot M_a^{.5} + X_v(w) \cdot M_v^{.5}}$$

Thermal conductivity

$$k_{av}(T_a, w) := \frac{X_a(w) \cdot k_a(T_a) \cdot M_a^{.33} + X_v(w) \cdot k_v(T_a) \cdot M_v^{.33}}{X_a(w) \cdot M_a^{.33} + X_v(w) \cdot M_v^{.33}}$$

#### A.4 Functions for the thermophysical properties of water:

Density

$$\rho_w(T_w) := \left( 1.49343 \cdot 10^{-3} - 3.7164 \cdot 10^{-6} \cdot T_w + 7.09782 \cdot 10^{-9} \cdot T_w^2 - 1.90321 \cdot 10^{-20} \cdot T_w^6 \right)^{-1}$$

Specific heat

$$c_{pw}(T_w) := \left( 8.15599 \cdot 10^3 - 2.80627 \cdot 10 \cdot T_w + 5.11283 \cdot 10^{-2} \cdot T_w^2 - 2.17582 \cdot 10^{-13} \cdot T_w^6 \right)$$

Dynamic viscosity

$$\mu_w(T_w) := 2.414 \cdot 10^{-5} \cdot 10^{\frac{247.8}{T_w - 140}}$$

Thermal conductivity

$$k_w(T_w) := -6.14255 \cdot 10^{-1} + 6.9962 \cdot 10^{-3} \cdot T_w - 1.01075 \cdot 10^{-5} \cdot T_w^2 + 4.74737 \cdot 10^{-12} \cdot T_w^4$$

**Appendix B - Thermal design sample calculation****Input parameters**

<b>Description</b>	<b>Symbol and value</b>	<b>Units</b>
<b><u>Initial values</u></b>		
Assumed initial water velocity	$v_{wi} = 2$	$\frac{m}{s}$
Assumed initial air face velocity	$v_{ai} = 3$	$\frac{m}{s}$
<b><u>Water Data</u></b>		
Flow rate	$m_w = 98.75$	$\frac{kg}{s}$
Inlet Temperature	$T_{wi} = 353.15$	K
Outlet temperature	$T_{wo} = 318.15$	K
<b><u>Ambient Conditions</u></b>		
Air gas constant	$R_{air} = 287.08$	$\frac{J}{kgK}$
Ambient temperature at ground level	$T_{a1} = 293.15$	K
Atmospheric pressure at ground level	$p_{a1} = 1 \times 10^5$	Pa
Temperature at inlet of heat exchanger	$T_{a5} = 293.111$	K
<b><u>Tube Geometry</u></b>		
Tube outside diameter	$d_o = 0.0254$	m
Tube wall thickness	$t_w = 2.11 \times 10^{-3}$	m
Tube thermal conductivity	$k_t = 58$	$\frac{W}{mK}$
Transverse pitch	$P_{tr} = 0.0635$	m
Finned tube length	$L_t = 9$	m
Number of tube rows	$n_r = 4$	
Number of passes	$n_p = 4$	
<b><u>Fin Geometry</u></b>		
Fin outside diameter	$d_{fo} = 0.057$	m
Fin root diameter	$d_r = 0.0254$	m

Uniform fin thickness	$t_f = 4.06 \times 10^{-4}$	m
Fin thermal conductivity	$k_f = 230$	$\frac{W}{mK}$
Fins per inch	$f_{pi} = 10$	

### **Heights and losses**

Number of supports	$n_{ts} = 8$	
Diameter of supports	$d_{ts} = 0.2$	m
Support coefficient of drag (Figure 2.5.1)	$C_{Dts} = 1.25$	
Height of windwall (i.e. no windwall)	$H_w = 0$	m
Dry Adiabatic Lapse Rate	$DALR = 9.75 \times 10^{-3}$	$\frac{K}{m}$
Upstream loss coefficient (Figure 6.4.1)	$K_{up} = 0.6$	
Downstream loss coefficient (Figure 6.4.2)	$K_{do} = 0.05$	
Conical shroud inlet loss coefficient (Figure 6.4.7)	$K_{Fsi} = 0.1$	

### **Fan Installation Specifications**

Number of fans per bay	$n_{Fbay} = 2$	
Fan diameter	$d_F = 3.8678$	m
	$d_{ft} = 12.6895$	ft
Fan tip clearance	$t_{fan} = 0.019$	m
Fan hub diameter	$d_h = 0.4$	m
Fan rotational speed	$N_F = 260.3911$	rpm

### **Fan Reference data**

Reference fan rotational speed	$N_{Fr} = 216$	rpm
Reference air density	$\rho_r = 1$	$\frac{kg}{m^3}$
Reference fan diameter	$d_{Fr} = 4.265$	m
	$d_{fr} = 13.9926$	ft

### **Reference fan curve**

The reference fan static pressure can be calculated as follows:

$$\Delta P_{FSR} := \left( a_1 + b_1 \cdot V_{Fr} + c_1 \cdot V_{Fr}^2 + d_1 \cdot V_{Fr}^3 \right)$$

where:

$$a_1 := 140.224$$

$$b_1 := 0.877$$

$$c_1 := -0.01$$

$$d_1 := 1.5075 \cdot 10^{-5}$$

Fan shaft power at the reference condition:

$$P_{Fr} := \left[ a_2 + b_2(V_{Fr}) + c_2 \cdot V_{Fr}^2 + d_2 \cdot V_{Fr}^3 + e_2 \cdot V_{Fr}^4 \right]$$

where:

$$a_2 := 31.62$$

$$b_2 := -0.990$$

$$c_2 := 0.01$$

$$d_2 := -1.4427 \cdot 10^{-4}$$

$$e_2 := 3.7075 \cdot 10^{-7}$$

### **Nozzle data**

Inlet nozzle size	$d_{Ni} = 4$	inch
Outlet nozzle size	$d_{No} = 4$	inch
Inlet nozzle inside diameter	$d_{ni} = 0.0873$	m
Outlet nozzle inside diameter	$d_{no} = 0.0873$	m
Number of inlet nozzles	$n_{Ni} = 2$	
Number of outlet nozzles	$n_{No} = 2$	

### **Iteration Parameters**

Outlet air temperature	$T_{a6} = 323.2878$	K
Air mass flow rate	$m_a = 475.9472$	$\frac{kg}{s}$
Final water velocity	$v_w = 1.4244$	$\frac{m}{s}$
Final air velocity	$v_a = 3.5841$	$\frac{m}{s}$
Number of bundles per bay	$n_b = 2$	
Number of bays	$n_{bay} = 2$	

### Water properties at mean temperature

Arithmetic mean temperature

$$T_{wm} := \frac{T_{wi} + T_{wo}}{2} \quad T_{wm} = 335.65 \quad \text{K}$$

Specific heat using Equation A.4.2  $c_{pw}(T_{wm}) = 4.1858 \times 10^3 \quad \frac{\text{J}}{\text{kgK}}$

Thermal conductivity using Equation A.4.4  $k_w(T_{wm}) = 0.6556 \quad \frac{\text{W}}{\text{mK}}$

Dynamic viscosity using Equation A.4.3  $\mu_w(T_{wm}) = 4.4595 \times 10^{-4} \quad \frac{\text{kg}}{\text{ms}}$

Density using Equation A.4.1  $\rho_w(T_{wm}) = 981.8819 \quad \frac{\text{kg}}{\text{m}^3}$

Prandtl number

$$\text{Pr}_w := \frac{c_{pw}(T_{wm}) \cdot \mu_w(T_{wm})}{k_w(T_{wm})} \quad \text{Pr}_w = 2.8474$$

### Air properties at mean temperature

Arithmetic mean air temperature

$$T_{am} := \frac{T_{a5} + T_{a6}}{2} \quad T_{am} = 308.1994 \quad \text{K}$$

Properties of air flowing through the heat exchanger evaluated at the arithmetic mean temperature (using equations in Appendix A.1):

Specific heat using Equation A.1.2  $c_{pa}(T_{am}) = 1.0073 \times 10^3 \quad \frac{\text{J}}{\text{kgK}}$

Dynamic viscosity using Equation A.1.3  $\mu_a(T_{am}) = 1.8844 \times 10^{-5} \quad \frac{\text{kg}}{\text{ms}}$

Thermal conductivity using Equation A.1.4  $k_a(T_{am}) = 0.0269 \quad \frac{\text{W}}{\text{mK}}$

Prandtl number

$$\text{Pr}_{am} := \frac{c_{pa}(T_{am}) \cdot \mu_a(T_{am})}{k_a(T_{am})} \quad \text{Pr}_{am} = 0.7068$$



**Geometry Calculation**

Fin pitch

$$P_f := \frac{d_r}{f_{pi}} \quad P_f = 2.54 \times 10^{-3} \quad \text{m}$$

Longitudinal pitch

$$P_l := \cos\left(\frac{30}{180} \cdot \pi\right) \cdot P_{tr} \quad P_l = 0.055 \quad \text{m}$$

Diagonal pitch

$$P_d := \sqrt{\left(\frac{P_{tr}}{2}\right)^2 + P_l^2} \quad P_d = 0.0635 \quad \text{m}$$

Inside tube diameter

$$d_i := d_o - 2 \cdot t_w \quad d_i = 0.0212 \quad \text{m}$$

Estimated flow area required per pass

$$A_{req} := \frac{\dot{m}_w}{\rho_w(T_{wm}) \cdot v_w} \quad A_{req} = 0.0706 \quad \text{m}^2$$

Cross-sectional flow area per tube

$$A_t := \frac{\pi}{4} \cdot d_i^2 \quad A_t = 3.5232 \times 10^{-4} \quad \text{m}^2$$

Total number of tubes required per pass

$$n_{t,req} = \left\lceil \frac{A_{req}}{A_t} \right\rceil \quad n_{t,req} = 201$$

Total number of tubes per pass per bay

$$n_{t,bay} = \left\lceil \frac{n_{t,req}}{n_{bay}} \right\rceil \quad n_{t,bay} = 101$$

Number of tubes per pass per bundle

$$n_{tp} = \left\lceil \frac{n_{t,bay}}{n_b} \right\rceil \quad n_{tp} = 50$$

Ratio of tube passes to tube rows

$$p_r := \frac{n_r}{n_p} \quad p_r = 1$$

Number of tubes per row per bundle

$$n_{tr} := \frac{n_{tp}}{p_r} \quad n_{tr} = 50$$

Number of tubes per bundle

$$n_{tb} := n_{tr} \cdot n_r \quad n_{tb} = 200$$

Width of bundle

$$W := d_{fo} + (n_{tr} - 0.5) \cdot p_{tr} \quad W = 3.2003 \quad m$$

Frontal area per bundle

$$A_{fr} := W \cdot L_t \quad A_{fr} = 28.8023 \quad m^2$$

Total frontal area

$$A_{ftr} := A_{fr} \cdot n_b \cdot n_{bay} \quad A_{ftr} = 115.209 \quad m^2$$

Total tube length

$$L_{tot} := n_b \cdot n_{bay} \cdot n_{tr} \cdot n_r \cdot L_t \quad L_{tot} = 7.2 \times 10^3 \quad m$$

## Energy Equation

Reynolds number

$$Re_w := \frac{\rho_w(T_{wm}) \cdot v_w \cdot d_i}{\mu_w(T_{wm})} \quad Re_w = 6.6424 \times 10^4$$

Friction factor (Filonenko, 1954) from Equation 2.2.10

$$f_D := (1.82 \log(Re_w) - 1.64)^{-2} \quad f_D = 0.0196$$

Nusselt number (Gnielinski, 1975) from Equation 3.2.29

$$Nu_w := \frac{\left(\frac{f_D}{8}\right) \cdot (Re_w - 1000) \cdot Pr_w \cdot \left[1 + \left(\frac{d_i}{L_{tot}}\right)^{0.67}\right]}{1 + 12.7 \left(\frac{f_D}{8}\right)^{0.5} \cdot (Pr_w^{0.67} - 1)} \quad Nu_w = 278.9729$$

Water heat transfer coefficient

$$h_w := \frac{k_w(T_{wm}) \cdot Nu_w}{d_i} \quad h_w = 8.6347 \times 10^3 \quad \frac{W}{m^2 K}$$

Minimum flow are through bundle

$$A_c := A_{\text{frt}} - \frac{(n_{\text{tr}} \cdot L_t \cdot n_b \cdot n_{\text{bay}}) \cdot [d_{\text{fo}} \cdot t_f + (P_f - t_f) \cdot d_r]}{P_f} \quad A_c = 60.3972 \quad \text{m}^2$$

Air mass velocity from Equation 2.1.4

$$G_c := \frac{\dot{m}_a}{A_c} \quad G_c = 7.8803 \quad \frac{\text{kg}}{\text{m}^2 \cdot \text{s}}$$

Air-side Reynolds number

$$\text{Re}_a := \frac{G_c \cdot d_r}{\mu_a(T_{\text{am}})} \quad \text{Re}_a = 1.0622 \times 10^4$$

Ratio: Air-side area to root area  $\left(\frac{A}{A_r}\right)$  from Equation 5.5.4

$$A_{\text{Ar}} := \frac{\left(\frac{d_{\text{fo}}^2 - d_r^2}{2}\right) + d_{\text{fo}} \cdot t_f + d_r \cdot (P_f - t_f)}{d_r \cdot P_f} \quad A_{\text{Ar}} = 21.3787 \quad \text{m}^2$$

Air-side Nusselt number (Ganguli, 1985) from Equation 5.5.4

$$\text{Nu}_a := 0.38 \text{Re}_a^{0.6} \cdot \text{Pr}_{\text{am}}^{0.333} \cdot A_{\text{Ar}}^{-0.15} \quad \text{Nu}_a = 55.6966$$

Air-side heat transfer coefficient

$$h_a := \frac{k_a(T_{\text{am}}) \cdot \text{Nu}_a}{d_r} \quad h_a = 58.8845 \quad \frac{\text{W}}{\text{m}^2 \cdot \text{K}}$$

Fin efficiency parameter b from Equation 3.3.4

$$b := \sqrt{2 \cdot \frac{h_a}{k_f \cdot t_f}} \quad b = 35.5131 \quad \text{m}^{-1}$$

Fin efficiency parameter  $\phi$  from Equation 3.3.13

$$\phi := \left(\frac{d_{\text{fo}}}{d_r} - 1\right) \cdot \left(1 + 0.35 \ln\left(\frac{d_{\text{fo}}}{d_r}\right)\right) \quad \phi = 1.5961$$

Fin efficiency from Equation 3.3.12

$$\eta_f := \frac{\tanh\left(\frac{b \cdot d_r \cdot \phi}{2}\right)}{\frac{b \cdot d_r \cdot \phi}{2}} \quad \eta_f = 0.8569$$

Exposed root area per fin

$$A_{r,\text{fin}} := \pi \cdot (P_f - t_f) \cdot d_r \quad A_{r,\text{fin}} = 1.7029 \times 10^{-4} \quad \text{m}^2$$

Exposed area per fin

$$A_{f,\text{fin}} := \frac{2 \cdot \pi}{4} \cdot (d_{fo}^2 - d_r^2) + \pi \cdot d_{fo} \cdot t_f \quad A_{f,\text{fin}} = 4.1628 \times 10^{-3} \quad \text{m}^2$$

Total exposed area per fin

$$A_{\text{fin}} := A_{r,\text{fin}} + A_{f,\text{fin}} \quad A_{\text{fin}} = 4.3331 \times 10^{-3} \quad \text{m}^2$$

Total air-side heat transfer area

$$A_a := \frac{L_t \cdot n_b \cdot n_{\text{bay}} \cdot n_r \cdot n_{tr} \cdot A_{\text{fin}}}{P_f} \quad A_a = 1.2283 \times 10^4 \quad \text{m}^2$$

Surface effectiveness from Equation 3.3.11

$$e_f := 1 - \frac{A_{f,\text{fin}} \cdot (1 - \eta_f)}{A_{\text{fin}}} \quad e_f = 0.8625$$

Total water-side heat transfer area

$$A_w := \pi \cdot n_r \cdot n_{tr} \cdot n_b \cdot n_{\text{bay}} \cdot L_t \cdot d_i \quad A_w = 479.0803 \quad \text{m}^2$$

Overall heat transfer coefficient times Area from Equation 3.1.26

$$UA := \left( \frac{1}{h_a \cdot e_f \cdot A_a} + \frac{\ln\left(\frac{d_o}{d_i}\right)}{2 \cdot \pi \cdot k_t \cdot L_{\text{tot}}} + \frac{1}{h_w \cdot A_w} \right)^{-1} \quad UA = 5.2246 \times 10^5 \quad \frac{\text{W}}{\text{K}}$$

Overall heat transfer coefficient based on air-side area

$$U_a := \frac{UA}{A_a} \quad U_a = 42.5357 \quad \frac{\text{W}}{\text{m}^2 \text{K}}$$

Water heat capacity rate

$$C_w := m_w \cdot c_{pw}(T_{wm}) \quad C_w = 4.1335 \times 10^5 \quad \frac{\text{W}}{\text{K}}$$

Air heat capacity rate

$$C_a := m_a \cdot c_{pa}(T_{am}) \quad C_a = 4.7941 \times 10^5 \quad \frac{\text{W}}{\text{K}}$$

Minimum heat capacity rate

$$C_{\text{min}} := \min(C_w, C_a) \quad C_{\text{min}} = 4.1335 \times 10^5 \quad \frac{\text{W}}{\text{K}}$$

Maximum heat capacity rate

$$C_{\max} := \max(C_w, C_a) \quad C_{\max} = 4.7941 \times 10^5 \quad \frac{\text{W}}{\text{K}}$$

Number of transfer units

$$\text{NTU} := \frac{UA}{C_{\min}} \quad \text{NTU} = 1.264$$

Heat capacity ratio

$$C_r := \frac{C_{\min}}{C_{\max}} \quad C_r = 0.8622$$

Effectiveness according to Table 3.5.1 for Counterflow

$$e := \frac{1 - \exp[-\text{NTU} \cdot (1 - C_r)]}{1 - C_r \cdot \exp[-\text{NTU} \cdot (1 - C_r)]} \quad e = 0.58$$

Rate of heat transfer according to Equation 8.1.2 in terms of the effectiveness of the heat exchanger

$$Q_e := e \cdot C_{\min} \cdot (T_{wi} - T_{a5}) \quad Q_e = 1.4393 \times 10^7 \quad \text{W}$$

Air-side heat transfer rate according to Equation 8.1.1

$$Q_a := m_a \cdot c_{pa} \cdot (T_{a6} - T_{a5}) \quad Q_a = 1.4467 \times 10^7 \quad \text{W}$$

Process-side heat transfer rate according to Equation 8.1.1

$$Q_p := m_w \cdot c_{pw} \cdot (T_{wi} - T_{wo}) \quad Q_p = 1.4467 \times 10^7 \quad \text{W}$$

### LMTD method

Logarithmic mean temperature difference from Equation 3.5.8

$$\Delta T_{\text{lm}} := \frac{(T_{wi} - T_{a6}) - (T_{wo} - T_{a5})}{\ln\left(\frac{T_{wi} - T_{a6}}{T_{wo} - T_{a5}}\right)} \quad \Delta T_{\text{lm}} = 27.3798$$

Dimensionless temperature changes of the two streams defined by Equations B.3 and B.4

$$\phi_1 := \frac{T_{wi} - T_{wo}}{T_{wi} - T_{a5}} \quad \phi_1 = 0.583$$

$$\phi_2 := \frac{T_{a6} - T_{a5}}{T_{wi} - T_{a5}} \quad \phi_2 = 0.5026$$

Dimensionless mean temperature difference for counter flow from Equation B.5

$$\phi_3 := \frac{\phi_1 - \phi_2}{\ln\left(\frac{1 - \phi_2}{1 - \phi_1}\right)} \quad \phi_3 = 0.456$$

Where matrix needed for temperature correction factor from Table B.7

$$a := \begin{pmatrix} -3.39 \cdot 10^{-1} & 2.77 \cdot 10^{-2} & 1.79 \cdot 10^{-1} & -1.99 \cdot 10^{-2} \\ 2.38 \cdot 10^0 & -9.99 \cdot 10^{-2} & -1.21 & 4 \cdot 10^{-2} \\ 5.62 \cdot 10^0 & 9.04 \cdot 10^{-2} & 2.62 & 4.94 \cdot 10^{-2} \\ 3.9 \cdot 10^0 & -8.54 \cdot 10^{-4} & -1.81 & -9.81 \cdot 10^{-2} \end{pmatrix}$$

Temperature correction factor from Equation B.6

$$F_t = \sum_{i=0}^3 \sum_{k=0}^3 \left[ a_{i,k} \cdot (1 - \phi_3)^k \cdot \sin\left(2 \cdot i \cdot \text{atan}\left(\frac{\phi_1}{\phi_2}\right)\right) \right] \quad F_t = 1$$

Heat transfer based on LMTD from Equation 3.5.16

$$Q_{\text{EMTD}} := F_t \cdot UA \cdot \Delta T_{\text{lmr}} \quad Q_{\text{EMTD}} = 1.4305 \times 10^7$$

### Draft Equation

Plenum height

$$H_{\text{pl}} := \begin{cases} 0.6 & \text{if } d_F < 1.828 \\ 1 & \text{otherwise} \end{cases} \quad H_{\text{pl}} = 1 \quad \text{m}$$

Fan height above ground level according to Equation 8.3.2

$$X_1 := -\ln(0.985 - 0.96) \quad X_1 = 3.6889$$

$$H_3 := \max\left(d_F, \frac{6.35 d_F X_1}{1 + \frac{45}{n_{\text{Fbay}}}}\right) \quad H_3 = 4 \quad \text{m}$$

Height at outlet of heat exchanger

$$H_6 := H_3 + H_{\text{pl}} \quad H_6 = 5 \quad \text{m}$$

Approximate air temperature at the fan inlet, according to Equation 8.1.16:

$$T_{a3} := T_{a1} - \text{DALR} \cdot H_3 \quad T_{a3} = 293.111 \quad \text{K}$$

Corresponding density from Equation 8.1.11:

$$\rho_{a3} := \frac{p_{a1}}{R_{air} \cdot T_{a3}} \quad \rho_{a3} = 1.1884 \quad \frac{\text{kg}}{\text{m}^3}$$

Air density at heat exchanger inlet from Equation 8.1.12

$$\rho_{a5} := \frac{p_{a1}}{R_{air} \cdot T_{a5}} \quad \rho_{a5} = 1.1884 \quad \frac{\text{kg}}{\text{m}^3}$$

Air density at heat exchanger outlet

$$\rho_{a6} := \frac{p_{a1}}{R_{air} \cdot T_{a6}} \quad \rho_{a6} = 1.0775 \quad \frac{\text{kg}}{\text{m}^3}$$

Average air density through heat exchanger from Equation 8.1.13

$$\rho_{a56} := \frac{2 \cdot p_{a1}}{R_{air} \cdot (T_{a5} + T_{a6})} \quad \rho_{a56} = 1.1302 \quad \frac{\text{kg}}{\text{m}^3}$$

Corresponding specific heat according to Appendix A.1:

$$c_{pa}(T_{a3}) = 1.0067 \times 10^3 \quad \frac{\text{J}}{\text{kgK}}$$

Total number of fans

$$n_{F,tot} := n_{Fbay} \cdot n_{bay} \quad n_{F,tot} = 4$$

Actual volume flow rate through each fan is:

$$V_F := \frac{\dot{m}_a}{\rho_{a3} \cdot n_{F,tot}} \quad V_F = 100.123 \quad \frac{\text{m}^3}{\text{s}}$$

Fan laws were employed, since the conditions are not the same as at the fan reference condition:

Volume flow rate from Equation 6.2.1:

$$V_{Fr} := V_F \left( \frac{N_{Fr}}{N_F} \right) \cdot \left( \frac{d_{Fr}}{d_F} \right)^3 \quad V_{Fr} = 111.3587 \quad \frac{\text{m}^3}{\text{s}}$$

At this flow rate the reference fan static pressure is:

$$\Delta P_{FSr} := \left( a_1 + b_1 \cdot V_{Fr} + c_1 \cdot V_{Fr}^2 + d_1 \cdot V_{Fr}^3 \right) \quad \Delta P_{FSr} = 85.1595 \quad \text{Pa}$$

Actual change in fan static pressure from Equation 6.2.2:

$$\Delta P_{Fs} := \Delta P_{FSr} \cdot \left( \frac{N_F}{N_{Fr}} \right)^2 \cdot \left( \frac{\rho_{a3}}{\rho_r} \right) \cdot \left( \frac{d_F}{d_{Fr}} \right)^2 \quad \Delta P_{Fs} = 120.958 \quad \text{Pa}$$

Fan shaft power at the reference condition:

$$P_{Fr} := \left[ a_2 + b_2(V_{Fr}) + c_2 \cdot V_{Fr}^2 + d_2 \cdot V_{Fr}^3 + e_2 \cdot V_{Fr}^4 \right] \quad P_{Fr} = 14.7372 \quad \text{W}$$

Actual fan shaft power from Equation 6.2.3:

$$P_F := P_{Fr} \cdot \left( \frac{N_F}{N_{Fr}} \right)^3 \cdot \left( \frac{\rho_{a3}}{\rho_r} \right) \cdot \left( \frac{d_F}{d_{Fr}} \right)^5 \quad P_F = 18.8202 \quad \text{W}$$

Actual tip clearance from Equation 6.2.10

$$t_{Fan} := t_{fan} \cdot \left( \frac{d_F}{d_{Fr}} \right)^{0.8} \cdot \left( \frac{P_F}{P_{Fr}} \right)^{0.1} \quad t_{Fan} = 0.018 \quad \text{m}$$

Total fan casing area:

$$A_{fc} := \frac{\pi}{4} \cdot n_{F,tot} \cdot (d_F + 2 \cdot t_{Fan})^2 \quad A_{fc} = 47.8772 \quad \text{m}^2$$

Flow area into support structure

$$A_2 := H_3 \cdot [2 \cdot (L_t + W \cdot n_{bay} \cdot n_b) - n_{ts} \cdot d_{ts}] \quad A_2 = 168.008 \quad \text{m}^2$$

Support loss coefficient from Equation 2.6.9

$$K_{ts} := \frac{H_3 \cdot n_{ts} \cdot d_{ts} \cdot C_{Dts}}{A_2} \quad K_{ts} = 0.0476$$

Fan static pressure rise coefficient from Equation 8.1.7

$$K_{Fs} := 2 \cdot \Delta P_{Fs} \cdot \frac{\rho_{a3}}{\left( \frac{m_a}{A_{fc}} \right)^2} \quad K_{Fs} = 2.9092$$

Characteristic flow parameter from Equation 5.4.11

$$Ry := \frac{m_a}{A_{frt} \cdot \mu_a(T_{am})} \quad Ry = 2.1923 \times 10^5$$

Plenum recovery factor, according to section 6.4.2:

$$K_{rec} := 0.3 \quad \text{since} \quad 15 \leq K_{he} \leq 24$$

$$\frac{H_{pl}}{d_c} > 0.3$$



Heat Exchanger Pressure drop (Robinson and Briggs, 1966) from Equation 5.5.6

$$Eu := 18.93 n_r Re_a^{-0.316} \left( \frac{P_{tr}}{d_r} \right)^{-0.927} \left( \frac{P_{tr}}{P_d} \right)^{0.515} \quad Eu = 1.73$$

Pressure drop

$$D_{he} := \frac{Eu \cdot G_c^2}{\rho_{a56}} \quad D_{he} = 95.052$$

Heat exchanger loss coefficient from Equation 5.4.3

$$K_{he} := \frac{2 \cdot D_{he} \cdot \rho_{a56}}{\left( \frac{m_a}{A_{frit}} \right)^2} \quad K_{he} = 12.5896$$

Corresponding heat exchanger outlet kinetic energy correction factor, according to Equation 6.4.5:

$$\alpha_{e6} := 1.6 - 0.48 \frac{A_{fc}}{A_{frit}} - 0.012 K_{he} \quad \alpha_{e6} = 1.2495$$

Heat exchanger effectiveness due to maldistribution of the air-side flow, using Equation 5.10.1:

$$e_{nu} := 1.05 - 0.05 \alpha_{e6} \quad e_{nu} = 0.9875$$

Effective fan area:

$$A_e := n_{F,tot} \frac{\pi}{4} \left[ (d_F + 2t_{Fan})^2 - d_h^2 \right] \quad A_e = 47.3746 \quad m^2$$

Since no windwall is present,

LHS = 0, Equation 8.1.9:

$$H_7 := H_6 + H_w \quad H_7 = 5$$

$$LHS := p_{a1} \left[ \left( 1 - DALR \cdot \frac{H_7 - H_6}{T_{a6}} \right)^{3.5} - \left( 1 - DALR \cdot \frac{H_7 - H_6}{T_{a1}} \right)^{3.5} \right]$$

$$LHS = 0$$

RHS of draft equation is given by Equation 8.1.9:

$$\begin{aligned} \text{RHS} := & K_{ts} \cdot \frac{\left(\frac{m_a}{A_2}\right)^2}{2 \cdot \rho_{a3}} + K_{Fsi} \cdot \frac{\left(\frac{m_a}{A_{fc}}\right)^2}{2 \cdot \rho_{a3}} + K_{up} \cdot \frac{\left(\frac{m_a}{A_e}\right)^2}{2 \cdot \rho_{a3}} - (K_{Fs} + K_{rec}) \cdot \left[ \frac{\left(\frac{m_a}{A_{fc}}\right)^2}{2 \cdot \rho_{a3}} \right] \dots \\ & + K_{do} \cdot \frac{\left(\frac{m_a}{A_e}\right)^2}{2 \cdot \rho_{a3}} + D_{he} + \alpha_{e6} \cdot \frac{\left(\frac{m_a}{A_{frt}}\right)^2}{2 \cdot \rho_{a6}} \end{aligned}$$

$$\text{RHS} = 3.4368$$

$$\text{diff} := \text{RHS} - \text{LHS}$$

$$\text{diff} = 3.4368$$

### Tube side pressure drop

Flow area of nozzle inlet

$$A_{Ni} := \frac{\pi \cdot d_{ni}^2}{4} \quad A_{Ni} = 5.9885 \times 10^{-3} \quad \text{m}^2$$

Inlet velocity

$$v_{12} := \frac{m_w}{\rho_w(T_{wi}) \cdot A_{Ni} \cdot n_{Ni} \cdot n_b \cdot n_{bay}} \quad v_{12} = 2.1216 \quad \frac{\text{m}}{\text{s}}$$

Inlet nozzle pressure drop

$$K_{12} := 1.0 \quad (\text{Fried and Idelchik})$$

$$\Delta p_{12} := \frac{K_{12} \cdot \rho_w(T_{wi}) \cdot v_{12}^2}{2} \quad \Delta p_{12} = 2.3177 \times 10^3$$

Flow area of nozzle outlet

$$A_{No} := \frac{\pi \cdot d_{no}^2}{4} \quad A_{No} = 5.9885 \times 10^{-3} \quad \text{m}^2$$

Outlet velocity

$$v_{56} := \frac{m_w}{\rho_w(T_{wo}) \cdot A_{No} \cdot n_{No} \cdot n_b \cdot n_{bay}} \quad v_{56} = 2.0814 \quad \frac{\text{m}}{\text{s}}$$

Area ratio of outlet nozzle

$$\sigma_{56} := 0$$

Jet contraction ratio

$$\sigma_c := 0.61375 + 0.13318\sigma_{56} - 0.26095\sigma_{56}^2 + 0.51145\sigma_{56}^3$$

Loss coefficient

$$K_c := 1 - \frac{2}{\sigma_c} + \frac{1}{\sigma_c^2} \quad K_c = 0.3961$$

Outlet nozzle pressure drop

$$\Delta p_{56} := \frac{\rho_w (T_{wi}) v_{56}^2}{2} \cdot \left[ (1 - \sigma_{56}^2) + K_c \right] \quad \Delta p_{56} = 2.9379 \times 10^3$$

Area ratio of tube entrance and tube exit

$$\sigma_{23} := 0$$

$$\sigma_{45} := 0$$

Entrance loss coefficient

$$K_{c23} := 1 - \frac{2}{\sigma_c} + \frac{1}{\sigma_c^2} \quad K_{c23} = 0.3961$$

Pressure drop across tube entrance

$$\Delta p_{23} := \frac{\rho_w (T_{wm}) \cdot v_w^2}{2} \cdot \left[ (1 - \sigma_{23}^2) + K_{c23} \right] \quad \Delta p_{23} = 1.3905 \times 10^3$$

Pressure drop across tube exit

$$K_{45} := 1.0 \quad (\text{the same as expansion coefficient of nozzle inlet})$$

$$\Delta p_{45} := \frac{K_{45} \cdot \rho_w (T_{wm}) \cdot v_w^2}{2} \quad \Delta p_{45} = 1.0558 \times 10^3$$

Frictional pressure drop inside tubes

$$\Delta p_{f34} := \frac{f_D \cdot n_p \cdot L_t \cdot \rho_w (T_{wm}) \cdot v_w^2}{2 \cdot d_i} \quad \Delta p_{f34} = 3.324 \times 10^4$$

Nozzle-to-nozzle pressure drop across the bundle

$$\Delta p_{16} = \Delta p_{12} + \Delta p_{23} + \Delta p_{f34} + \Delta p_{45} + \Delta p_{56}$$

$$\Delta p_{16} = 48.28 \text{ kPa}$$

## Appendix C - Mechanical design sample calculation

### Input parameters

	Symbol and value	Unit
<b><u>General</u></b>		
Design Temperature	$T_1 = 150$	°C
Design Pressure	$P_1 = 2.7$	MPa
Corrosion Allowance	$C_a = 3$	
Short side ligament efficiency	$E_1 = 0.5$	
Attachment Factor	$C_{af} = 0.2$	
<b><u>Geometry - header</u></b>		
Plug hole diameter	$d_h = 28.575$	mm
Tube outside diameter	$d_{to} = 25.4$	mm
Tube wall thickness	$t_w = 2.77$	mm
Tube length	$t_l = 6300$	mm
Tube pitch (transversal)	$p_t = 63.5$	mm
Tube pitch (longitudinal)	$p_l = 68$	mm
Number of tubes per bundle	$n_t = 258$	
Number of rows per bundle	$n_r = 6$	
Number of passes	$n_p = 6$	
Number of stay plates	$n_{st} = 3$	
Number of compartments	$n_c = 4$	
Side plate (short) thickness	$t_1 = 30$	mm
Gasket depth	$g = 2.5$	mm
Tube sheet (long) plate thickness	$t_2 = 27.5$	mm

End plate thickness	$t_3 = 16$	mm
Header joint Efficiency	$E_{hj} = 1$	
Partition plate thickness	$t_p = 12$	mm
Spacing between header plate and tube	$S_{tt} = 30$	mm
Sum of the number of tube rows minus one	$n_1 = 2$	
Max number of tube rows inside any compartment	$n_{co} = 1$	

### **Geometry - process nozzles**

Outside diameter	$d_o = 88.9$	mm
Wall thickness	$t = 9.74$	mm
Nozzle joint efficiency	$E_{nj} = 1$	

### **Loads**

Force in the x-direction	$F_x = 6000$	N
Force in the y-direction	$F_y = 5070$	N
Force in the z-direction	$F_z = 6000$	N
Moment in the x-direction	$M_x = 1230$	Nm
Moment in the y-direction	$M_y = 1830$	Nm
Moment in the z-direction	$M_z = 1230$	Nm

### **Allowable stresses**

Nozzle at design temperature	$S_n = 117.9$	MPa
Plug material at design temperature	$S_{dp} = 137.9$	MPa
Reinforcement element at design temperature	$S_p = 117.9$	MPa
Header at design temperature	$S_d = 137.9$	MPa
Tube material	$S_a = 92.4$	MPa

### Overall Header Geometry

Side plate length

$$H := \max \left[ \text{ceil} \left[ 2 \left( \frac{d_o}{2} - t + C_a + \max \left( 12, \frac{t_1}{2} \right) \right) \right], d_o + 10 \right] \quad H = 106 \quad \text{mm}$$

Tubesheet length

$$L := n_1 \cdot p_1 + n_{st} \cdot (2 \cdot S_{tt} + t_p) + 2 \cdot S_{tt} \quad L = 412 \quad \text{mm}$$

### Corroded Conditions

Side plate thickness

$$t_{1\text{corr}} := t_1 - C_a \quad t_{1\text{corr}} = 27 \quad \text{mm}$$

Tube sheet thickness

$$t_{2\text{corr}} := t_2 - C_a \quad t_{2\text{corr}} = 24.5 \quad \text{mm}$$

Partition plate thickness

$$t_{p\text{corr}} := t_p - 2 \cdot C_a \quad t_{p\text{corr}} = 6 \quad \text{mm}$$

Side plate length

$$H_{\text{corr}} := H + 2 \cdot C_a \quad H_{\text{corr}} = 112 \quad \text{mm}$$

Effective Tube sheet length

$$L_{\text{eff}} := (n_{co} \cdot p_1 + 2 \cdot S_{tt} + 2 \cdot C_a) \cdot n_c + n_{st} \cdot t_{p\text{corr}} \quad L_{\text{eff}} = 554 \quad \text{mm}$$

Distance to stay plate

$$h := \frac{L_{\text{eff}} - n_{st} \cdot t_{p\text{corr}}}{n_c} \quad h = 134 \quad \text{mm}$$

Ligament efficiency

$$E_2 := \frac{p_t - d_h}{p_t} \quad E_2 = 0.55$$

### Header Design

Moment of inertia of short-side plate

$$I_1 := \frac{t_{1\text{corr}}^3}{12} \quad I_1 = 1640.25 \quad \text{mm}^4$$

Moment of inertia of long-side plate

$$I_2 := \frac{t_{2\text{corr}}^3}{12} \quad I_2 = 1225.5104 \quad \text{mm}^4$$

Rectangular vessel parameter

$$\alpha := \frac{H_{\text{corr}}}{h} \quad \alpha = 0.8358$$

Vessel parameter

$$K := \frac{I_2}{I_1} \cdot \alpha \quad K = 0.6245$$

### **Membrane Stress**

Side plate

$$S_{\text{ms}} := \frac{P_1 \cdot h}{2 \cdot t_{1\text{corr}} \cdot E_1} \left[ 3 - \left[ \frac{6 + K \cdot (11 - \alpha^2)}{3 + 5K} \right] \right] \quad S_{\text{ms}} = 12.988 \quad \text{MPa}$$

Tube sheet plate

$$S_{\text{ml}} := \frac{P_1 \cdot H_{\text{corr}}}{2 \cdot t_{2\text{corr}} \cdot E_2} \quad S_{\text{ml}} = 11.2208 \quad \text{MPa}$$

Stay plate

$$S_{\text{mst}} := \frac{P_1 \cdot h}{2 \cdot t_{\text{pcorr}}} \left[ \frac{6 + K \cdot (11 - \alpha^2)}{3 + 5K} \right] \quad S_{\text{mst}} = 61.2269 \quad \text{MPa}$$

### **Bending Stress**

Distance to extreme fibre

$$c_s := \frac{t_{1\text{corr}}}{2} \quad c_s = 13.5 \quad \text{mm}$$

$$c_1 := \frac{t_{2\text{corr}}}{2} \quad c_1 = 12.25 \quad \text{mm}$$

Side plate

$$S_{bN} := \frac{P_1 \cdot c_s}{24 \cdot I_1 \cdot E_1} \cdot \left[ -3 \cdot H_{\text{corr}}^2 + 2 \cdot h^2 \cdot \left( \frac{3 + 5 \cdot \alpha^2 \cdot K}{3 + 5 \cdot K} \right) \right] \quad S_{bN} = -13.4078 \quad \text{MPa}$$

$$S_{bQs} := \frac{P_1 \cdot h^2 \cdot c_s}{12 \cdot I_1} \cdot \left( \frac{3 + 5 \cdot \alpha^2 \cdot K}{3 + 5 \cdot K} \right) \quad S_{bQs} = 28.1405 \quad \text{MPa}$$

Tube sheet plate

$$S_{bM} := \frac{P_1 \cdot h^2 \cdot c_1}{12 \cdot I_2 \cdot E_2} \cdot \left[ \frac{3 + K \cdot (6 - \alpha^2)}{3 + 5 \cdot K} \right] \quad S_{bM} = 75.6831 \quad \text{MPa}$$

$$S_{bQl} := \frac{P_1 \cdot h^2 \cdot c_1}{12 \cdot I_2} \cdot \left( \frac{3 + 5 \cdot \alpha^2 \cdot K}{3 + 5 \cdot K} \right) \quad S_{bQl} = 34.1765 \quad \text{MPa}$$

**Total Stresses**

Side plate

$$S_{TN} := |S_{ms}| + |S_{bN}| \quad S_{TN} = 26.3958 \quad \text{MPa}$$

$$S_{TQs} := |S_{ms}| + |S_{bQs}| \quad S_{TQs} = 41.1286 \quad \text{MPa}$$

Tube sheet

$$S_{TM} := |S_{ml}| + |S_{bM}| \quad S_{TM} = 86.9039 \quad \text{MPa}$$

$$S_{TQl} := |S_{ml}| + |S_{bQl}| \quad S_{TQl} = 45.3973 \quad \text{MPa}$$

Stay plate

$$S_{Tst} := |S_{mst}| \quad S_{Tst} = 61.2269 \quad \text{MPa}$$

Allowable membrane stress

$$S_{ab} := S_{dp} \quad S_{ab} = 137.9 \quad \text{MPa}$$

Allowable total stress

$$S_{aT} := 1.5 S_{dp} \quad S_{aT} = 206.85 \quad \text{MPa}$$



## End Plate Design

End plate thickness

$$t_{3\text{corr}} := t_3 - C_a \qquad t_{3\text{corr}} = 13 \quad \text{mm}$$

Shortspan of tubesheet

$$d := \min(h, H_{\text{corr}}) \qquad d = 112 \quad \text{mm}$$

Long span of tubesheet

$$D := \max(h, H_{\text{corr}}) \qquad D = 134 \quad \text{mm}$$

Noncircular head factor

$$Z := \min\left[\left(3.4 - \frac{2.4d}{D}\right), (2.5)\right] \qquad Z = 1.394$$

Minimum required wall thickness according to UG-34 of ASME VIII div 1 (2007)

$$t_{3\text{min}} := d \cdot \sqrt{\frac{Z \cdot C_{af} \cdot P_1}{S_d \cdot E_{hj}}} + C_a \qquad t_{3\text{min}} = 11.275 \quad \text{mm}$$

## Nozzle Design

Thickness of nozzle

$$t_n := t - C_a \qquad t_n = 6.74 \quad \text{mm}$$

Inside diameter of nozzle

$$d_i := d_o - 2 \cdot t_n \qquad d_i = 75.42 \quad \text{mm}$$

Minimum required wall thickness (corroded) under internal pressure according to UG-27 of ASME VIII div 1 (2007)

$$t_m := \frac{P_1 \cdot d_i}{2 \cdot (S_n \cdot E_{nj} - 0.6 P_1)} + C_a \qquad t_m = 3.8756 \quad \text{mm}$$

Circumferential stress

$$S_h := \frac{P_1 \cdot d_i}{2 \cdot t_n} \qquad S_h = 15.1064 \quad \text{MPa}$$

## Cross sectional area

$$A_{\text{cross}} := \frac{\pi}{4} \cdot (d_o^2 - d_i^2) \quad A_{\text{cross}} = 1739.6833 \quad \text{mm}^2$$

Tensile stress due to  $F_y$ 

$$S_t := \frac{F_y}{A_{\text{cross}}} \quad S_t = 2.9143 \quad \text{MPa}$$

## Resultant moment

$$M_r := \sqrt{M_x^2 + M_z^2} \quad M_r = 1739.4827 \quad \text{MPa}$$

## Moment of inertia

$$I := \frac{\pi}{64} \cdot (d_o^4 - d_i^4) \quad I = 1477794.2646 \quad \text{MPa}$$

## Section modulus

$$Z_n := \frac{2 \cdot I}{d_o} \quad Z_n = 33246.2152 \quad \text{MPa}$$

## Bending stress

$$S_b := \frac{1000 M_r}{Z_n} \quad S_b = 52.3212 \quad \text{MPa}$$

## Resultant stress

$$S_r := S_h + S_t + S_b \quad S_r = 70.3419 \quad \text{MPa}$$

## Shear stresses

$$\tau_x := \frac{2 \cdot F_x}{\pi \cdot d_o \cdot t_n} \quad \tau_x = 6.3748 \quad \text{MPa}$$

$$\tau_y := \frac{2 \cdot F_y}{\pi \cdot d_o \cdot t_n} \quad \tau_y = 5.3867 \quad \text{MPa}$$

$$\tau_z := \frac{2000 M_y}{\pi \cdot d_o^2 \cdot t_n} \quad \tau_z = 21.871 \quad \text{MPa}$$

Resultant shear stress

$$\tau_r := \tau_x + \tau_y + \tau_z \quad \tau_r = 33.6325 \quad \text{MPa}$$

Equivalent stress

$$S_e := \sqrt{S_r^2 + 4 \cdot \tau_r^2} \quad S_e = 97.3272 \quad \text{MPa}$$

Allowable stress

$$S_n = 117.9 \quad S_n = 117.9 \quad \text{MPa}$$

## Tube-to-tubesheet welds

Fillet weld leg

$$a_f = 1 \quad \text{mm}$$

Groove weld leg

$$a_g = 3 \quad \text{mm}$$

Length of combined weld legs

$$a_c = 4 \quad \text{mm}$$

Allowable stress in tube

$$S_a = 92.4 \quad S_a = 92.4 \quad \text{MPa}$$

Allowable stress in weld

$$S_w := \min(S_a, S_d) \quad S_w = 92.4 \quad \text{MPa}$$

Weld strength factor

$$f_w := \frac{S_a}{S_w} \quad f_w = 1$$

Axial tube strength

$$F_t := \pi \cdot t_w \cdot (d_{to} - t_w) \cdot S_a \quad F_t = 18196.429 \quad \text{N}$$

Design strength

$$F_d := F_t \quad F_d = 18196.429 \quad \text{N}$$

Fillet weld strength

$$F_f := \min\left[0.55 \pi \cdot a_f \cdot (d_{to} + 0.67 \cdot a_f) \cdot S_w, F_t\right] \quad F_f = 4162.2251 \quad \text{N}$$

Groove weld strength

$$F_g := \min\left[0.85 \pi \cdot a_g \cdot (d_{to} + 0.67 \cdot a_g) \cdot S_w, F_t\right] \quad F_g = 18196.429 \quad \text{N}$$

Ratio of design strength to tube strength

$$f_d := \frac{F_d}{F_t} \quad f_d = 1$$

Ratio of fillet weld strength to design strength

$$f_f := 1 - \frac{F_g}{f_d \cdot F_t} \quad f_f = 0$$

Max allowable axial load in either direction on tube-to-tubesheet joint

$$L_{\max} := F_t \quad L_{\max} = 18196.429 \quad \text{N}$$

Figure UW-20.1 of ASME VIII Div 1 (2007)

sketch (a):

$$a_{ra} := \sqrt{(0.75 d_{to})^2 + 2.73 t_w \cdot (d_{to} - t_w) \cdot f_w \cdot f_d} - 0.75 d_{to} \quad a_{ra} = 4.0592 \quad \text{mm}$$

$$a_{fa} := \max(a_{ra}, t_w) \quad a_{fa} = 4.0592 \quad \text{mm}$$

sketch (b):

$$a_{rb} := \sqrt{(0.75 d_{to})^2 + 1.76 t_w \cdot (d_{to} - t_w) \cdot f_w \cdot f_d} - 0.75 d_{to} \quad a_{rb} = 2.7038 \quad \text{mm}$$

$$a_{gb} := \max(a_{rb}, t_w) \quad a_{gb} = 2.77 \quad \text{mm}$$

sketch (c):

$$a_{rc} := \sqrt{(0.75 d_{to})^2 + 1.07 t_w \cdot (d_{to} - t_w) \cdot f_w \cdot f_d} - 0.75 d_{to} \quad a_{rc} = 1.6859 \quad \text{mm}$$

$$a_{cc} := \max(a_{rc}, t_w) \quad a_{cc} = 2.77 \quad \text{mm}$$

$$a_{fc} := \frac{a_{cc}}{2} \quad a_{fc} = 1.385 \quad \text{mm}$$

$$a_{gc} := \frac{a_{cc}}{2} \quad a_{gc} = 1.385 \quad \text{mm}$$

sketch (d):

$$a_{rd} := \sqrt{(0.75d_{to})^2 + 2.03t_w(d_{to} - t_w) \cdot f_w \cdot f_d \cdot f_f} - 0.75d_{to} \quad a_{rd} = 0 \quad \text{mm}$$

$$a_{cd} := \max(a_{rd} + a_g, t_w) \quad a_{cd} = 3 \quad \text{mm}$$

$$a_{fd} := a_{cd} - a_g \quad a_{fd} = 0 \quad \text{mm}$$

Use sketch (d), therefore:

$$a_{c.\text{required}} := a_{cd} \quad a_{c.\text{required}} = 3 \quad \text{mm}$$

$$a_{f.\text{required}} := a_{fd} \quad a_{f.\text{required}} = 0 \quad \text{mm}$$

Weld is acceptable if:

$$a_c > a_{c(\text{required})}$$

$$a_f > a_{f(\text{required})}$$

**Appendix D – Measured data and results of wind tunnel experiment****Table D.1: Isothermal Test**

Run no.	$P_{atm}$ [Pa]	$T_{wb}$ [°C]	$T_{ai}$ [°C]	$\Delta P_b$ [Pa]	$\Delta P_{inl}$ [Pa]	$\Delta P_{noz}$ [Pa]
1	100460.00	15.30	15.87	163.18	899.66	1065.70
2	100460.00	15.30	15.79	126.66	666.09	779.47
3	100460.00	15.30	15.75	93.36	463.62	533.53
4	100460.00	15.30	15.68	63.99	296.15	334.29
5	100460.00	15.30	15.67	39.31	164.23	181.46
6	100460.00	15.30	15.73	19.83	69.94	74.75

**Table D.2: Measured data of whole bundle (Test 1)**

Run no.	$T_{ai}$ [°C]	$T_{ao}$ [°C]	$T_{wi}$ [°C]	$T_{wo}$ [°C]	$m_w$ [kg/s]	$\Delta P_b$ [Pa]	$\Delta P_{inl}$ [Pa]	$\Delta P_{noz}$ [Pa]	$\Delta T_w$ [°C]
1	18.27	48.20	58.03	53.02	3071.99	152.93	821.33	955.44	0.09
2	18.32	50.32	59.01	54.28	3076.30	118.26	602.69	693.93	0.09
3	18.41	52.26	59.20	55.18	3076.46	86.73	418.17	473.17	0.09
4	18.36	54.45	59.40	56.04	3069.27	59.16	264.74	293.00	0.09
5	18.47	56.69	59.70	57.07	3059.36	36.16	146.31	158.33	0.09
6	18.56	58.37	59.83	58.08	3058.70	17.96	62.42	64.31	0.09

**Table D.3: Results of whole bundle (Test 1)**

Run no.	$m_{av}$ [kg/s]	LMTD	$Q_a$ [kW]	$Q_w$ [kW]	$Q_a/Q_w$	$h_a$ [W/m <sup>2</sup> K]	$Ry \times 10^3$ [m <sup>-1</sup> ]	$Ny \times 10^3$ [m <sup>-1</sup> ]
1	2.21	19.74	67.36	64.11	1.05	56.08	202.39	299.75
2	1.88	19.20	61.34	60.54	1.01	52.12	171.85	275.18
3	1.55	17.89	53.51	51.17	1.05	46.42	141.35	253.50
4	1.22	16.12	44.78	42.58	1.05	41.75	110.66	231.51
5	0.89	13.94	34.66	32.99	1.05	36.02	80.63	202.72
6	0.56	11.54	22.74	21.61	1.05	26.81	50.68	155.39

**Table D.4: Measured data of whole bundle (Test 2)**

Run no.	$T_{ai}$ [°C]	$T_{ao}$ [°C]	$T_{wi}$ [°C]	$T_{wo}$ [°C]	$m_w$ [kg/s]	$\Delta P_b$ [Pa]	$\Delta P_{inl}$ [Pa]	$\Delta P_{noz}$ [Pa]	$\Delta T_w$ [°C]
1	19.19	48.43	58.12	53.20	3049.75	152.95	815.36	951.15	0.07
2	18.80	50.09	58.48	54.02	3039.02	118.10	600.28	689.87	0.07
3	18.97	52.34	59.22	55.25	3032.98	86.65	415.34	471.00	0.07
4	18.77	54.46	59.44	56.13	3038.52	59.31	263.12	292.80	0.07
5	18.62	56.69	59.69	57.06	3023.11	36.26	145.50	157.59	0.07
6	18.51	58.41	59.85	58.08	3023.11	17.96	61.90	64.22	0.07

**Table D.5: Results of whole bundle (Test 2)**

Run no.	$m_{av}$ [kg/s]	LMTD	$Q_a$ [kW]	$Q_w$ [kW]	$Q_a/Q_w$	$h_a$ [W/m <sup>2</sup> K]	$Ry \times 10^3$ [m <sup>-1</sup> ]	$Ny \times 10^3$ [m <sup>-1</sup> ]
1	2.20	19.37	65.60	63.15	1.04	55.87	201.35	296.41
2	1.87	18.70	59.77	57.04	1.05	50.99	171.16	275.57
3	1.55	17.68	52.57	50.49	1.04	46.21	140.73	251.69
4	1.22	16.06	44.23	42.09	1.05	41.28	110.44	229.05
5	0.89	13.89	34.40	33.04	1.04	36.06	80.33	201.90
6	0.56	11.52	22.73	21.96	1.03	27.13	50.53	155.65

**Table D.6: Measured data of whole bundle (Test 3)**

Run no.	$T_{ai}$ [°C]	$T_{ao}$ [°C]	$T_{wi}$ [°C]	$T_{wo}$ [°C]	$m_w$ [kg/s]	$\Delta P_b$ [Pa]	$\Delta P_{inl}$ [Pa]	$\Delta P_{noz}$ [Pa]	$\Delta T_w$ [°C]
1	18.08	47.35	57.46	52.41	3018.61	152.82	817.68	958.51	0.06
2	18.21	50.09	59.01	54.31	3012.52	117.81	599.93	694.10	0.06
3	18.30	52.10	59.23	55.14	3010.43	86.35	415.22	472.54	0.06
4	18.25	54.20	59.43	56.00	3017.73	59.03	263.52	294.15	0.06
5	17.95	56.45	59.61	56.91	3012.07	35.97	145.05	157.45	0.06
6	17.60	58.38	59.95	58.09	3007.88	17.77	62.04	64.30	0.06

**Table D.7: Results of whole bundle (Test 3)**

Run no.	$m_{av}$ [kg/s]	LMTD	$Q_a$ [kW]	$Q_w$ [kW]	$Q_a/Q_w$	$h_a$ [W/m <sup>2</sup> K]	$Ry \times 10^3$ [m <sup>-1</sup> ]	$Ny \times 10^3$ [m <sup>-1</sup> ]
1	2.21	19.81	66.03	64.46	1.02	55.32	202.98	292.40
2	1.88	19.44	61.16	59.70	1.02	50.74	172.04	270.97
3	1.55	18.08	53.43	51.96	1.03	46.26	141.39	250.45
4	1.22	16.45	44.75	43.55	1.03	41.27	111.05	226.28
5	0.89	14.26	34.86	34.08	1.02	35.92	80.59	199.40
6	0.56	11.97	23.33	23.22	1.00	27.22	50.81	153.79

**Table D.8: Measured data of whole bundle (Test 4)**

Run no.	$T_{ai}$ [°C]	$T_{ao}$ [°C]	$T_{wi}$ [°C]	$T_{wo}$ [°C]	$m_w$ [kg/s]	$\Delta P_b$ [Pa]	$\Delta P_{inl}$ [Pa]	$\Delta P_{noz}$ [Pa]	$\Delta T_w$ [°C]
1	17.48	47.42	57.93	52.70	3032.70	153.31	826.68	966.29	0.09
2	17.42	49.56	58.70	53.93	3027.86	118.26	606.83	700.91	0.09
3	17.51	51.81	59.23	55.07	3020.60	86.50	419.33	477.08	0.09
4	17.49	53.96	59.37	55.85	3034.10	58.93	266.04	296.58	0.09
5	17.32	56.32	59.65	56.83	3022.10	35.85	146.39	158.53	0.09
6	17.26	58.26	59.82	57.98	3028.15	17.40	62.43	64.56	0.09

**Table D.9: Results of whole bundle (Test 4)**

Run no.	$m_{av}$ [kg/s]	LMTD	$Q_a$ [kW]	$Q_w$ [kW]	$Q_a/Q_w$	$h_a$ [W/m <sup>2</sup> K]	$Ry \times 10^3$ [m <sup>-1</sup> ]	$Ny \times 10^3$ [m <sup>-1</sup> ]
1	2.24	20.44	68.14	66.14	1.03	55.11	205.05	292.64
2	1.90	19.76	62.23	60.14	1.03	50.51	173.97	272.01
3	1.57	18.58	54.69	52.24	1.05	45.48	142.90	249.76
4	1.23	16.82	45.76	44.20	1.04	41.10	112.13	226.75
5	0.90	14.63	35.61	35.14	1.01	35.93	81.35	198.59
6	0.57	12.00	23.65	22.59	1.05	26.91	51.29	155.81



**Table D.10: Measured data of whole bundle (Test 5)**

Run no.	$T_{ai}$ [°C]	$T_{ao}$ [°C]	$T_{wi}$ [°C]	$T_{wo}$ [°C]	$m_w$ [kg/s]	$\Delta P_b$ [Pa]	$\Delta P_{inl}$ [Pa]	$\Delta P_{noz}$ [Pa]	$\Delta T_w$ [°C]
1	17.34	47.40	58.10	52.81	3025.02	153.78	830.02	970.60	0.08
2	17.28	49.75	59.07	54.25	3023.60	118.47	610.50	704.29	0.08
3	17.25	51.64	59.18	55.00	3029.72	86.55	421.30	478.80	0.08
4	17.18	53.83	59.39	55.83	3026.67	59.00	267.84	298.14	0.08
5	17.42	56.27	59.62	56.85	3025.19	35.80	147.44	159.65	0.08
6	17.57	58.25	59.91	58.00	3021.71	17.42	62.95	64.48	0.08

**Table D.11: Results of whole bundle (Test 5)**

Run no.	$m_{av}$ [kg/s]	LMTD	$Q_a$ [kW]	$Q_w$ [kW]	$Q_a/Q_w$	$h_a$ [W/m <sup>2</sup> K]	$Ry \times 10^3$ [m <sup>-1</sup> ]	$Ny \times 10^3$ [m <sup>-1</sup> ]
1	2.25	20.66	68.71	66.81	1.03	54.98	205.96	291.84
2	1.91	20.06	63.18	60.86	1.04	50.36	174.85	271.80
3	1.58	18.76	55.14	52.75	1.05	45.44	143.72	249.47
4	1.24	17.06	46.28	44.77	1.03	40.99	112.89	226.13
5	0.90	14.64	35.71	34.60	1.03	35.61	81.92	199.10
6	0.57	12.14	23.53	23.38	1.01	27.03	51.42	152.99

**Table D.12: Measured data of row 1**

Run no.	$T_{ai}$ [°C]	$T_{ao}$ [°C]	$T_{wi}$ [°C]	$T_{wo}$ [°C]	$m_w$ [kg/s]	$\Delta P_b$ [Pa]	$\Delta P_{inl}$ [Pa]	$\Delta P_{noz}$ [Pa]	$\Delta T_w$ [°C]
1	16.96	24.50	60.19	58.68	3061.98	160.00	877.35	1029.10	0.06
2	17.32	25.53	60.19	58.77	3057.34	124.10	654.48	745.76	0.06
3	17.74	26.97	60.18	58.86	3050.98	91.14	456.01	507.99	0.06
4	17.86	28.53	60.22	59.00	3056.53	61.94	285.22	313.54	0.06
5	17.95	30.98	60.25	59.14	3058.39	37.52	157.17	165.71	0.06
6	18.01	35.09	60.30	59.37	3057.95	18.28	66.44	63.96	0.06

**Table D.13: Results of row 1**

Run no.	$m_{av}$ [kg/s]	LMTD	$Q_a$ [kW]	$Q_w$ [kW]	$Q_a/Q_w$	$h_a$ [W/m <sup>2</sup> K]	$Ry \times 10^3$ [m <sup>-1</sup> ]	$Ny \times 10^3$ [m <sup>-1</sup> ]
1	2.39	38.62	18.34	18.59	0.99	45.97	225.56	42.18
2	2.04	37.95	17.00	17.39	0.98	42.84	191.81	39.44
3	1.68	37.02	15.78	16.04	0.98	40.00	157.97	37.21
4	1.32	36.21	14.32	14.84	0.97	36.78	123.72	34.13
5	0.95	34.89	12.65	13.44	0.94	33.48	89.24	30.87
6	0.58	32.62	10.16	11.01	0.92	27.99	54.38	25.86

**Table D.14: Measured data of row 2**

Run no.	$T_{ai}$ [°C]	$T_{ao}$ [°C]	$T_{wi}$ [°C]	$T_{wo}$ [°C]	$m_w$ [kg/s]	$\Delta P_b$ [Pa]	$\Delta P_{inl}$ [Pa]	$\Delta P_{noz}$ [Pa]	$\Delta T_w$ [°C]
1	15.37	24.11	60.19	58.43	3037.25	160.30	890.32	1042.63	0.08
2	15.88	25.21	60.19	58.58	3021.86	124.21	657.98	755.67	0.08
3	16.03	26.39	60.24	58.75	3034.54	90.75	456.02	515.33	0.08
4	16.11	27.98	60.27	58.91	3026.08	61.42	289.77	318.83	0.08
5	16.09	30.45	60.34	59.13	3029.84	36.80	159.95	168.16	0.08
6	16.15	34.80	60.37	59.34	3026.16	17.55	67.93	64.79	0.08

**Table D.15: Results of row 2**

Run no.	$m_{av}$ [kg/s]	LMTD	$Q_a$ [kW]	$Q_w$ [kW]	$Q_a/Q_w$	$h_a$ [W/m <sup>2</sup> K]	$Ry \times 10^3$ [m <sup>-1</sup> ]	$Ny \times 10^3$ [m <sup>-1</sup> ]
1	2.42	39.47	21.50	21.81	0.99	56.42	229.00	50.19
2	2.06	38.71	19.54	19.70	0.99	50.44	194.72	45.79
3	1.70	38.12	17.95	18.22	0.99	46.02	160.59	42.13
4	1.34	37.30	16.16	16.50	0.98	41.31	125.93	38.20
5	0.97	36.06	14.14	14.70	0.96	36.64	90.81	33.93
6	0.59	33.62	11.28	12.27	0.92	30.88	55.43	28.25

**Table D.16: Measured data of row 3**

Run no.	$T_{ai}$ [°C]	$T_{ao}$ [°C]	$T_{wi}$ [°C]	$T_{wo}$ [°C]	$m_w$ [kg/s]	$\Delta P_b$ [Pa]	$\Delta P_{inl}$ [Pa]	$\Delta P_{noz}$ [Pa]	$\Delta T_w$ [°C]
1	16.73	25.68	60.12	58.36	3044.81	159.57	882.39	1035.86	0.08
2	16.72	26.57	60.16	58.50	3038.90	123.43	651.53	752.10	0.08
3	16.73	27.70	60.20	58.66	3028.28	90.28	451.82	512.27	0.08
4	16.60	29.20	60.25	58.84	3045.81	61.09	287.46	317.54	0.08
5	16.62	31.58	60.27	59.03	3039.97	36.60	158.34	167.63	0.08
6	16.56	35.51	60.33	59.32	3040.60	17.29	66.90	64.81	0.08

**Table D.17: Results of row 3**

Run no.	$m_{av}$ [kg/s]	LMTD	$Q_a$ [kW]	$Q_w$ [kW]	$Q_a/Q_w$	$h_a$ [W/m <sup>2</sup> K]	$Ry \times 10^3$ [m <sup>-1</sup> ]	$Ny \times 10^3$ [m <sup>-1</sup> ]
1	2.40	37.92	21.86	21.75	1.01	60.70	226.64	53.70
2	2.05	37.53	20.52	20.44	1.00	56.32	193.09	50.40
3	1.69	37.01	18.88	18.84	1.00	51.13	159.14	46.39
4	1.33	36.36	17.06	17.14	1.00	45.67	124.94	41.91
5	0.96	35.11	14.66	15.03	0.98	39.52	90.15	36.45
6	0.59	32.98	11.41	12.09	0.94	31.54	55.13	29.18

**Table D.18: Measured data of row 4**

Run no.	$T_{ai}$ [°C]	$T_{ao}$ [°C]	$T_{wi}$ [°C]	$T_{wo}$ [°C]	$m_w$ [kg/s]	$\Delta P_b$ [Pa]	$\Delta P_{inl}$ [Pa]	$\Delta P_{noz}$ [Pa]	$\Delta T_w$ [°C]
1	16.36	25.21	60.12	58.35	3009.74	158.41	881.47	1037.57	0.05
2	16.40	26.00	60.20	58.54	3005.77	122.32	650.81	752.57	0.05
3	16.24	26.91	60.24	58.70	3007.40	89.41	451.47	512.82	0.05
4	16.32	28.58	60.29	58.89	3028.02	60.38	287.00	317.68	0.05
5	16.31	31.12	60.29	59.04	3013.67	36.05	157.81	167.65	0.05
6	16.27	35.12	60.37	59.35	3026.30	17.03	66.77	64.72	0.05

**Table D.19: Results of row 4**

Run no.	$m_{av}$ [kg/s]	LMTD	$Q_a$ [kW]	$Q_w$ [kW]	$Q_a/Q_w$	$h_a$ [W/m <sup>2</sup> K]	$Ry \times 10^3$ [m <sup>-1</sup> ]	$Ny \times 10^3$ [m <sup>-1</sup> ]
1	2.41	38.34	21.67	21.86	0.99	59.62	227.10	52.53
2	2.05	38.03	20.01	20.53	0.97	54.45	193.45	48.21
3	1.70	37.71	18.37	18.98	0.97	49.07	159.64	43.97
4	1.33	36.87	16.60	17.25	0.96	44.16	125.22	39.97
5	0.96	35.52	14.52	15.26	0.95	39.10	90.29	35.62
6	0.59	33.38	11.35	12.49	0.91	31.65	55.15	28.65

**Table D.20: Measured data of row 5**

Run no.	$T_{ai}$ [°C]	$T_{ao}$ [°C]	$T_{wi}$ [°C]	$T_{wo}$ [°C]	$m_w$ [kg/s]	$\Delta P_b$ [Pa]	$\Delta P_{inl}$ [Pa]	$\Delta P_{noz}$ [Pa]	$\Delta T_w$ [°C]
1	15.73	24.79	60.15	58.37	3044.80	157.14	880.85	1039.06	0.07
2	16.18	25.93	60.22	58.55	3040.24	121.22	649.85	752.91	0.07
3	16.40	27.28	60.25	58.71	3038.59	88.44	450.48	512.99	0.07
4	16.75	29.07	60.29	58.89	3033.07	59.69	285.88	317.23	0.07
5	16.83	31.59	60.32	59.10	3033.21	35.71	157.69	167.77	0.07
6	16.92	35.89	60.36	59.34	3039.02	16.76	66.59	64.67	0.07

**Table D.21: Results of row 5**

Run no.	$m_{av}$ [kg/s]	LMTD	$Q_a$ [kW]	$Q_w$ [kW]	$Q_a/Q_w$	$h_a$ [W/m <sup>2</sup> K]	$Ry \times 10^3$ [m <sup>-1</sup> ]	$Ny \times 10^3$ [m <sup>-1</sup> ]
1	2.41	38.89	22.21	22.12	1.00	59.83	228.03	53.16
2	2.06	38.19	20.39	20.67	0.99	55.02	193.87	48.99
3	1.70	37.45	18.77	19.00	0.99	50.29	159.68	45.40
4	1.33	36.40	16.70	17.12	0.98	44.88	125.07	40.80
5	0.97	35.06	14.48	14.95	0.97	39.13	90.30	35.98
6	0.59	32.62	11.42	12.24	0.93	32.28	55.07	29.56

**Table D.22: Measured data of row 6**

Run no.	$T_{ai}$ [°C]	$T_{ao}$ [°C]	$T_{wi}$ [°C]	$T_{wo}$ [°C]	$m_w$ [kg/s]	$\Delta P_b$ [Pa]	$\Delta P_{inl}$ [Pa]	$\Delta P_{noz}$ [Pa]	$\Delta T_w$ [°C]
1	17.58	26.46	60.18	58.40	3017.43	156.34	874.58	1031.96	0.08
2	17.79	27.40	60.17	58.53	3023.89	120.67	644.85	749.10	0.08
3	18.00	28.62	60.21	58.70	3017.62	88.33	446.87	510.30	0.08
4	18.03	30.15	60.22	58.86	3012.16	59.58	284.09	315.63	0.08
5	17.86	32.21	60.27	59.07	3014.75	35.82	156.62	167.63	0.08
6	17.81	36.09	60.35	59.36	3013.38	17.06	66.24	65.15	0.08

**Table D.23: Results of row 6**

Run no.	$m_{av}$ [kg/s]	LMTD	$Q_a$ [kW]	$Q_w$ [kW]	$Q_a/Q_w$	$h_a$ [W/m <sup>2</sup> K]	$R_{yx}10^3$ [m <sup>-1</sup> ]	$N_{yx}10^3$ [m <sup>-1</sup> ]
1	2.39	37.16	21.62	21.45	1.01	61.88	224.99	54.51
2	2.04	36.61	19.93	19.88	1.00	56.31	191.57	50.22
3	1.68	35.95	18.17	18.15	1.00	50.73	157.82	45.90
4	1.32	35.18	16.30	16.25	1.00	44.87	123.69	41.33
5	0.96	34.21	14.00	14.16	0.99	38.25	89.55	35.62
6	0.59	32.13	10.97	11.51	0.95	30.93	54.81	28.76

## Appendix E - Wind tunnel experiment sample calculation

The following sample calculation was done according to Kroger (2004). It shows how the measured data was used to calculate the performance characteristics of the finned tube bundle of Test 3, speed 1 (Appendix D, Table D.6 and Table D.7).

### Details of fin

Thermal conductivity	$k_f = 230$	$\frac{W}{mK}$
Fin diameter	$d_f = 57.2$	mm
Fin root diameter	$d_r = 25.4$	mm
Fin root thickness	$t_{fr} = 0.406$	mm
Fin thickness (mean)	$t_{fm} = 0.406$	mm
Fin tip thickness	$t_{ft} = 0.406$	mm
Fin pitch	$P_f = 2.8$	mm

### Details of tubes

Thermal conductivity	$k_t = 58$	$\frac{W}{mK}$
Tube outside diameter	$d_o = 0.0254$	m
Tube inside diameter	$d_i = 0.0194$	m
Number of tube rows	$n_r = 6$	
Number of tubes per row (effective)	$n_{etr} = 12.5$	
Number of tubes per row (actual)	$n_{atr} = 13$	
Transversal tube pitch	$P_t = 0.0635$	m
Longitudinal pitch	$P_l = 0.05499$	m
Length of finned tube	$L_t = 0.75$	m
Mean thermal contact resistance	$R_c = 0$	$\frac{m^2K}{w}$

### Measured data

Cross-sectional area of tunnel in front of nozzle plate	$A_{tus} = 1.44$	$m^2$
Frontal area	$A_{fr} = 0.5865$	$m^2$
Atmospheric pressure	$P_{atm} = 1.0003 \times 10^5$	Pa
Air inlet wet bulb temperature	$T_{wb} = 291.15$	K
Air inlet temperature	$T_{ai} = 291.22742$	K
Air outlet temperature	$T_{ao} = 320.50494$	K

Water inlet temperature	$T_{wi} = 330.61438$	K
Water outlet temperature	$T_{wo} = 325.55821$	K
Change in water temp due to losses	$dT_w = 0.05862$	K
Diameter of elliptical nozzle	$d_n = 0.2509$	nr
Pressure drop across elliptical nozzle	$dP_n = 957.30956$	Pa
Pressure drop across bundle for nozzle inlet	$dP_b = 817.27961$	Pa
Measure bundle pressure drop	$P = 151.97222$	Pa
Air specific heat ratio (Cp/Cv)	$C = 1.4$	
Mass flow rate of water	$m_w = 3.08494$	$\frac{\text{kg}}{\text{s}}$
Molar mass of air	$M_a = 28.97$	$\frac{\text{kg}}{\text{mole}}$
Molar mass of water vapour	$M_v = 18.016$	$\frac{\text{kg}}{\text{mole}}$
Pressure upstream of the nozzle	$dP_{up} := P_{atm} - dP_b$	
	$dP_{up} = 9.92127 \times 10^4$	Pa
Diagonal pitch		
	$P_d := \sqrt{P_1^2 + \left(\frac{P_t}{2}\right)^2}$	
	$P_d = 0.0635$	nr
Vapour Pressure from equation A.2.1	$P_{va} := P_v(T_{wb})$	
	$P_{va} = 2.0627 \times 10^3$	Pa
Humidity ratio from equation A.3.5	$w_a := w(T_{ai}, T_{wb}, P_{atm}, P_{va})$	
	$w_a = 0.01313$	
<b>Properties of dry air</b>		
Arithmetic mean air temperature	$T_{am} := \frac{T_{ai} + T_{ao}}{2}$	
	$T_{am} = 305.86618$	K
Specific heat	$c_{pa}(T_{am}) = 1.00718 \times 10^3$	$\frac{\text{J}}{\text{kgK}}$
Dynamic viscosity	$\mu_a(T_{am}) = 1.87377 \times 10^{-5}$	$\frac{\text{kg}}{\text{ms}}$
Thermal conductivity	$k_a(T_{am}) = 0.02667$	$\frac{\text{W}}{\text{mK}}$

Prandtl number

$$\text{Pr}_{\text{am}} := \frac{c_{\text{pa}}(T_{\text{am}}) \cdot \mu_{\text{a}}(T_{\text{am}})}{k_{\text{a}}(T_{\text{am}})} \quad \text{Pr}_{\text{am}} = 0.70751$$

### Properties of water vapour

Specific heat  $c_{\text{pv}}(T_{\text{am}}) = 1.89161 \times 10^3 \frac{\text{J}}{\text{kgK}}$

Dynamic viscosity  $\mu_{\text{v}}(T_{\text{am}}) = 1.02265 \times 10^{-5} \frac{\text{kg}}{\text{ms}}$

Thermal conductivity  $k_{\text{v}}(T_{\text{am}}) = 0.01913 \frac{\text{W}}{\text{mK}}$

Prandtl number

$$\text{Pr}_{\text{v}} := \frac{c_{\text{pa}}(T_{\text{am}}) \cdot \mu_{\text{a}}(T_{\text{am}})}{k_{\text{a}}(T_{\text{am}})} \quad \text{Pr}_{\text{v}} = 0.70751$$

### Properties of mixture of dry air and water vapour

Density  $\rho_{\text{avm}} := \rho_{\text{av}}(w_{\text{a}}, P_{\text{atm}}, T_{\text{am}}) \quad \rho_{\text{avm}} = 1.13029 \frac{\text{kg}}{\text{m}^3}$

Specific heat  $c_{\text{pavm}} := c_{\text{pav}}(T_{\text{am}}, w_{\text{a}}) \quad c_{\text{pavm}} = 1.01864 \times 10^3 \frac{\text{J}}{\text{kgK}}$

Dynamic viscosity  $\mu_{\text{avm}} := \mu_{\text{av}}(T_{\text{am}}, w_{\text{a}}) \quad \mu_{\text{avm}} = 1.85983 \times 10^{-5} \frac{\text{kg}}{\text{ms}}$

Thermal conductivity  $k_{\text{avm}} := k_{\text{av}}(T_{\text{am}}, w_{\text{a}}) \quad k_{\text{avm}} = 0.02654 \frac{\text{W}}{\text{mK}}$

Prandtl number

$$\text{Pr}_{\text{avm}} := \frac{c_{\text{pavm}} \cdot \mu_{\text{avm}}}{k_{\text{avm}}} \quad \text{Pr}_{\text{avm}} = 0.71382$$

### Properties of water

Arithmetic mean water temperature

$$T_{\text{wm}} := \frac{T_{\text{wi}} + T_{\text{wo}}}{2} \quad T_{\text{wm}} = 328.08629 \text{ K}$$

Specific heat  $c_{\text{pw}}(T_{\text{wm}}) = 4.18112 \times 10^3 \frac{\text{J}}{\text{kgK}}$

Dynamic viscosity  $\mu_{\text{w}}(T_{\text{wm}}) = 5.01438 \times 10^{-4} \frac{\text{kg}}{\text{ms}}$

Thermal conductivity  $k_{\text{w}}(T_{\text{wm}}) = 0.64813 \frac{\text{W}}{\text{mK}}$



Prandtl number

$$\text{Pr}_{\text{wm}} := \frac{c_{\text{pw}}(T_{\text{wm}}) \cdot \mu_{\text{w}}(T_{\text{wm}})}{k_{\text{w}}(T_{\text{wm}})} \quad \text{Pr}_{\text{wm}} = 3.2348$$

### **Calculation**

Air density after bundle and before nozzle from equation A.3.1

at air outlet temperature

$$\rho_{\text{avo}} := \rho_{\text{av}}(w_{\text{a}}, dP_{\text{up}}, T_{\text{ao}}) \quad \rho_{\text{avo}} = 1.06985 \quad \frac{\text{kg}}{\text{m}^3}$$

Dynamic viscosity of dry air from equation A.1.3

$$\mu_{\text{a}}(T_{\text{ao}}) = 1.9402 \times 10^{-5} \quad \frac{\text{kg}}{\text{ms}}$$

Dynamic viscosity of water vapour from equation A.2.3

$$\mu_{\text{v}}(T_{\text{ao}}) = 1.06829 \times 10^{-5} \quad \frac{\text{kg}}{\text{ms}}$$

Dynamic viscosity of moist air from equation A.3.3

$$\mu_{\text{avo}} := \mu_{\text{av}}(T_{\text{ao}}, w_{\text{a}}) \quad \mu_{\text{avo}} = 1.92592 \times 10^{-5} \quad \frac{\text{kg}}{\text{ms}}$$

Gas expansion factor from equation 5.2.3

$$\Phi_{\text{g}} := 1 - \frac{3 \cdot dP_{\text{n}}}{4 \cdot (dP_{\text{up}}) \cdot C} \quad \Phi_{\text{g}} = 0.99483$$

Elliptical nozzle area

$$A_{\text{n}} := \frac{\pi}{4} \cdot d_{\text{n}}^2 \quad A_{\text{n}} = 0.04944 \quad \text{m}^2$$

Approach velocity factor from equation 5.2.4

$$Y := 1 + 0.5 \cdot \left( \frac{A_{\text{n}}}{A_{\text{tus}}} \right)^2 + 2 \cdot \left( \frac{A_{\text{n}}}{A_{\text{tus}}} \right)^2 \cdot \frac{dP_{\text{n}}}{dP_{\text{up}} \cdot C} \quad Y = 1.00061$$

Assume  $C_{\text{n}} = 0.994$

With this value, the resultant air mass flow rate using equation 5.2.1

$$m_{\text{av}} := C_{\text{n}} \cdot \Phi_{\text{g}} \cdot Y \pi \cdot d_{\text{n}}^2 \cdot \frac{(2 \cdot \rho_{\text{avo}} \cdot dP_{\text{n}})^{0.5}}{4} \quad m_{\text{av}} = 2.21407 \quad \frac{\text{kg}}{\text{s}}$$

The nozzle Reynolds number is

$$\text{Re}_{\text{n}} := \frac{m_{\text{av}} \cdot d_{\text{n}}}{A_{\text{n}} \cdot \mu_{\text{avo}}} \quad \text{Re}_{\text{n}} = 5.83395 \times 10^5$$

Therefore

$$C_{n1} := \begin{cases} 0.954803 + 6.3781710^{-7} \cdot Re_n - 4.6539410^{-12} \cdot Re_n^2 \dots & \text{if } 30000 < Re_n < 100000 \\ + 1.3351410^{-17} \cdot Re_n^3 & \\ 0.9758 + 1.08 \cdot 10^{-7} \cdot Re_n - 1.6 \cdot 10^{-13} \cdot Re_n^2 & \text{if } 100000 < Re_n < 350000 \\ 0.994 & \text{otherwise} \end{cases}$$

$$C_{n1} = 0.994$$

Since  $C_n = C_{n1}$ . The iteration has converged

Energy Balance from equations (4.12) and (4.13)

$$Q_a := m_{av} \cdot c_{pavm} \cdot (T_{ao} - T_{ai}) \quad Q_a = 6.6031 \times 10^4 \quad \text{W}$$

$$Q_w := m_w \cdot c_{pw} (T_{wm}) \cdot (T_{wi} - T_{wo} - dT_w) \quad Q_w = 6.44609 \times 10^4 \quad \text{W}$$

$$\%Error := \left( \frac{Q_a - Q_w}{Q_a} \right) \cdot (100) \quad \%Error = 2.37784$$

$$Q_m := \frac{Q_a + Q_w}{2} \quad Q_m = 6.52459 \times 10^4$$

Determine the water side heat transfer coefficient

Reynolds number

$$Re_w := \frac{4 \cdot m_w}{n_{atr} \cdot \pi \cdot d_i \cdot \mu_w (T_{wm})} \quad Re_w = 3.10594 \times 10^4$$

Friction factor for smooth tubes

$$f_w := (1.82 \log(Re_w) - 1.64)^{-2} \quad f_w = 0.02341$$

Effective length

$$L_{te} := n_r \cdot L_t \quad L_{te} = 4.5 \quad \text{m}$$

Nusselt number (Gnielinski)

$$Nu := \frac{\left( \frac{f_w}{8} \right) \cdot (Re_w - 1000) \cdot Pr_{wm} \left[ 1 + \left( \frac{d_i}{L_{te}} \right)^{0.67} \right]}{1 + 12.7 \left( \frac{f_w}{8} \right)^{0.5} \cdot (Pr_{wm}^{0.67} - 1)} \quad Nu = 160.27141$$

Water side heat transfer coefficient

$$h_w := \left( \frac{Nu \cdot k_w (T_{wm})}{d_i} \right) \quad h_w = 5.35447 \times 10^3$$

Logarithmic mean temperature difference

$$\Delta T_{lm} := \frac{(T_{wo} - T_{ai}) - (T_{wi} - T_{ao})}{\ln\left(\frac{T_{wo} - T_{ai}}{T_{wi} - T_{ao}}\right)} \quad \Delta T_{lm} = 19.81178$$

Effective air side fin surface area

$$A_f := n_r \cdot n_{etr} \cdot \frac{L_t}{P_f} \cdot \frac{\pi \cdot \left[ \frac{2}{4} \cdot (d_f^2 - d_r^2) + d_f t_{ft} \right]}{1000} \quad A_f = 84.35365$$

Total air side surface area

$$A_a := A_f + \frac{\pi \cdot n_r \cdot n_{etr} \cdot L_t \cdot d_r \cdot \frac{P_f - t_{fr}}{P_f}}{1000} \quad A_a = 88.19136$$

Total water side surface area

$$A_w := n_r \cdot n_{etr} \cdot \pi \cdot d_i \cdot L_t \quad A_w = 3.42826$$

$$\text{sum} := \frac{1}{n_r \cdot n_{etr} \cdot L_t} \left[ \frac{\ln\left(\frac{d_o}{d_i}\right)}{2 \cdot \pi \cdot k_t} + \left( \frac{R_c}{\pi \cdot d_o} \right) + \frac{\ln\left(\frac{d_r}{1000}\right)}{2 \cdot \pi \cdot k_f} \right] \quad \text{sum} = 1.31459 \times 10^{-5}$$

$$\text{where sum} = \sum_n \frac{R_n}{A_n}$$

For cross flow

$$F_t = 1$$

Heat transfer parameter

$$N_y := \left[ \left( \frac{F_t \cdot \Delta T_{lm}}{Q_m} - \frac{1}{h_w \cdot A_w} \right) \cdot \left( A_{fr} \cdot k_{avm} \cdot Pr_{avm}^{0.33} \right) \right]^{-1} \quad N_y = 2.88165 \times 10^5$$

Corresponding characteristic flow parameter

$$R_y := \frac{m_{av}}{\mu_{avm} \cdot A_{fr}} \quad R_y = 2.02978 \times 10^5$$

Fin efficiency parameter using equation 3.3.13

$$\phi := \left( \frac{d_f}{d_r} - 1 \right) \cdot \left( 1 + 0.35 \ln \left( \frac{d_f}{d_r} \right) \right) \quad \phi = 1.60769$$

Fin efficiency parameter using equation 3.3.4

$$b := \left( \frac{2 \cdot h_a \cdot 1000}{k_f \cdot t_{fm}} \right)^{0.5} \quad b = 34.4209$$

Fin efficiency using equation 3.3.12

$$\eta_f := \frac{\tanh \left( b \cdot d_r \cdot \frac{\phi}{2000} \right)}{b \cdot d_r \cdot \frac{\phi}{2000}} \quad \eta_f = 0.86247$$

Surface effectiveness

$$e_f := A_a - A_f (1 - \eta_f) \quad e_f = 76.5901$$

Assume  $h_a = 55.31824$

From equation 5.3.7 the air side heat transfer coefficient

$$h_{a1} := \left[ e_f \left( F_t \cdot \frac{\Delta T_{lm}}{Q_m} - \frac{1}{h_w \cdot A_w} - \text{sum} \right) \right]^{-1} \quad h_{a1} = 55.31825$$

Since  $h_a = h_{a1}$ . The iteration has converged

Minimum flow area

$$A_c := \left( n_{etr} \cdot \frac{L_t \cdot 1000}{P_f} \right) \cdot \left[ P_t \cdot \left( \frac{P_f}{1000} \right) - (d_f - d_r) \cdot t_{fm} \cdot 10^{-6} - P_f \cdot d_r \cdot 10^{-6} \right] \quad A_c = 0.31396$$

Colburn j-factor from equation 5.4.4

$$j := \frac{h_a \cdot Pr_{avm}^{0.67}}{\left( \frac{m_{av}}{A_c} \right) \cdot c_{pavm}} \quad j = 6.14372 \times 10^{-3}$$

Reynolds number based on the root diameter

$$Re_a := \frac{m_{av} \cdot \left( \frac{d_r}{1000} \right)}{A_c \cdot \mu_{avm}}$$

Ratio of total air-side area to the root area  $\frac{A}{A_r}$

$$A_r := \frac{\frac{d_f^2 - d_r^2}{2} + d_f t_{ft} + d_r (P_f - t_{fr})}{d_r \cdot P_f} \quad A_r = 19.64807 \quad \text{m}^2$$

Mass velocity based on minimum flow area

$$G_c := \frac{m_{av}}{A_c} \quad G_c = 7.0521 \quad \frac{\text{kg}}{\text{m}^2 \text{ s}}$$

Non-isothermal Euler number

$$Eu := \frac{\rho_{avm} \cdot P}{G_c^2} \quad Eu = 3.45394$$

Area ratio

$$\sigma := \frac{A_c}{A_{fr}} \quad \sigma = 0.53531$$

Air density before bundle at air inlet temperature

$$\rho_{avi} := \rho_{av}(w_a, P_{atm}, T_{ai}) \quad \rho_{avi} = 1.1871 \quad \frac{\text{kg}}{\text{m}^3}$$

Conversion to isothermal Euler number

$$Eu_{iso} := \left[ P - \left[ \frac{G_c^2}{2} \cdot (1 + \sigma^2) \cdot \left( \frac{1}{\rho_{avo}} - \frac{1}{\rho_{avi}} \right) \right] \right] \cdot \left( \frac{\rho_{avm}}{G_c^2} \right)$$

$$Eu_{iso} = 3.38682$$